Georgia Tech Sponsored Research

Project	E-25-W22
Project director	Glezer Ari
Title	Control of Natural Convection Along a Heated, Inclined Plate
Close-out	1/29/1999

(new) #1 E-95-022

APPENDIX D

ANNUAL NSF GRANT PROGRESS REPORT

NSF Program: Thermal Systems and Engineering

NSF Award Number: CST 9318332

PI Name:

Period Covered By This Report: Sept. 93 - Sept. 94

PI Institution: Georgia Tech

Date: March 28, 1995

PI Address: School of Mechanical Engr., Georgia Institute of Technology, Atlanta, GA 30332-0405

[X] **Check if Continued Funding is Requested**

Please include the following information:

1. Brief summary of progress to date and work to be performed during the succeeding period;
2. Statement of funds estimated to remain unobligated --if more than 20%-- at the end of the period for which NSF currently is providing support (not required for participants in the Federal Demonstration Project);
3. Proposed budget for the ensuing year in the NSF format, only if the original award letter did not indicate specific incremental amounts or if adjustments to a planned increment exceeding the greater of 10% or $10,000 are being requested;
4. Current information about other research support of senior personnel, if changed from the previous submission;
5. Any other significant information pertinent to the type of project supported by NSF or as specified by the terms and conditions of the grant;
6. A statement describing any contribution of the project to the area of education and human-resource development, if changed from any previous submission; and
7. Updated information on animal care and use, Institutional Biohazard Committee and Human Subject Certification, if changed substantially from those originally proposed and approved.

I certify that to the best of my knowledge (1) the statements herein (excluding scientific hypotheses and scientific opinions) are true and complete, and (2) the text and graphics in this report as well as any accompanying publications or other documents, unless otherwise indicated, are the original work of the signatories or individuals working under their supervision. I understand that the willful provision of false information or concealing a material fact in this report or any other communication submitted to NSF is a criminal offense (U.S. Code, Title 18, Section 1001.)

P.I. Signature: Ari Glezer

NSF Form 1328 (1/94)

CONTROL OF NATURAL CONVECTION ALONG A HEATED, INCLINED PLATE

Annual Progress Report

Sept 1993 - Sept 1994

NSF Grant CST-9318332

Ari Glezer

G. W. Woodruff School of Mechanical Engineering

Georgia Institute of Technology

I. Introduction

The research work performed under NSF Grant CST-9318332 is concerned with active control of the onset, evolution, and breakdown to turbulence of streamwise vortices in a free convection boundary layer along a heated inclined surface.

The study of thermally-driven boundary layer flows owes much of its importance to engineering applications in passive (nonmechanical) surface cooling technologies (ranging from electronic packages to nuclear reactors), and chemical vapor deposition processes (e.g., in fabrication of microelectronic and optical components). These flows may become buoyantly unstable on inclined surfaces and lead to the appearance of longitudinal (streamwise) vortices (rolls) having their axes aligned in the streamwise direction. Because the appearance of these vortices is accompanied by significant changes in transport phenomena near the surface, active control of their onset and evolution can become a powerful tool for the manipulation of various measures of performance (such as heat transfer or surface deposition) in free convection boundary layer flows of practical interest. To this end, the proposed research focuses on the effect of active control on the origin and evolution of the streamwise vortices in a flat plate boundary layer along an inclined heated surface.

The onset and development of free convection boundary layers along heated inclined surfaces was studied experimentally both for constant-temperature surfaces by Sparrow and Husar (1969) and Lloyd and Sparrow (1970), and for constant heat flux surfaces by Shaukatullah and Gebhart (1978). The appearance of streamwise vortices was first observed by Sparrow and Husar who used a Thymol-blue technique for flow visualization. In this technique an acidic solution is changed into a basic solution by a proton transfer process occurring at a negative electrode. Concomitantly with the pH change, the color of the (clear) solution becomes deep blue. Sparrow and Husar also showed that at large angles of inclination, neighboring vortices merge prior to break up to turbulence.

Lloyd and Sparrow (1970) showed that free convection flat plate boundary layers become unstable in two different modes depending on the vertical inclination angle α. When the plate is nearly vertical (i.e., $\alpha < 14^{o}$), the instability is in the form of transverse traveling waves. However, when α exceeds 17^{o} the instability leads to the formation of the longitudinal vortices previously observed by Sparrow and Husar. The critical Rayleigh number for the onset of these instabilities decreases from $Ra = 10^{9}$ for $\alpha = 0^{o}$ to 10^{6} at $\alpha = 60^{o}$. Lloyd (1974) found that the critical spanwise wavelength of the vortices is independent of the angle of inclination, but that it varies with the temperature difference between the plate and the bulk fluid. Lloyd et al. (1972) used a mass transfer technique to

illustrate spanwise concentration variation along an inclined plate. Shaukatullah and Gebhart (1978) carried out detailed temperature and velocity surveys along an inclined constant heat flux plate. Their results were qualitatively similar to those of Sparrow and his coworkers for a constant-temperature plate.

The present experiments differ substantially from previous work in this area in that instability modes will be *externally excited and controlled.* External excitation of isolated instability modes allows for direct comparison with theoretical results. Moreover, the use of such excitation has also proven to be a powerful tool for control of flow instabilities and, in particular, for their suppression or enhancement as was demonstrated by Liepmann et al. (1982) for Tollmien-Schlichting waves in a flat plate Blasius boundary layer. The development of similar control methodology for the suppression and enhancement of flow instabilities in free convection boundary layers is important in a number of practical applications. For example, in chemical vapor deposition processes it is desirable to suppress flow instabilities in order to achieve deposition uniformity. On the other hand, in applications involving passive cooling such as in electronic packaging, it is important to exploit flow instabilities in order to enhance heat transfer by promoting earlier transition to turbulent convection. Thus active control of these instabilities is the focus of the present investigation.

II. Progress Report

The experiments under the present grant will be conducted in water, and the flow instabilities leading to the formation of the streamwise vortices will be manipulated using novel heating actuators embedded in the surface of a submerged test surface. The experiments will be conducted in a water tank measuring 107 cm on the side. The flat-plate model is shown schematically in Figure 1 . The test surface will be 61 cm wide and 66 cm long and will rest on an insulated substrate, hinged along its span to a submerged base. The work during the first year of the grant was primarily focused on the design and construction of the water tank and the flat plate model.

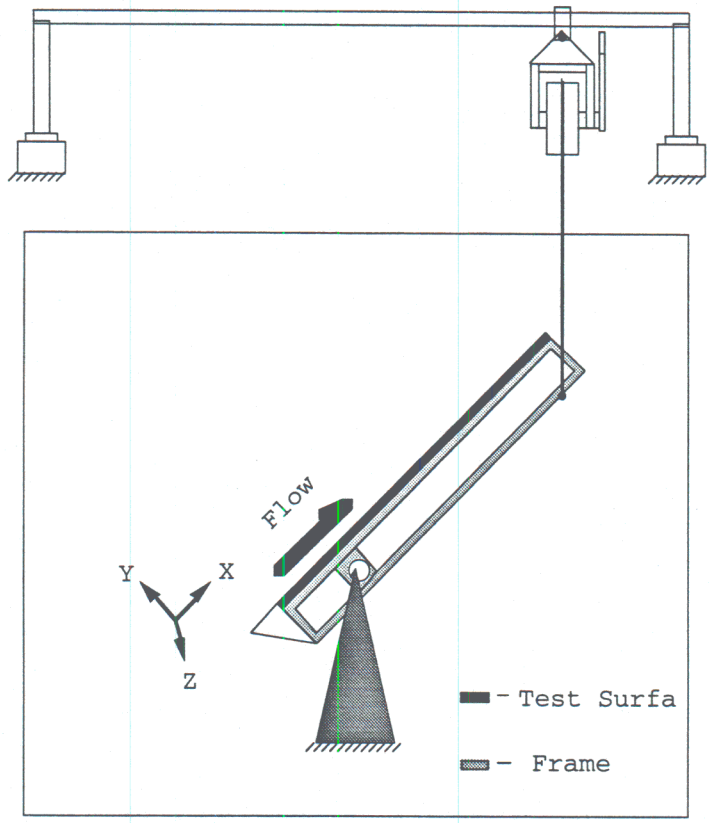

Fig.

II.1 Heated test surface

The test surface (measuring 61 cm x 61 cm) will be operated in a constant heat flux mode using a resistive heating of a 0.0254 mm thick Inconel 600 foil (having a nominal resistance of 0.04 Ω) with controlled current injection. The heater foil is connected to spanwise electrodes along its upstream and downstream edges. The electrodes are built into the support structure and will provide the nominal current necessary for constant heat flux operation of the surface. Flow instabilities will be excited or suppressed by current

injection into a rectangular grid of nodes (each cell measuring 2.5 x 5 cm) where each node is a wire that is soldered to the surface from below and passes through the ceramic substrate. Control will be effected by the injection or removal of current from the surface using a bank of 36 DC amplifiers (one for each node) that can be directly controlled from the laboratory computer. Rayleigh numbers in excess of 10^{14} will be achieved. The spanwise width of the surface is equivalent to over 100 wavelengths of the spanwise instability that leads to the formation of streamwise vortices.

The Inconel foil is bonded to a 1.25 cm thick mica-glass ceramic substrate plate flat to within ±0.1 mm that has a maximum continuous operating temperature of 400°C, thermal conductivity of 0.001 cal-cm/(sec-cm^2-°C), volume resistivity of $10^{12}\,\Omega \bullet cm$, and high resistance to water absorption. The mechanical properties of this material are similar to acrylic and it is machinable using standard carbide tooling. The bonding process is carried out in a press using a TFP (Teflon) sealing film at moderate temperature and pressure (330°C and 100 psi). During the bonding process, the active submerged surface of the heater is also coated with a 0.02 mm thick TFP film for electrical isolation from the surrounding water. The surface coating is necessary to prevent electrolysis due to the voltage drop along the foil and thus the formation of bubbles that may disrupt the flow on the surface.

The test surface is instrumented with two linear arrays of equally spaced (2.5 cm) miniature chromel-constantan thermocouples at z = 30.5 cm , and x =10.25 cm. The thermocouples are attached to the underside of the Inconel sheet with a thermally conductive epoxy and the wires are connected through 0.03 cm holes in the ceramic substrate. The thermocouple measurements will be used to measure the streamwise variation of the surface temperature and to verify spanwise uniformity. It is anticipated that for increasing levels of heat flux, the spanwise rows will provide temperature measurements for the laminar, transitional and turbulent regimes of free convection boundary layers. The thermocouple sensors will be used extensively in the control experiments and for calculations of the heat transfer from the surface.

The underside of the ceramic substrate is thermally insulated using a 2.5 cm thick extruded polystyrene plate (ρ = 35 kg/m^3, k = 0.029 W/m-K). The low thermal mass and conductivity of the insulation material allows for minimal heat losses through the underside of the ceramic, so that once steady state conditions are reached, virtually all the heat flux from the test surface is conducted to the adjacent fluid.

II.2 Control Methodology

In the present experiments, controlled excitation will be effected using a novel heating actuation technique whereby current is injected or removed from a rectangular grid of control nodes in a resistive heating foil using a dedicated DC amplifier. Control of the surface heat flux by localized current sourcing or sinking at the nodal points leads to corresponding localized changes in current density and thus to *incremental localized heating or cooling of the surface* relative to the time-invariant constant heat flux (which determines the flow's Rayleigh number). Thus, this technique allows, in effect, for the introduction of three-dimensional vorticity perturbations into the flow boundary layer by exploiting the dependence of the viscosity on temperature (Liepmann et al. 1982).

The inherently fast response time of film heating actuators and current injection coupled with the fact that the current density at each node is controlled by a dedicated DC amplifier, allows for complex spatial and temporal heat flux waveforms to be generated at the test surface. The heat flux excitation is in essence reconfigurable on the fly from the laboratory computer through a D/A interface to the control amplifiers.

The feasibility of current control in a thin foil has been demonstrated in a simulation that is based on elements of electromagnetic theory. For a thin conducting sheet, time invariant or quasi time invariant voltage potential Φ of the sheet satisfies the two dimensional Laplace equation

$$\frac{\partial^2 \Phi}{\partial x^2} + \frac{\partial^2 \Phi}{\partial y^2} = 0$$

The restriction concerning the time invariance is a result of the coupling between magnetic and electric field under dynamic conditions. This field coupling could not be described by the homogeneous Laplace equation and would require a solution of Maxwell's equation. For the purpose of the simulation, only quasi steady electric fields will be produced by the voltage potential on the foil and thus this coupling need not be considered.

The current density and the heat flux at a position x and y can be obtained by the following relationships:

$$j_i = \sigma \frac{\partial \Phi}{\partial x_i} \tag{1}$$

$$q''(x,y) = \sigma\left(\sum_{i=1}^{2} \left(\frac{\partial \Phi}{\partial x_i}\right)^2_{x,y}\right) \tag{2}$$

Where j_i is the current density in the i direction, σ is the electrical conductivity of the metal foil, and q" is the heat flux at any location on the foil.

Equation 1 can easily be solved analytically for the rectangular foil in the absence of current injection at the nodal points. However, the presence of singular points of current injection (or sinking) makes the use of a finite difference solution of the foil potential more practical. In the simulation, a prescribed voltage distribution was set across the nodes of the numerical mesh. Note that the mesh nodes correspond to the actual control nodes of the test foil. By altering the values of the mesh nodes, the resulting potential of all other points can be determined. The solutions to several voltage distributions have been provided to demonstrate the versatility of obtainable heat flux patterns of the proposed control scheme.

In each of the five examples presented in figure 2, a constant voltage drop is maintained between the top and bottom edges of the mesh. In Figure 2a, an the voltage at the center row of nodes is slightly increased and a spanwise-regular array of hot spots results from the increase in current density around the perturbed nodes with respect to the unperturbed voltage distribution. In each of the remaining four cases (Figures 2b-e) the pattern of voltage perturbations introduced in the numerical mesh was varied to demonstrate the flexibility of this powerful excitation technique in synthesis of complex surface heating peturbations. Of particular note is the capability of this methodology to introduce local heat flux that is can be higher or lower than the unperturbed surface heat flux.

II.3 Manufacturing Process of Test Surface

The test surface is constructed in several stages, a brief outline of the procedure is given below.

The hole pattern for the control nodes and thermocouples is drilled into the ceramic substrate using carbide tooling, and slots for cables and strain relief are milled into the backside of the ceramic using CNC machines. Thermocouples are embedded in the substrate so that their sensing elements are flush with the foil side (before the foil is bonded) using a special high-temperature, thermally conductive epoxy. This allows for a polishing of the ceramic substrate, before the bonding of the heater foil.

The Inconel foil and layers of TFP are then placed onto the ceramic, and pressed using a flat metal plate. The control nodes are soldered using a 95% Ag 5% Cd solder having liquidus temperature of 390^{o}C which is above the bonding temperature (330^{o}C). The nodes are soldered to the foil from the backside of the ceramic *before* the bonding process because this results in a smoother surface.

The composite package is then placed in a Wabash high-pressure high-temperature press available at Georgia Tech. The press has controllable loading of up to 50 tons and a

Normalized Heat Flux
On Heated Test Surface
(Planform View)

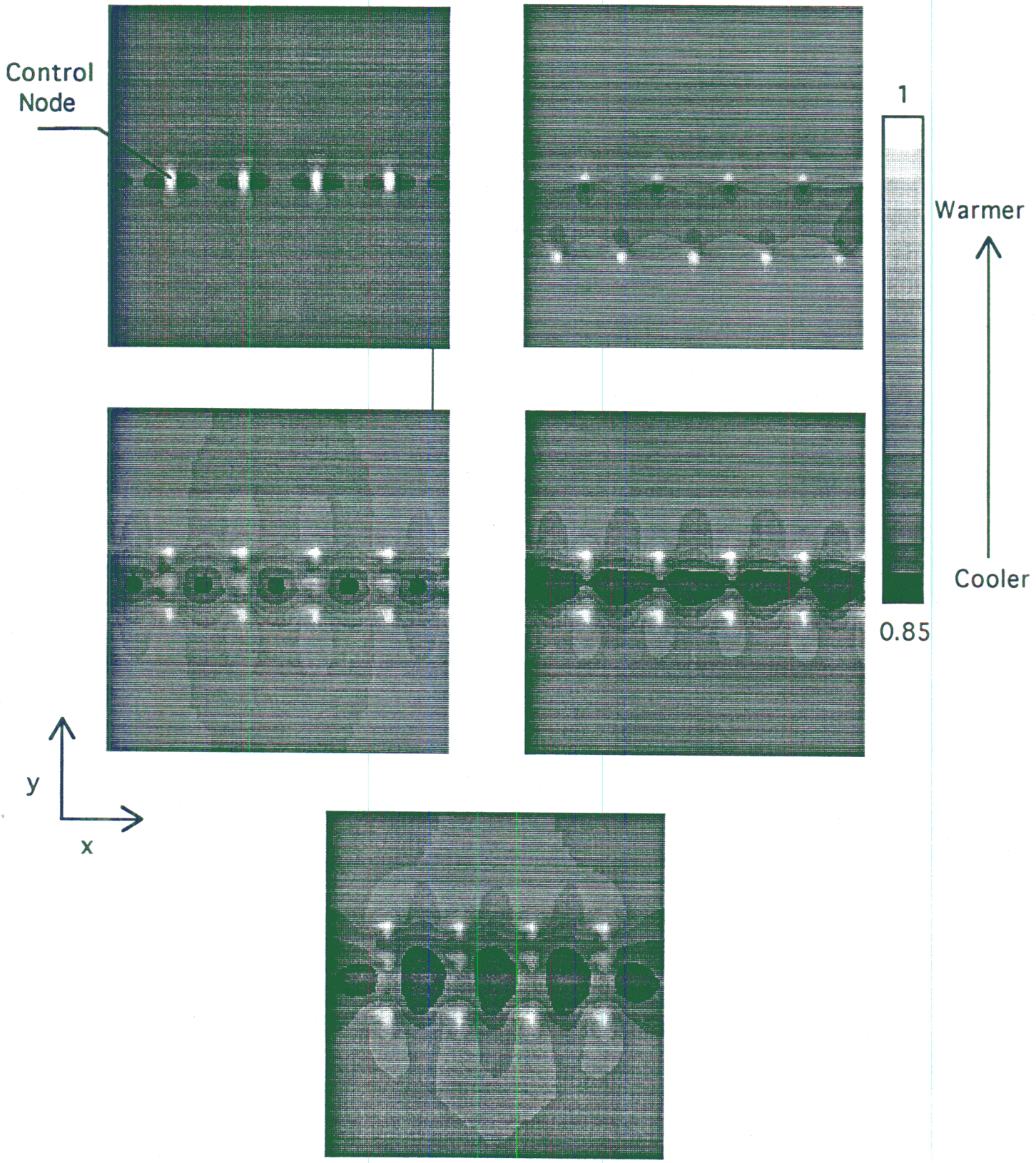

Fig. 2

maximum temperature of 1000°C. The bonding of the test surface is carried out at 1000 lbf at 330°C for 2 hours. This ensures the complete melting and strong adhesion of the TFP film to the foil and to the ceramic substrate. The result of this process is a smooth flat plate, instrumented with thermocouples and control nodes for flow actuation.

II.4 Test Surface Housing

The heated test surface assembly forms the top cover of a shallow, sealed, water-tight box having rectangular cross sections in the planform and vertical planes. The container is constructed around an inner frame measuring 61 cm x 61 cm x 9.5 cm as shown in Figure 3 and houses the heated surface assembly (described above) and the wiring for surface instrumentation. The prevention of water leaks into the container and the stainless steel tube that is a conduit for the wires was an important design consideration because the current that will be necessary to heat the test surface will exceed 100 A. In order to minimize deflections of the test surface owing to the hydrostatic pressure differential across the top and bottom surfaces of the heater plate, the test surface assembly is internally supported at regularly-spaced locations. The two side walls of the container in the streamwise direction extend 10 cm above the test surface and serve as endplates to reduce edge effects on the buoyancy-driven flow. The leading edge section is flush with the test surface and is designed to fix the upstream stagnation point, to deflect part of the buoyancy-driven flow to the underside of the container and to provide a known unheated upstream section for the test surface. This assembly forms a flat, smooth surface from the leading edge to the trailing edge for boundary layer development.

The test surface housing rests on and rotates about the centerline of a stainless steel tube (that also serves as a wire conduit) that is supported by the two side windows of the tank. The angle of inclination of the test surface α is continuously adjustable between 0^o and 90^o using a cable and pulley system that is driven by a stepper motor.

II.5 Tank

A water tank constructed of a stainless steel frame and four removable acrylic side windows was been designed and constructed for the purpose of the present experiments. The design drawings for the tank are shown in Figures 4. The frame is constructed of welded sections of 3" x 3" x 1/4" stainless steel angle and the windows are attached using standard 1/2" UNC studs that are welded around the perimeter of the frame. Each of the four identical square windows (measuring 105 cm on the side) is made of 2.5 cm thick acrylic sheet and can be easily removed from the frame. The flat plate model is attached to

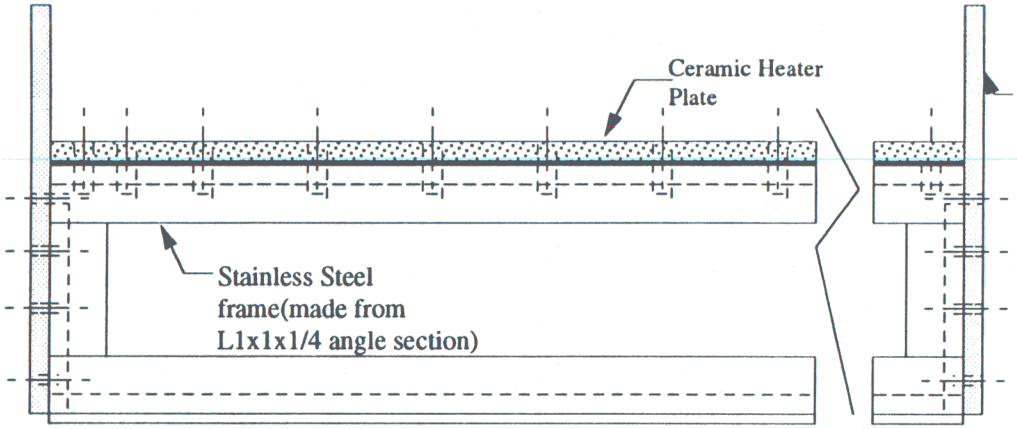

Fig. 3

Test Surface Frame:

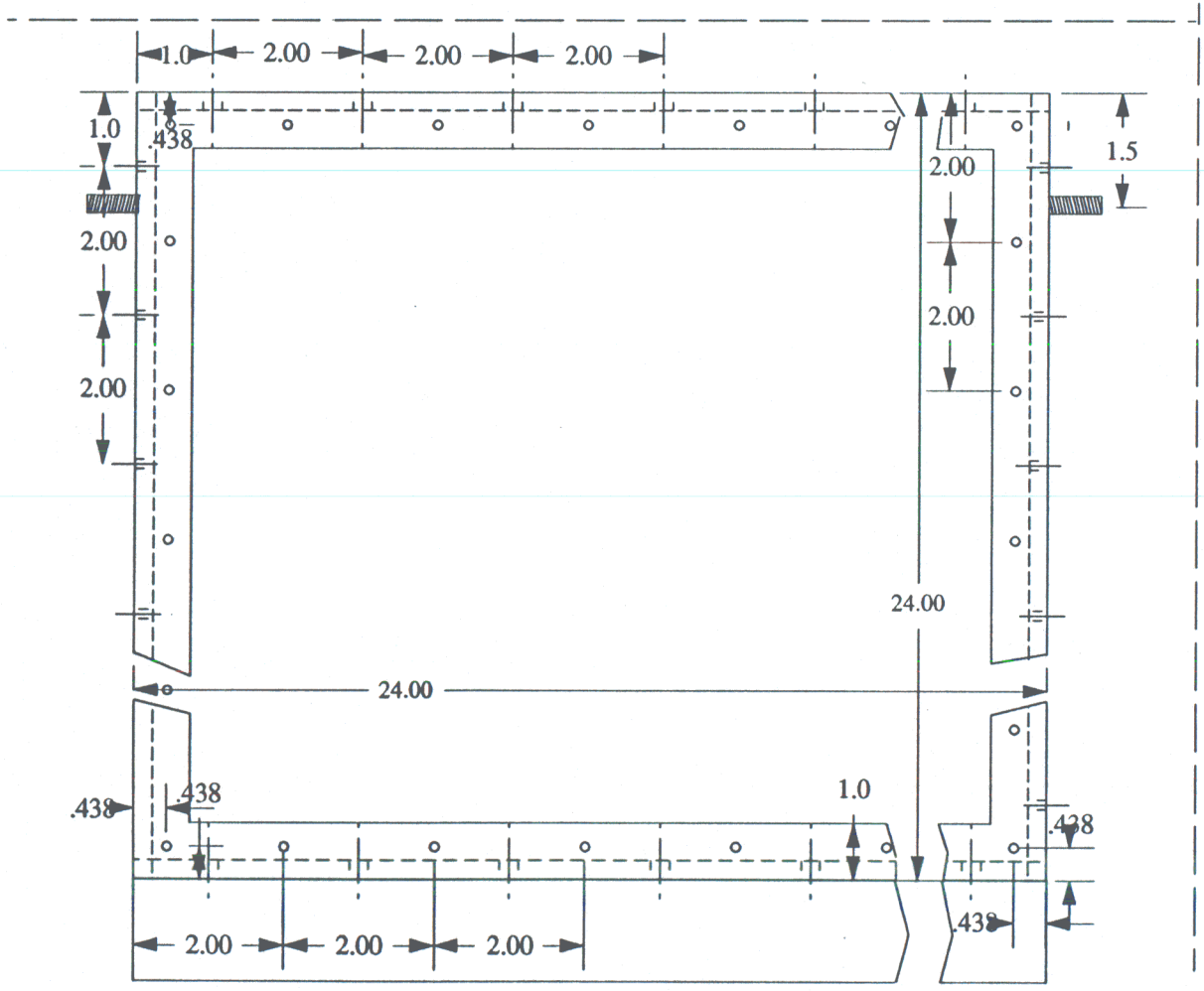

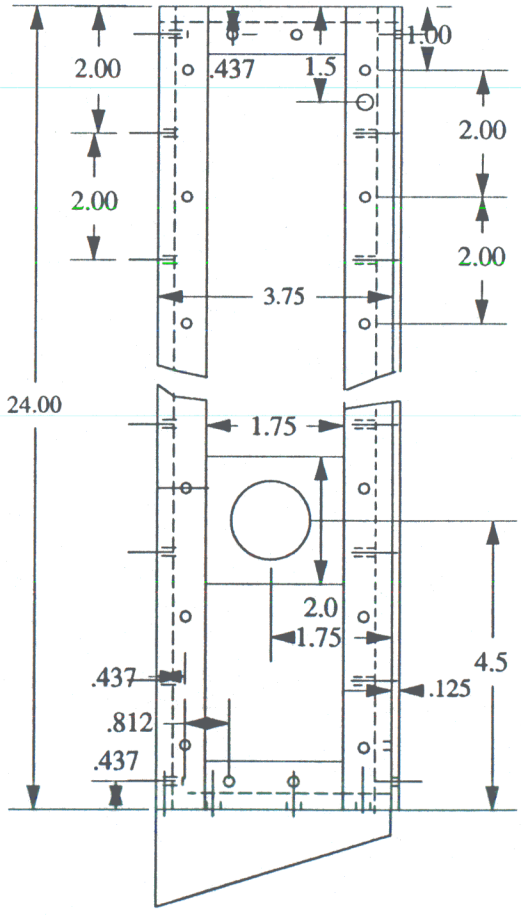

Water Tank Test Facility

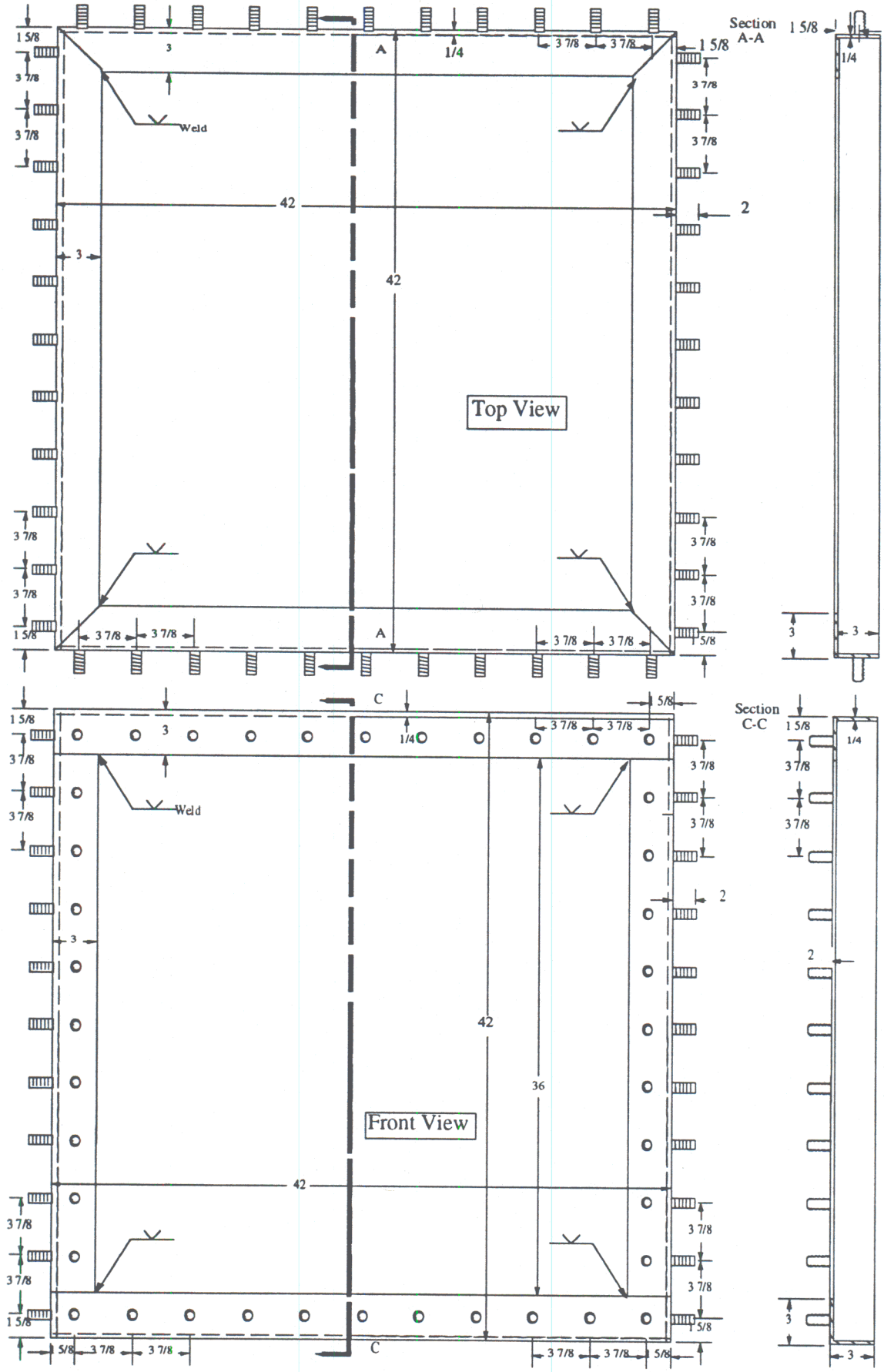

Fig. 4

a 2.5 cm stainless steel tube that is mounted on the windows using special brackets and Swagelock fittings that allow for tilting of the plate.

The present tank is designed to be considerably larger than tanks in previous investigations (e.g., Shaukatullah and Gebhart 1978) to allow for longer experiments before the ambient temperature stratification becomes substantial. It is estimated that experimental runs as long as 25 minutes can be attained before a significant bulk temperature gradient arises (0.05°C/cm). The tank will be equipped with a recirculating pump that will allow for cooling and filtering of the working liquid. Once the experimental hardware is operational, the possibility of extending the test time by cooling the liquid near the free surface will be investigated. It is noted however, that the addition of a heat exchanger at the free surface will give rise to a buoyancy driven circulation within the tank and thus alter the natural convection flow over the surface.

The tank is equipped with an off line circulation and filter system and an auxiliary storage tank. The water in the main tank can be cooled using a circulation heat exchanger which is connected to the laboratory's chilled water system.

II.5 Instrumentation

II.5.1 DC Power Amplifiers

A 36-channel power amplifier unit has been built to supply the current to the control nodes of the test surface. The key component of these units is the LM12 CL/K power op amp capable of driving ±35V at ±10A. Larger currents are obtained by connecting a number of these devices in parallel. Each device is mounted on a common heat sink that are cooled by fans. Power is supplied by two Brute Series 1200 W high power-adjustable DC power supplies manufactured by Adtech Power.

The output current of the amplifiers is voltage controlled by a sensing circuit that allows for computer control of the current distribution to the test surface.

II.5.2 Main Power Supply

The projected maximum heat flux density for the present experiments is 0.2 W/cm^2 (the foil resistivity is $\rho = 1\text{x-}6\,\Omega \bullet m$, its length and thickness are 61 cm and 0.0254 cm, respectively, and thus its resistance is approximately 0.04 Ω). Thus, the main power supply that will provide the base current to the foil should be capable of delivering 130 A at 6 Volts (2 of HP6260B-027 10V @ 100A CV/CC power supply).

II.5.3 Thermocouple Sensors

Surface temperature measurements will be made with 0.0254 cm type E thermocouples embedded in the ceramic substrate. The thermocouples are constructed in house using an existing argon environment thermocouple welder. The measurements are taken using a Fluke 2190A digital thermometer which is connected to two Fluke 2300A scanners scanners. The composite system allows for the continuous monitoring of up to 20 thermocouples with a resolution of 0.1°C.

II.5.4 Multi-Channel Cold Wire Thermometer

Time-dependent temperature distributions will be made using rakes of up to 32 miniature cold-wire sensors. We will construct two types of rakes for measurements along the y-axis (y-rake) and along the z-axis (z-rake) at a given y elevation above the test surface. The sensors will be made of 10 μm platinum wire welded to a pair of stainless steel prongs 1 mm apart. In the y-rake, the sensors will be closely spaced to allow for detailed measurements within the thermal boundary layer. In the z-rake, the spacing of the sensors will be dictated by the spanwise spacing of the longitudinal vortices and will correspond to approximately 6-7 sensors per vortical structure. The rakes will be mounted on a sting, which will be traversed in the y and z directions using a computer-controlled two-axis small traverse that will be mounted on rails along each side of the tank. The ancillary electronics have already been constructed and the technology for the construction of such rakes that are suitable for use in water has been developed. The present rakes have a temperature resolution of 0.03° C and frequency response of at least 1 kHz. The temperature data will be sampled by a dedicated laboratory computer via an A/D interface, which will also be used for data processing. The same computer will generate the excitation waveform for the control node actuators via a D/A.

Global and planform distributions of heat flux from the test surface to the adjacent fluid will be calculated from our experimental data. The global heat transfer will be computed from measurements of the total power input to the Inconel foil. (The insulated substrate is designed so that virtually all of the heat flux from the test surface will be into the adjacent fluid after an initial transient period.) Planform distributions of heat flux will be calculated from temperature gradients at the test surface (these gradients will be available from detailed measurements of cold-wire temperature distributions normal to the test surface). Of particular interest is the incremental change in heat transfer compared to the unforced flow.

III. Statement of Work for Year II

III.1 Calibration Runs

- Complete construction of the heated test surface.
- The uniformity of temperature distribution of the constant-heat flux test surface will be checked using the embeded thermocouple probes.
- Spanwise uniformity of temperature distribution of the constant-heat-flux test surfaces will also be checked.
- The x and y velocity components will be measured at a number of spanwise and streamwise stations using the LDV system.
- The spanwise uniformity of the velocity field of each plate will be verified at subcritical Rayleigh numbers.

III.2 Experiments

- The onset and evolution of the longitudinal vortices in the unforced thermal boundary layer will be compared with results from previous investigations.
- The formation and evolution of longitudinal vortices will be studied using a time-invariant forcing program.
- Excitation waveforms having various spanwise wavelengths will be studied and compared with the theory and with the unforced flow.
- The stability experiments will be conducted at a number of subcritical and supercritical Ra numbers (at different inclination angles).
- The controlled excitation used in the stability experiments will employed.
- An array of surface sensors will measure temperature and shear stress disturbances upstream of the formation of the streamwise vortices.

References

Godaux, F., Gebhart, B. "An Experimental Study of the Transition of Natural Convection Flow Adjacent to a Vertical Surface," *Int. J. Heat Mass Transfer*, **17**, 93-107, 1974.

Gebhart, B., "Natural Convection Flow, Instability and Transition," *J. Heat Transf.*, **18**, 293-309, 1969.

Knowles, C.P., Gebhart, B. , "The Stability of the Laminar Natural Convection Boundary Layer," *J. Fluid Mech.*, **34**, 657-686, 1968.

Liepmann, H. W., Brown, G. L. , and Nosenchuck, D. M. "Control of Laminar-Instability Waves using a New Technique," *J. Fluid Mech.*, **118**, 187-200, 1982.

Lloyd, J. R., Sparrow, E. M., and Eckert, E. R. G., "Laminar, Transition and Turbulent Natuaral Convection Adjacent to Inclined Vertical Surfaces," *Int. J. Heat Mass Transfer*, **15**, 457-473, 1972.

Merkin, J.H., "The Effect of Bouyancy Forces on the Boundary-Layer Flow over a Semi-Infinite Vertical Flat Plate in a Uniform Free Stream," *J. Fluid Mech.*, **35**, 439-450, 1969.

Sparrow, E.M., Gregg, J.L., "Laminar Free Convection From a Vertical Plate with Uniform Surface Heat Flux," *Trans. ASME*, 435-440, 1956.

Sparrow, E.M., Tsou, F.K.,Kurtz, E.F., "Stability of Laminar Free-Convection Flow on a Vertical Plate," *Phys. Fluids*, **8**, 1559-1561, 1965.

Shankatullah, E. M. and Gebhart, B., "An Experimental Investigation of Natural Convection Flow Over and Inclined Surface," *Int. J. Heat Mass Trans.*, **21**, 1481-1490, 1978.

CONTROL OF NATURAL CONVECTION ALONG A HEATED, INCLINED PLATE

NSF GRANT CST-9318332

ANNUAL PROGRESS REPORT

Sept 1994 - Sept 1995

submitted by

Ari Glezer
Woodruff School of Mechanical Engineering
Georgia Institute of Technology

I. INTRODUCTION

The research work performed under NSF Grant CST-9318332 is concerned with active control of the onset, evolution, and breakdown to turbulence of streamwise vortices in a free convection boundary layer along a heated inclined surface.

The study of thermally-driven boundary layer flows owes much of its importance to engineering applications in passive (non-mechanical) surface cooling technologies (ranging from electronic packages to nuclear reactors), and chemical vapor deposition processes (e.g., in fabrication of microelectronic and optical components). These flows may become buoyantly unstable on inclined surfaces and lead to the appearance of longitudinal (streamwise) vortices (rolls) having their axes aligned in the streamwise direction. Because the appearance of these vortices is accompanied by significant changes in transport phenomena near the surface, active control of their onset and evolution can become a powerful tool for the manipulation of various measures of performance (such as heat transfer or surface deposition) in free convection boundary layer flows of practical interest. To this end, the proposed research focuses on the effect of active control on the origin and evolution of the streamwise vortices in a flat plate boundary layer along an inclined heated surface.

The onset and development of free convection boundary layers along heated inclined surfaces was studied experimentally both for constant-temperature surfaces by Sparrow and Husar (1969) and Lloyd and Sparrow (1970), and for constant heat flux surfaces by Shaukatullah and Gebhart (1978). The appearance of streamwise vortices was first observed by Sparrow and Husar who used a Thymol-blue technique for flow visualization. In this technique an acidic solution is changed into a basic solution by a proton transfer process occurring at a negative electrode. Concomitantly with the pH change, the color of the (clear) solution becomes deep blue. Sparrow and Husar also showed that at large angles of inclination, neighboring vortices merge prior to break up to turbulence.

Lloyd and Sparrow (1970) showed that free convection flat plate boundary layers become unstable in two different modes depending on the vertical inclination angle α. When the plate is nearly vertical (i.e., $\alpha < 14^o$), the instability is in the form of transverse traveling waves. However, when α exceeds 17^o the instability leads to the formation of the longitudinal vortices previously observed by Sparrow and Husar. The critical Rayleigh number for the onset of these instabilities decreases from $Ra = 10^9$ for $\alpha = 0^o$ to 10^6 at $\alpha = 60^o$. Lloyd (1974) found that the critical spanwise wavelength of the vortices is independent of the angle of inclination, but that it varies with the temperature difference between the plate and the bulk fluid. Lloyd et al. (1972) used a mass transfer technique to illustrate spanwise concentration variation along an inclined plate. Shaukatullah and Gebhart (1978) carried out detailed temperature and velocity surveys along an

inclined constant heat flux plate. Their results were qualitatively similar to those of Sparrow and his coworkers for a constant-temperature plate.

The present experiments differ substantially from previous work in this area in that instability modes will be *externally excited and controlled*. External excitation of isolated instability modes allows for direct comparison with theoretical results. Moreover, the use of such excitation has also proven to be a powerful tool for control of flow instabilities and, in particular, for their suppression or enhancement as was demonstrated by Liepmann et al. (1982) for Tollmien-Schlichting waves in a flat plate Blasius boundary layer. The development of similar control methodology for the suppression and enhancement of flow instabilities in free convection boundary layers is important in a number of practical applications. For example, in chemical vapor deposition processes it is desirable to suppress flow instabilities in order to achieve deposition uniformity. On the other hand, in applications involving passive cooling such as in electronic packaging, it is important to exploit flow instabilities in order to enhance heat transfer by promoting earlier transition to turbulent convection. Thus active control of these instabilities is the focus of the present investigation.

II. EXPERIMENTAL APPARATUS AND DIAGNOSTICS

The experiments are conducted in a water tank using a submerged flat plate model (Figure 1). Flow instabilities leading to the formation of streamwise vortices are manipulated using a mosaic of novel surface heating actuators. The experimental hardware was specifically designed and constructed for the purpose of the present investigation. The water tank measures 107 cm on the side and the test surface is 66 cm long and 61 cm wide (i.e., approximately 100 wavelengths of the spanwise instability that leads to the formation of streamwise vortices), and is attached to an insulated substrate, hinged along its span to the sidewalls of the tank.

II.1 Heated Test Surface

The test surface is operated in a constant heat flux mode by a square mosaic of surface film heaters that is comprised of three identical segments each measuring 20 x 56 cm in the spanwise (z) and streamwise (x) directions, respectively (Figure 2a). The heater mosaic was designed in house and was fabricated by Minco. Each segment of the mosaic contains 32 streamwise-serpentined 40 Ω copper-nickel film elements (Figure 2b). Each element is 0.64 cm wide and 56 cm long, and the spanwise spacing between adjacent elements is 0.64 cm. Equally-spaced (.64 cm apart) node pads for external wiring (Figure 2c) allow for controlled addition or subtraction of current between any two nodes. The heating elements of each mosaic segment are laminated between two sheets of kapton each 0.0076 cm thick. The three segments of the heater mosaic are bonded side by side to a 1.25 cm thick mica-glass ceramic substrate plate that is flat to within ±0.1 mm and has a maximum continuous operating temperature of 400°C, thermal conductivity of 0.001 (cal-cm)/(sec-cm^2-°C), volume resistivity of $10^{12}\Omega \bullet cm$, and high resistance to water absorption. The mechanical properties of this material are similar to acrylic and it is machinable using standard carbide tooling. The bonding process is carried out in a press using an acrylic laminate at moderate temperature and pressure (180°C and 100 psi). The ceramic substrate was pre-drilled with access holes to the heaters nodes and for instrumentation with thermocouples.

All streamwise heating elements are connected to common spanwise electrodes along their upstream and downstream ends. These electrodes provide the nominal current that is necessary for constant heat flux operation of the surface. Rayleigh numbers in excess of 10^{14} can be achieved. Flow instabilities can be excited or suppressed by external addition or subtraction of current along heater segments that are 1.3, 3.0, 4.3, 7.3, 8.5, 9.8 cm long using pre-wired nodes. Each node is wired from below through the ceramic substrate and any number of nodes can be externally connected to achieve a desired spatial pattern. Current is added or subtracted using a bank of 32 amplifiers that can be directly controlled from the laboratory computer.

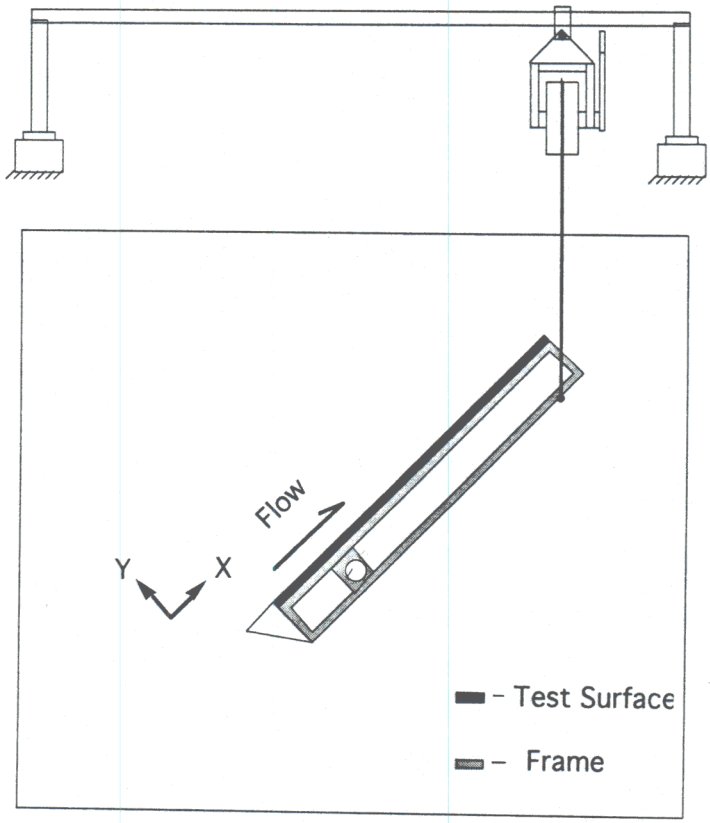

Fig. 1

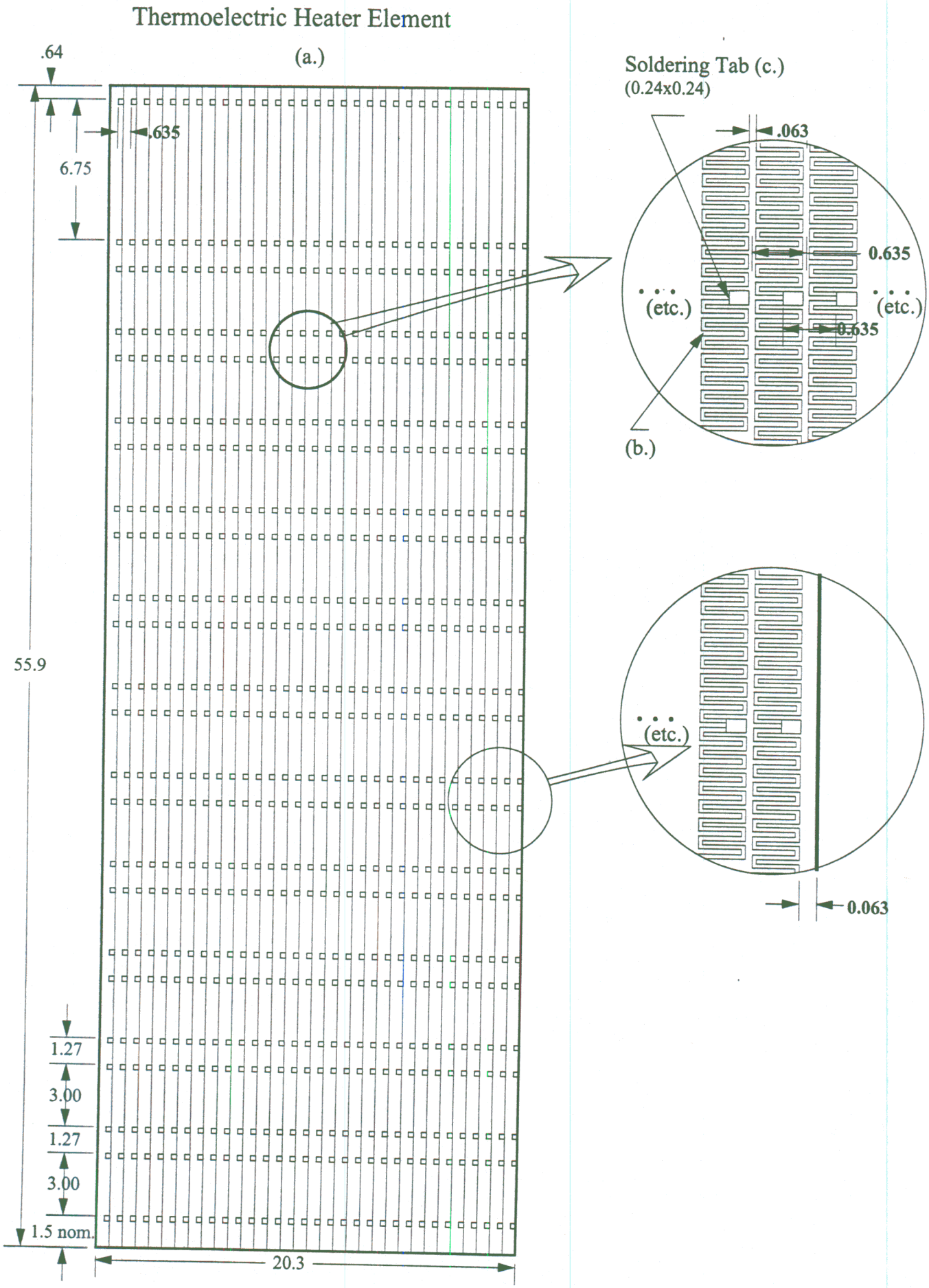
Thermoelectric Heater Element
(a.)
.64
.635
6.75
55.9
1.27
3.00
1.27
3.00
1.5 nom.
20.3
Soldering Tab (c.)
(0.24x0.24)
.063
0.635
(etc.)
(etc.)
0.635
(b.)
(etc.)
0.063

Fig. 2

The test surface is also instrumented with linear streamwise (at z = 0, plate centerline) and spanwise (at x = 10.25 cm) arrays of equally-spaced (2.5 cm apart) miniature chromel-constantan thermocouples. The thermocouples are attached to the underside of the heater with a thermally conductive epoxy and the wires are connected through 0.03 cm holes in the ceramic substrate. The thermocouples are used to measure the streamwise variation of the surface temperature and to verify spanwise uniformity. It is anticipated that for increasing levels of heat flux, the spanwise rows will provide temperature measurements for the laminar transitional and turbulent regimes of free convection boundary layers.

II.2 Test Surface Housing

The heated test surface assembly forms the top cover of a shallow, sealed, water-tight box having rectangular cross sections in the planform and vertical planes. The container is constructed around an inner frame measuring 61 cm x 61 cm x 9.5 cm (Figure 3) and houses the heated surface assembly (described above) and the wiring for surface instrumentation. The prevention of water leaks into the container and the stainless steel tube that is a conduit for the wires was an important design consideration because the current that will be necessary to heat the test surface can exceed 40 A. The two side walls of the container in the streamwise direction extend 10 cm above the test surface and serve as endplates to reduce edge effects on the buoyancy-driven flow. The leading edge section is flush with the test surface and is designed to fix the upstream stagnation point, to deflect part of the buoyancy-driven flow to the underside of the container and to provide a known unheated starting length. This assembly forms a flat, smooth surface from the leading edge to the trailing edge for boundary layer development.

The test surface housing rests on and rotates about the centerline of a stainless steel tube that is supported by the two side windows of the tank. The angle of inclination of the test surface α is continuously adjustable between 0° and 90° using a cable and pulley system.

II.3 Tank

A water tank constructed of a stainless steel frame and four removable acrylic side windows was designed and constructed for the purpose of the present experiments (Figures 4). The frame is constructed of welded sections of 3" x 3" x 1/4" stainless steel angle and the windows are attached using standard 1/2" threaded studs that are welded around the perimeter of the frame. Each of the four identical square windows (measuring 105 cm on the side) is made of 2.5 cm thick acrylic sheet and can be easily removed from the frame. The flat plate model is attached to a 2.5 cm stainless steel tube that is mounted on the windows using special brackets and fittings that allow for tilting of the plate.

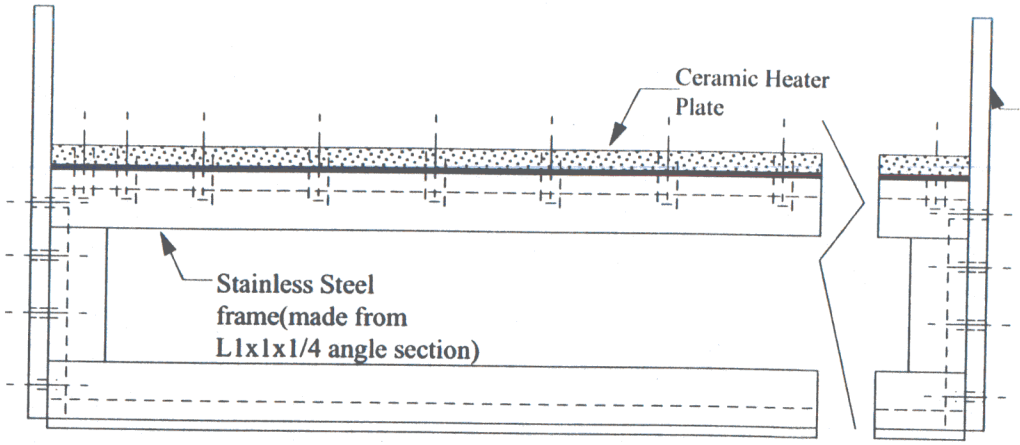

Fig. 3

Test Surface Frame:

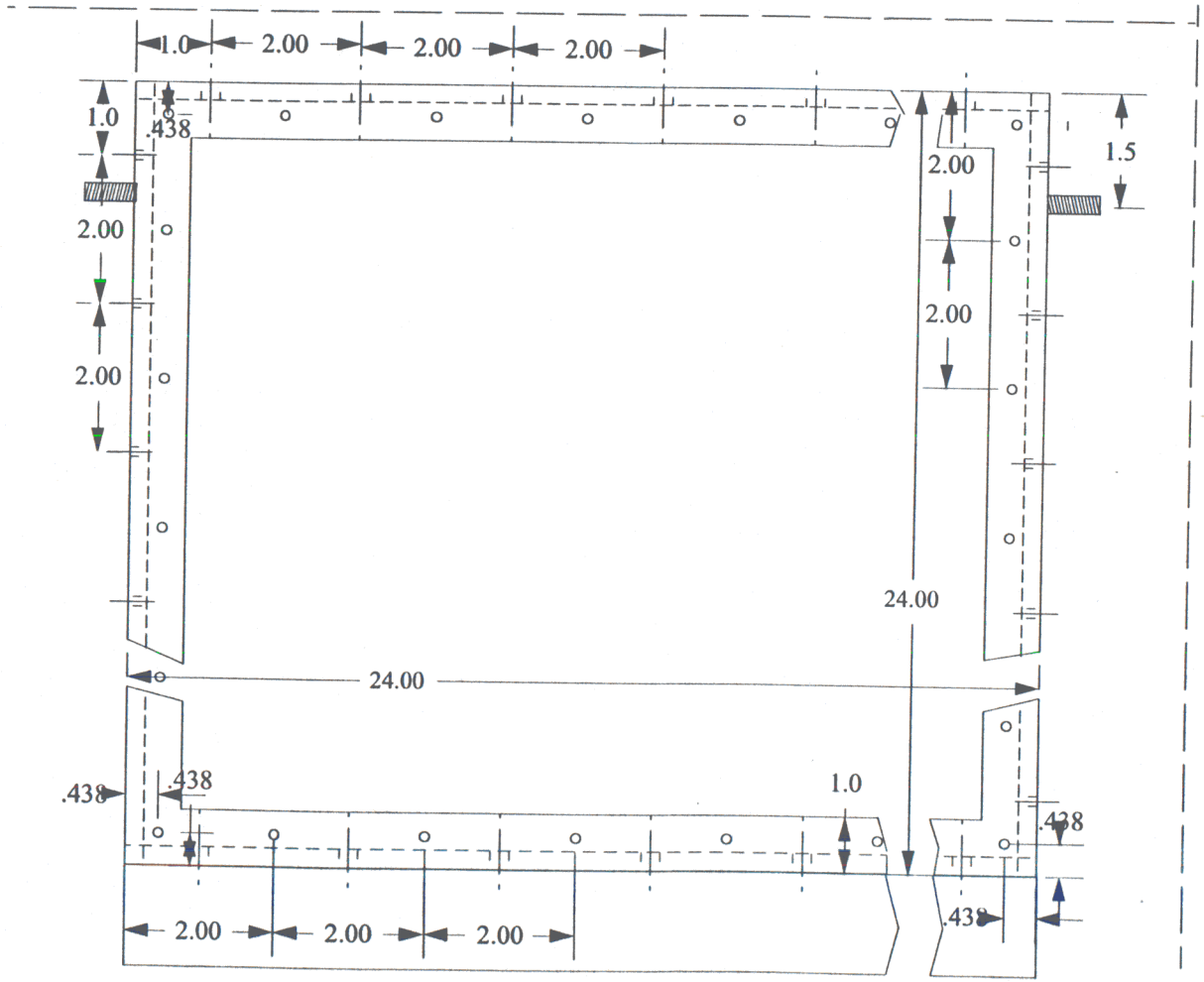

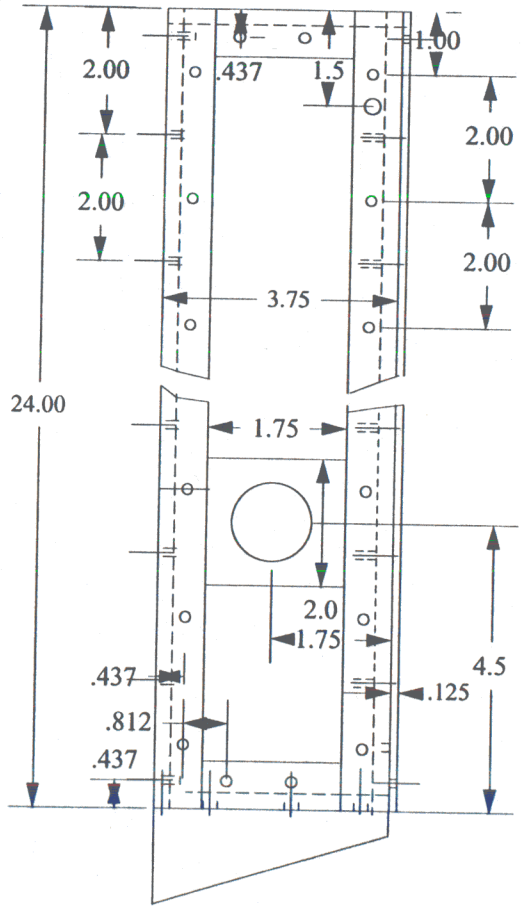

Water Tank Test Facility

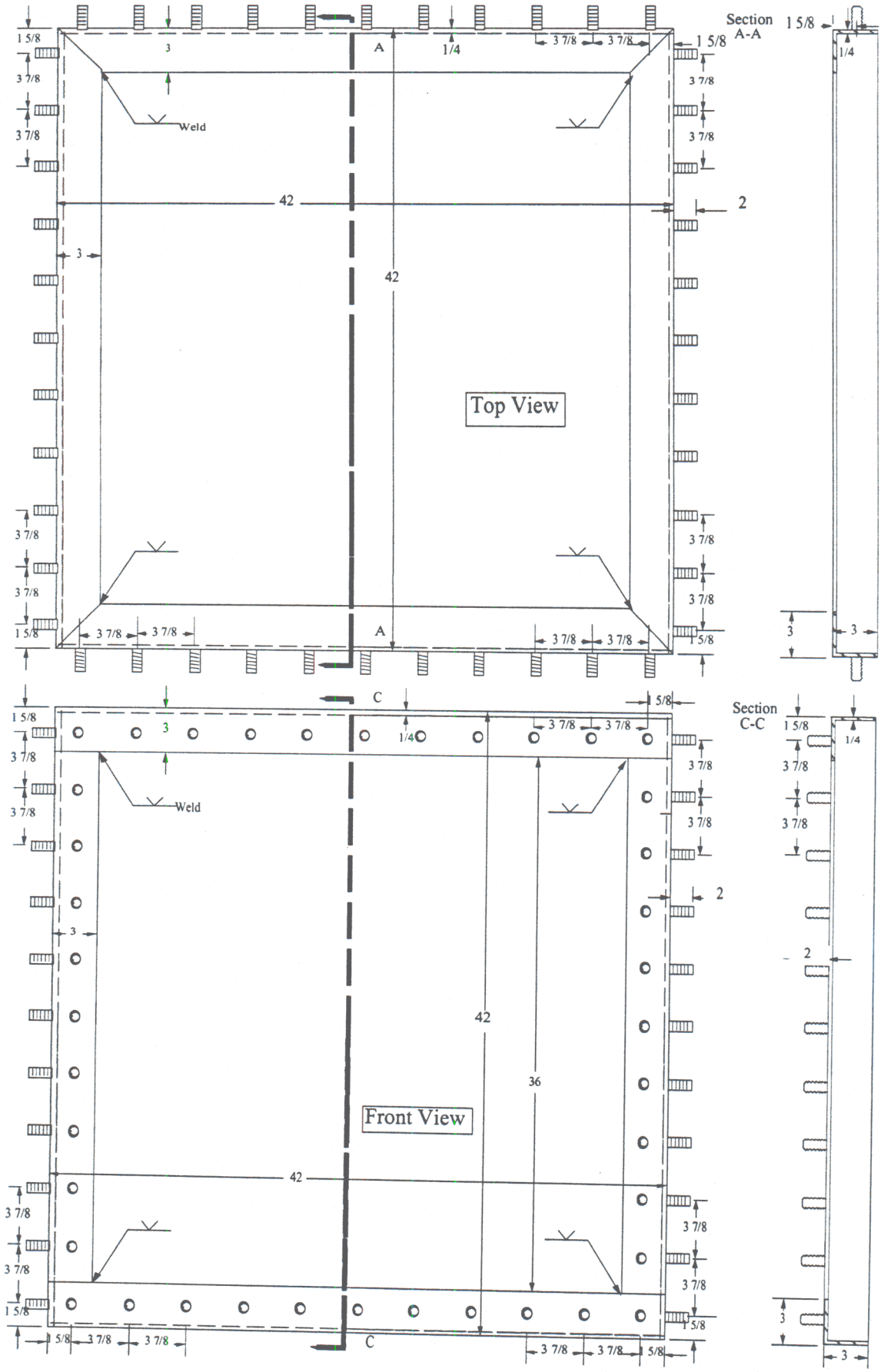

Fig. 4

The present tank is designed to be considerably larger than tanks that were used in previous investigations (e.g., Shaukatullah and Gebhart 1978) to allow for longer experiments before the ambient temperature stratification becomes substantial. Experimental runs in excess of 45 minutes can be attained before a significant bulk temperature gradient arises (0.05°C/cm). The tank is equipped with a recirculating pump that allows for cooling and filtering of the working liquid. The tank is equipped with an auxiliary storage tank. The water in the main tank can be cooled using a circulation heat exchanger which is connected to the laboratory's chilled water system.

II.4 Manufacturing Process of Test Surface

The hole pattern for the control nodes and thermocouples are drilled into the ceramic substrate using carbide tooling, and slots for cables and strain relief are milled into the backside of the ceramic using a milling machine. Thermocouples are embedded in the substrate so that their sensing elements are flush with the heater side (before the heater is bonded) using a special high-temperature, thermally conductive epoxy. This allows for a polishing of the ceramic substrate, before the bonding of the heater foil.

The heater mosaics and acrylic laminate are then placed onto the ceramic, and pressed using a flat metal plate. The control nodes are soldered using a standard SN60PB40 solder having liquidus temperature which is above the laminating temperature (180°C). The nodes are soldered to the soldering tabs of the heater from the backside of the ceramic *before* the laminating process because this results in a smoother surface.

The composite package is then placed in a Wabash high-pressure high-temperature press available at Georgia Tech. The press has controllable loading of up to 50 tons and a maximum temperature of 1000°C. The bonding of the test surface is carried out at 50 tons at 180°C for 30 minutes. This ensures complete lamination and strong adhesion of the acrylic film to the heater and to the ceramic substrate. The result of this process is a smooth flat plate, instrumented with thermocouples and control nodes for flow actuation.

II.5 Instrumentation

II.5.1 Power Amplifiers

A 32-channel power amplifier unit was built to supply the current to the control nodes of the test surface. Each channel can source or sink 1 A, which is enough to introduce the desired spatial and temporal disturbances into the base flow. Larger currents could be obtained by connecting a number of these devices in parallel. The output current of the amplifiers is voltage controlled by a sensing circuit that allows for computer control of the current distribution to the test surface. The input and output of the 32 channels are electrically isolated from each other by using input isolation amplifiers and individual transformer on each channel. Thus, the current output of

any amplifier does not affect other elements of the heater mosaic. In particular, actuators on the same streamwise heater segment can be independently activated.

II.5.2 Main Power Supply

The maximum heat flux density for the present experiments is 4000 W/m^2. A Hewlett Packard CC/CV 6269B DC power supply (0-40V 0-50A) provides the base power to achieve this heat flux level.

II.5.3 Flow Visualization

A double-pass shadowgraph system was constructed for flow visualization studies (Figure 5). The optical system consists of a fiber optic light source, a beam splitter, a lens having a focal length of 61 cm , and a thin (0.025 cm) stainless steel reflective surface that is in good thermal contact with the test surface. The shadowgraph images are recorded using a low light hi-resolution 1/2" 811 x 510 CCD camera. The optical components are mounted on a 1m optical rail that is attached to a Quickset tripod. Thus, the optical system can be tilted and rotated so that the optical axis is normal to the test surface, and traversed vertically along the projected streamwise direction of the flow. Spanwise motion of the optical system is achieved using a Velmex slider having 8" travel. This set up allows for quick alignment of the shadowgraph system over a wide range of test surface inclination angles.

II.5.4 Thermocouple Sensors

Surface temperature measurements are made using a 0.0254 cm type E thermocouples embedded in the ceramic substrate. The thermocouples are constructed in-house using an existing argon environment thermocouple welder. The measurements are taken using a Fluke 2190A digital thermometer which is connected to a pair of Fluke 2300A scanners. The composite system allows for the continuous monitoring of up to 20 thermocouples with a resolution of 0.1°C.

II.5.5 Multi-Channel Cold Wire Thermometer

Time-dependent temperature distributions will be made using rakes of up to 32 miniature cold-wire sensors. We will construct two types of rakes for measurements along the y-axis (y-rake) and along the z-axis (z-rake) at a given y elevation above the test surface. The sensors will be made of 10 μm platinum wire welded to a pair of stainless steel prongs 1 mm apart. In the y-rake, the sensors will be closely spaced to allow for detailed measurements within the thermal boundary layer. In the z-rake, the spacing of the sensors is dictated by the spanwise spacing of the longitudinal vortices and corresponds to approximately 6-7 sensors per vortical structure. The rakes will be mounted on a sting, which will be traversed in the y and z directions using a

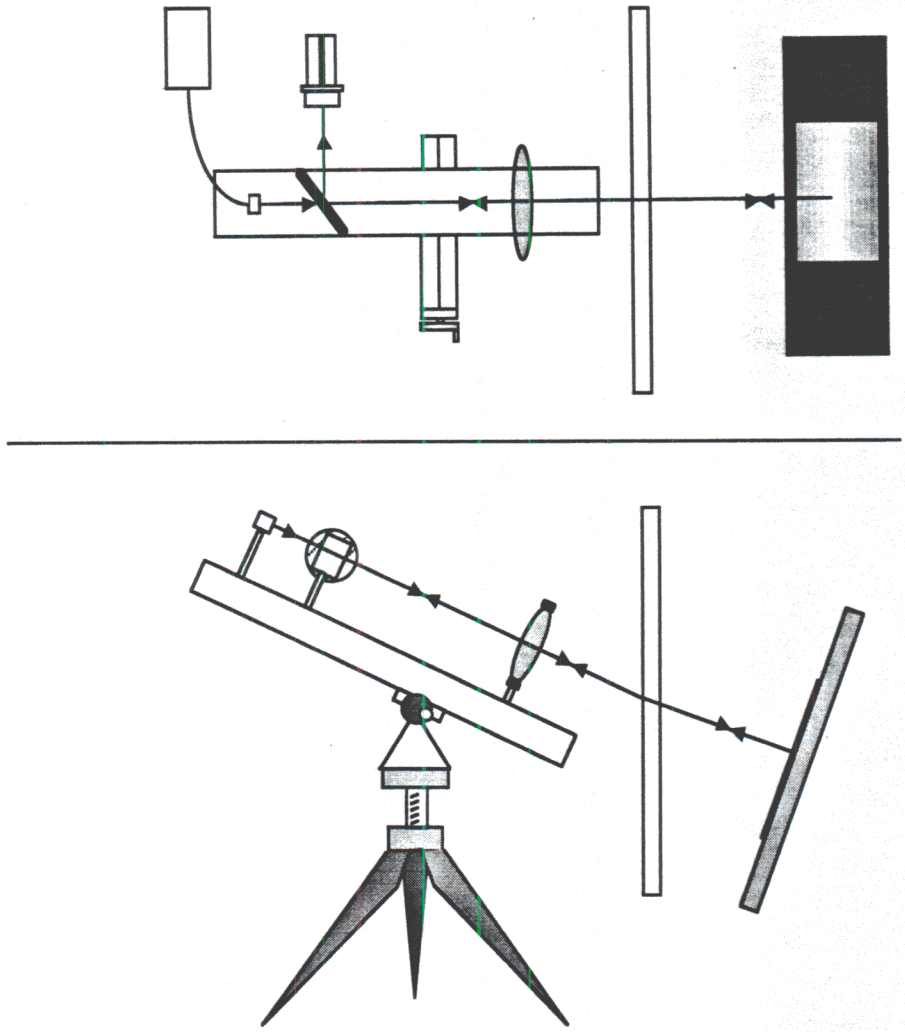

Shadowgraph System

Fig. 5

computer-controlled two-axis small traverse that will be mounted on rails along each side of the tank. The ancillary electronics have already been constructed and the technology for the construction of such rakes that are suitable for use in water has been developed. The present rakes have a temperature resolution of 0.03° C and frequency response of at least 1 kHz. The temperature data will be sampled by a dedicated laboratory computer via an A/D interface, which will also be used for data processing. The same computer generates the excitation waveform for the control node actuators via a D/A.

Global and planform distributions of heat flux from the test surface to the adjacent fluid will be calculated from our experimental data. The global heat transfer will be computed from measurements of the total power input to the heater mosaic. (The insulated substrate is designed so that virtually all of the heat flux from the test surface is into the adjacent fluid after an initial transient period.) Planform distributions of heat flux will be calculated from temperature gradients at the test surface (these gradients will be available from detailed measurements of cold-wire temperature distributions normal to the test surface). Of particular interest is the incremental change in heat transfer compared to the unforced flow.

II.5.6 Thermochromic Liquid Crystal

Distributions of surface temperatures will be measured using Thermochromic Liquid Crystal (TLC) . A calibration procedure for TLC is currently being developed by submerging sample TLC sheets in a thoroughly mixed heated water tank. The tank is allowed to cool down while it is continuously mixed. The temperature of the water is measured using a platinum RTD. A color CCD camera equipped with a polarizing filter is used to record the color image such that its optical axis is normal to the plane of the TLC sheet. (Because the color of the TLC image depends on the viewing angle, the camera cannot be moved.) Polarized white light co-aligned with the camera is used to illuminate the TLC sheet. The two polarizing filters create a cross polarized viewing system which enhances the signal to noise ratio by increasing the amount of circularly polarized light that is reflected from the TLC relative to the background light.

The CCD image is digitized on the laboratory computer and the dependence of color on illumination intensity is removed in software using a *Lab* color model introduced by the Commision Internationale d'Eclairage. Lab color consists of Luminance (L), and two chromatic components (a) and (b) which range from green to red and blue to yellow respectively. Since illumination intensity is decoupled from the color components, this color model is well suited for a color based measurement system. It is anticipated that a temperature resolution of 0.2 °C can be achieved with this system.

III EXPERIMENTAL RESULTS

In the present experiments, excitation is effected using a novel heating actuation technique whereby control current is added or subtracted locally from the baseline, time-invariant current that sets the Rayleigh number of the base flow by surface heating. The localized addition or subtraction of the control current through a rectangular grid of nodes of the streamwise heating elements leads to localized increase or decrease in heat flux and surface temperature. Thus, this technique allows, in effect, for the introduction of three-dimensional vorticity perturbations at the flow boundary by exploiting the dependence of the buoyancy force and viscosity on temperature (e.g., Liepmann et al. 1982).

The inherently fast response time of film heating actuators and current injection coupled with the fact that the current density at each node is controlled by a dedicated amplifier, allows for the synthesis of complex spatial and temporal heat flux distributions at the test surface. Furthermore, heat flux excitation is in essence reconfigurable on the fly from the laboratory computer through a D/A interface to the control amplifiers. It is anticipated that feedback from the system will be obtained from global surface temperature measurements using Thermochromic Liquid Crystals (TLC). Temperature distributions within the flow will be measured using cold wire sensors and temperature sensitive dyes.

III.1 Theoretical Considerations

The governing equations for laminar, natural convection along an inclined plate are:

$$\nabla \cdot \mathbf{V} = 0,$$

$$\frac{\partial \mathbf{V}}{\partial t} + \mathbf{V} \cdot \nabla \mathbf{V} = -\frac{1}{\rho} \nabla p - \mathbf{g}\beta(T - T_\infty) + \nu \nabla^2 \mathbf{V} \ ,$$

and

$$\frac{\partial T}{\partial t} + \mathbf{V} \cdot \nabla T = \alpha \nabla^2 T.$$

The vorticity equation is obtained by taking the curl of the momentum equation

$$\frac{\partial \Omega}{\partial t} + \mathbf{V} \cdot \nabla \Omega - \Omega \cdot \nabla \mathbf{V} = \beta \mathbf{g} \times \nabla T + \nu \nabla^2 \Omega,$$

The streamwise (x) component of the vorticity equation is:

$$\frac{D\Omega_x}{Dt} - (\Omega_x \frac{\partial u}{\partial x} + \Omega_y \frac{\partial u}{\partial y} + \Omega_z \frac{\partial u}{\partial z}) = -\beta g \sin\theta \frac{\partial T}{\partial z} + \nu \nabla^2 \Omega_x$$

At the wall (y = 0) this equation becomes:

$$\frac{\partial \Omega_x}{\partial t} = -\beta g \sin\theta \frac{\partial T}{\partial z} + \nu \nabla^2 \Omega_x$$

Thus, the magnitude and sign of the streamwise vorticity at the wall depend on the spanwise temperature gradient. Therefore, it is anticipated that naturally occurring or forced streamwise vorticity can be cancelled by generating vorticity of opposite sign at the wall. If the change of viscosity with temperature is significant, then this equation can be modified:

$$\frac{\partial \Omega_x}{\partial t} = -\beta g \sin\theta \frac{\partial T}{\partial z} + \nu \nabla^2 \Omega_x - \frac{\partial \nu}{\partial T} \frac{\partial T}{\partial z} \frac{\partial^2 v}{\partial y^2}$$

Thus, even without the influence of a normal force, streamwise vorticity can be generated if the change of viscosity with temperature is substantial or the spanwise temperature gradient is large enough.

III.2 Evolution of Instability Modes

It has been observed (e.g., Lloyd and Sparrow ,1970) that the inclination angle of the plate leads to three distinct instability modes of the flow. When the plate is nearly vertical (i.e., α < 14°), the instability is in the form of transverse traveling waves. When α exceeds 17°, the instability leads to the formation of the longitudinal vortices (Sparrow and Husar, 1969). The intermediate region is unstable to both modes.

III.2.1 Streamwise Vorticity Seeding

Figure 6 is a reproduction of a neutral stability curve from Haaland and Sparrow (1973) for streamwise vortex instabilities. In order to determine the experimental neutral stability curve, the modified Grashof number Gr and the disturbance wavenumber α must be varied independently. With a given disturbance wavelength, the generalized wavenumber α is varied while keeping Gr constant by changing the heat flux q" and the streamwise location of the disturbance.

Although Lloyd and Sparrow (1970) did not observe streamwise vortices for inclination angles smaller than 14°, the present experiments have demonstrated that streamwise vortices are

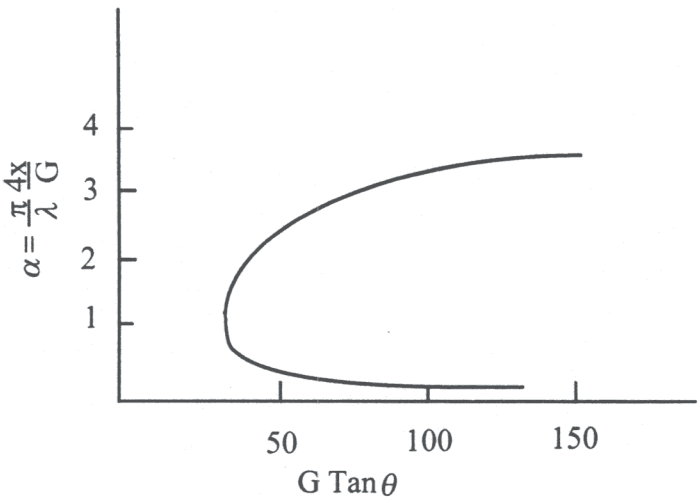

Fig. 6

easily triggered at inclination angles as small as 5° at high enough heat flux. This is a direct consequence of the ability to directly force spanwise temperature gradients that lead to the development of streamwise vorticity and thus allows for the determination of the neutral stability curve for the formation of streamwise vortices. To the best of our knowledge, the experimental determination of this instability mode has not been undertaken by other investigators and will be an important component of the present work.

The evolution of streamwise vortices is investigated using a row of 32 actuators each realized by a 0.64 cm wide heater segment measuring 4.3 cm in the streamwise direction and centered at x = 3 cm. Each actuator has three possible states, namely "heating" (H), "cooling" (C), or "neutral" (N). The "heating" and "cooling" states result from local addition and subtraction of current, respectively, from the base current that is used to heat the surface to the base heat flux. Note that "heating" and "cooling" correspond to local heat flux densities that are higher or lower than the base heat flux density. At the "neutral" state, the base heat flux is unchanged.

A typical shadowgraph image of the base flow for an inclination angles of 13° and $q"=1100 w/m^2$ is shown in Figure 7a. The field of view is square, measuring approximately 7.5 cm on the side, and is centered at midspan (z = o) and x = 20 cm. The upstream edge of the reflective surface is located 0.5 cm downstream from the trailing edge of the actuator row. The textured background results from imperfections in the finish of the reflective metal surface. The image in Figure 7a shows that within this streamwise domain, the base flow is nominally 2-D and that streamwise vortices are absent.

Figures 7b-g show the effect of excitation with six different excitation waveforms and demonstrate that time-invariant, spanwise-nonuniform excitation leads to the formation of streamwise vortices at virtually any spanwise wavelength that can be synthesized by the actuators. Actuation is achieved by setting given actuators to H, while keeping the rest of the actuators at N (as indicated in the figure). The spanwise temperature gradients that are induced by the heated actuators result in the formation of streamwise vortices that are depicted by dark streamwise bands. The shadowgraph images suggest that once a vortex is formed, it persists and grows as it is convected downstream.

Figures 8a-g were taken at an inclination angle θ = 25°, and $q"=2100 w/m^2$. Unlike the flow conditions in Figure 7, at this inclination angle the small spanwise temperature gradient between adjacent heaters leads to the formation of streamwise vortices at the spanwise wavelength of the streamwise heaters suggesting that at these flow conditions, this spanwise wavelength is within the neutral stability for 3-D disturbances. Figure 8a shows the base state and indicates incipient pairing of the streamwise vortices farther downstream. The shadowgraph image suggests that the streamwise vortices are stronger than in Figures 7b-g because the buoyancy force normal to the plate is larger.

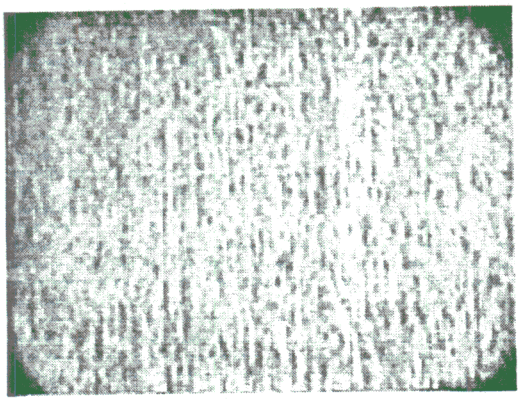

a.

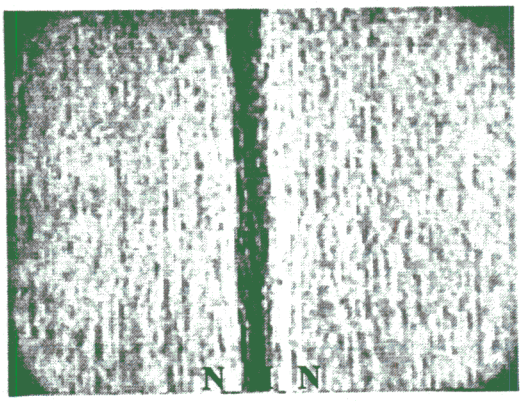

b.

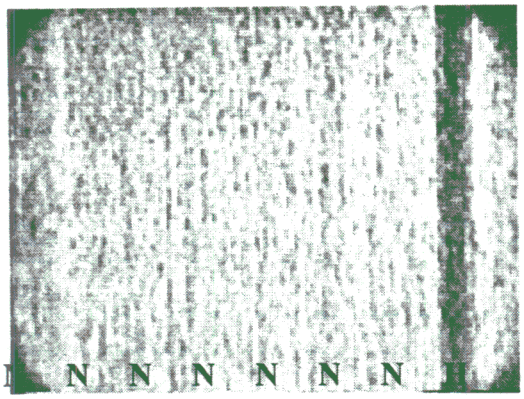

c.

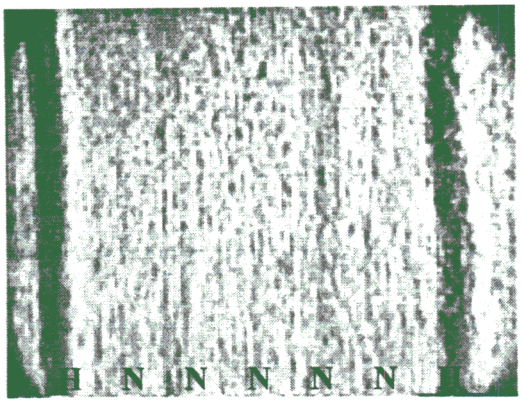

d.

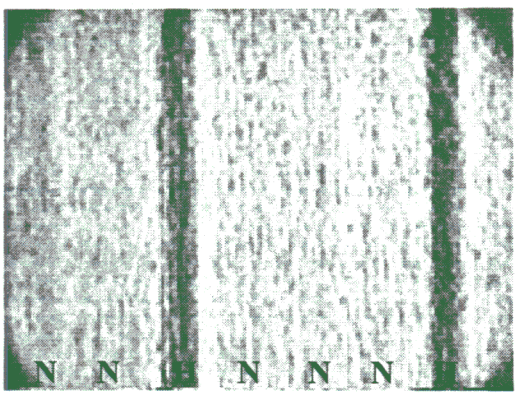

e.

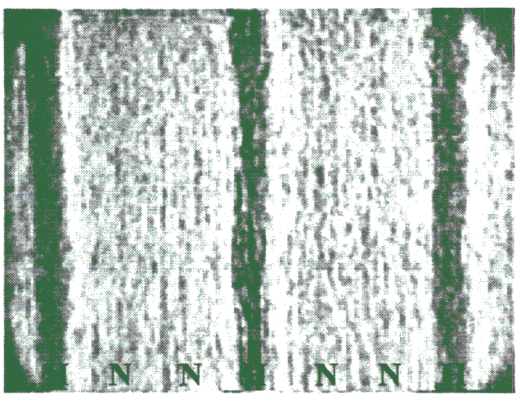

f.

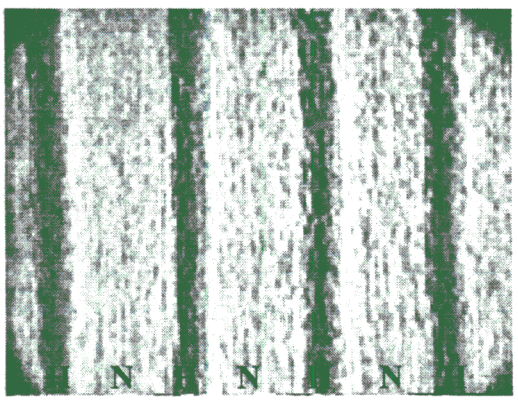

g.

Fig. 7

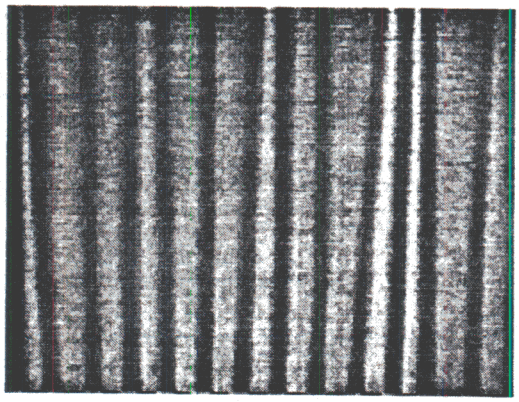

a.

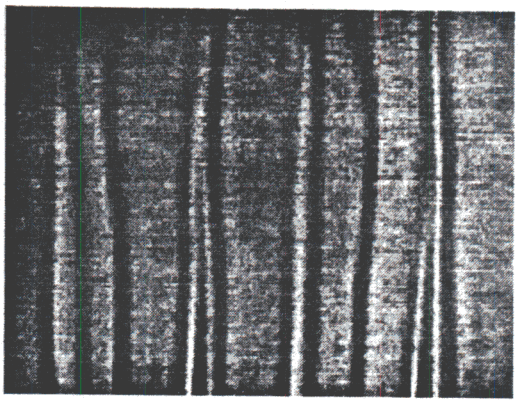

b.

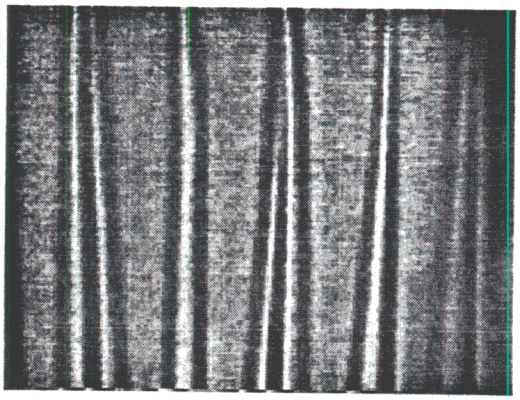

c.

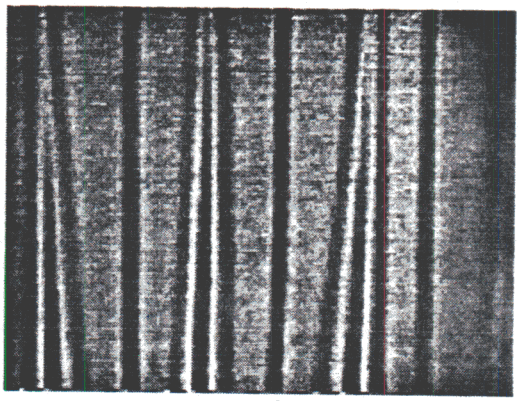

d.

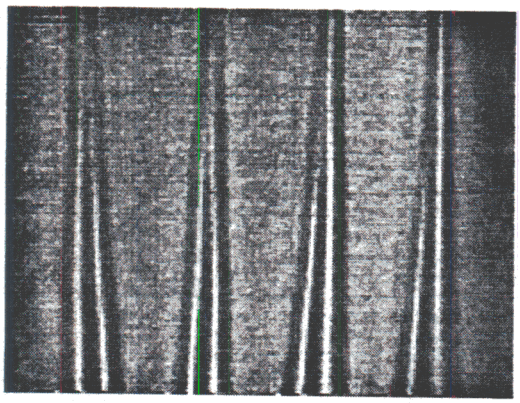

e.

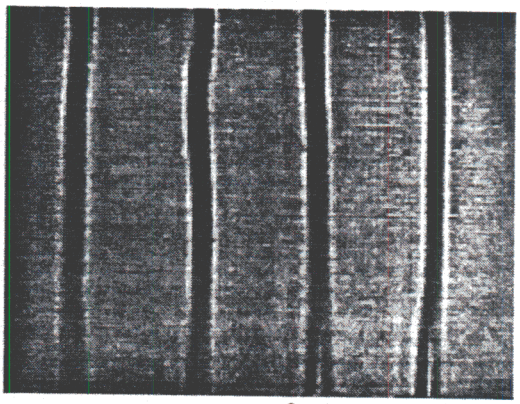

f.

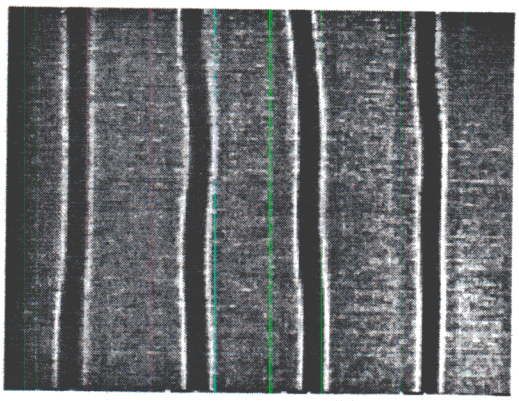

g.

Fig. 8

Sparrow and Husar (1968) observed vortex pairing at large angles of inclination (i.e. 35°). Although not directly stated, it could be seen from their work that the phenomenon of vortex pairing depended on the plate inclination angle. It is noteworthy that spanwise pairing can substantially affect heat transfer from the surface because, at high angles of inclination, transition to turbulence proceeds through the pairing process. The present investigation has shown that natural vortex pairing does not occur for inclination angles smaller than 20° for heat flux levels below 5500w/m^2. However, by implementing a time invariant forcing pattern on the base flow, a variety of merging patterns can be realized at inclination angles and heat flux levels that are substantially lower than in previous observations with important effects on the plate heat transfer.

Figures 8b-8g show the effect of deliberate spanwise nonuniform temperature gradient that is imposed on the flow that is already "seeded" with streamwise vortices at the spanwise wavelength of the heater elements. Each actuator apparently induces an additional streamwise vortex that attracts adjacent vortices already present in the flow and promotes spanwise pairing. In Figure 8b every sixth heater is activated and leads to grouping of three, two and single streamwise vortices. In Figure 8c, every fifth heater is activated and the result is groups of only three and two streamwise vortices. Activating every fourth heater, results in groups of three separated by single vortices (Figure 8d). Forcing with every third heater, leads to groups of three vortices (Figure 8e) when the shadowgraph system is translated in the streamwise direction it is shown that each group of three vortices merges into a single stable vortex farther downstream (Figures 8f and g). It is remarkable that no streamwise vortices are present or appear to re-emerge between vortex groups in Figures 8b-g.

III.2.2 Excitation of 2- and 3-D Instabilities

Previous investigations have established that the influence of 2-D forcing diminishes at increasing inclination angles while 3-D disturbances begin to amplify. At inclination angles between 14° and 17°, the flow is susceptible to both transverse waves and longitudinal vortices (Lloyd and Sparrow, 1970). The effectiveness of 2-D time-dependent forcing on the longitudinal vortices at a relatively small angle of inclination θ = 15° and q" = 3200w/m^2 is shown in Figure 9. The base flow is seeded with streamwise vortices at twice the wavelength of the heaters (by activating every other actuator) and is shown for reference in Figure 9a. The actuators are driven time-harmonically and the forcing frequency is slowly varied. At frequencies below 0.15Hz and above 0.5 Hz, the forcing has little effect and the disturbances are rapidly damped as they convect downstream (Figures 9b and e) . However, forcing at frequencies within this range has a dramatic effect on the flow and its transition to turbulent flow as is evidenced in Figures 9c and d. For these cases the streamwise vortices experience a massive distortion that is synchronized with the forcing

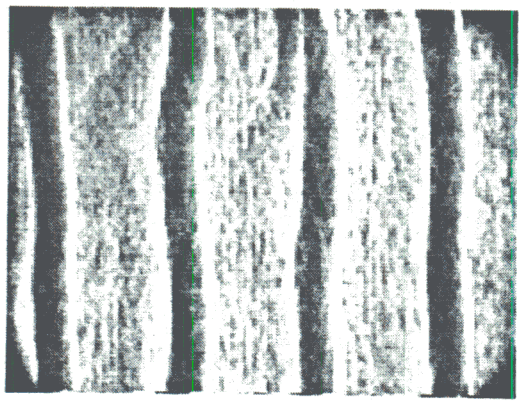

b.
HNHN f = 0

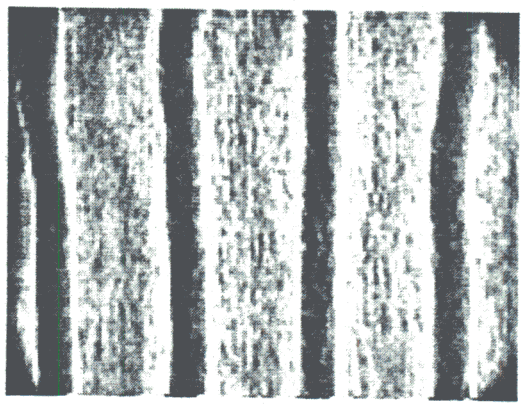

c.
HNHN f = 0.15

d.
HNHN f = 0.35

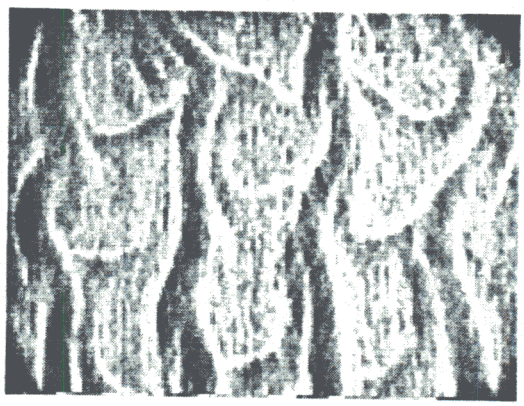

e.
HNHN f = 0.45

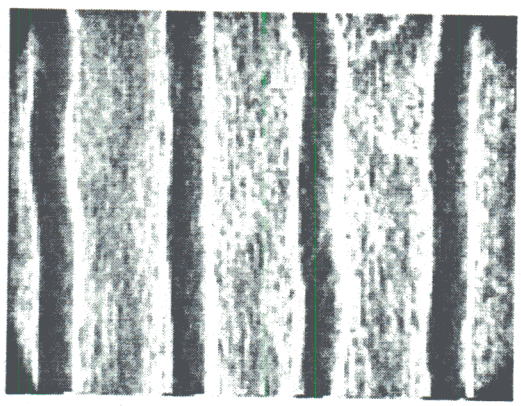

f.
HNHN f = 0.5

Fig. 9

frequency. It is expected that these changes in the flow state substantially affect the heat transfer from the plate.

The effect of a phase difference between the time-periodic excitation waveforms of adjacent actuators is shown in Figures 10a-e. The excitation waveform is spanwise-periodic with a period of two adjacent actuators and is $V_o\mathrm{Sin}(2\pi ft)$ and $V_o\mathrm{Sin}(2\pi ft+\Psi)$. Depending on the phase difference, the excitation waveform corresponds to a linear superposition of 2-D and equal and opposite oblique waves. The base flow, i.e., θ = 15° and q" = 3200w/m^2 is shown in figure 10a. In Figure 10b Ψ=0 and f= 0.5Hz and the forcing frequency is clearly noticeable in the spatial undulations of the streamwise vortices. As the phase Ψ is varied from 90° (Figure 10c) to 180° (Figure 10d), a varicose vortical pattern emerges. When the phase is Ψ=180°, the excitation is essentially equivalent to a family of two equal and opposite oblique waves. The addition of a DC offset to the excitation waveform, i.e., $V_o\mathrm{Sin}(2\pi ft)$ +V_o/2 and $V_o\mathrm{Sin}(2\pi ft+\Psi)$-$V_o$/2, stretches the varicose cells to such a degree that the vortices begin to break down (figure 10e). This effect leads to an increase in the amount of cooler fluid that is advected into the boundary layer and thus to an increase in the rate of heat transfer compared to the base flow.

The effect of 2-D waves of different frequencies on the evolution of existing streamwise vortices is shown in Figure 11 for θ = 7° and q" = 5500w/m^2. The base flow is shown for reference in Figure 11a. By exploiting the receptivity of the flow to both 2- and 3-D disturbances at low inclination angles, the flow appears to transition to a 3-D state well upstream of the unforced base flow.

The effect of nonuniform spanwise forcing is also being investigated. Figure 12 shows the evolution of the disturbance that results when the spanwise-uniform, time-harmonic (at 0.45 Hz) excitation waveform is disrupted by switching a group of actuators to the neutral state. In Figures 12a-e, while the center 1, 2, 4, 6, and 10 actuators are switched to neutral, respectively. As shown in Figure 12, the spanwise discontinuity results in substantial distortion of the 2-D wavetrain that widens as the number of neutral actuators increases. The effect of these distortions on the evolution of streamwise flow structures is investigated in more detail.

III.2.3 Stability of Transverse Waves

Previous numerical and experimental investigations have focused on the stability of natural convection over a *vertical* flat plate to transverse wave disturbances (e.g., Gebhart, 1969). Neutral stability curves were obtained as a function of the generalized disturbance frequency ß= $2\pi f\delta/U^*$ and the modified Grashof number Gr = $5(\mathrm{Gr}_x/5)^{1/5}$. It was shown that the shape and range of the neutral stability curve depend not only on the Prandtl number, but also on the amplitude of temperature disturbance at the surface s(0). It is noteworthy that for a plate with very large thermal capacitance s(0)=0 and thus surface temperature disturbances are zero, while low

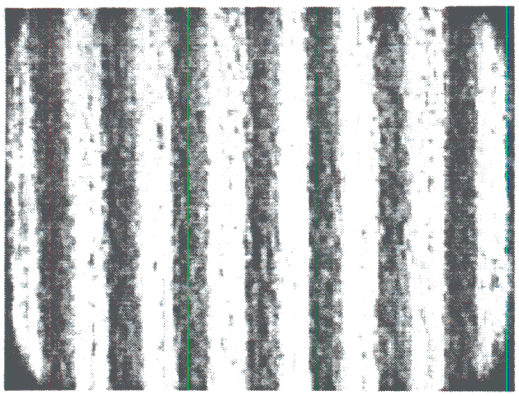

a.
Base flow

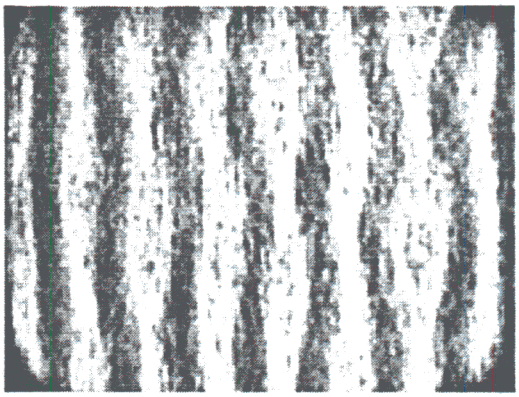

b.
$\psi = 0$

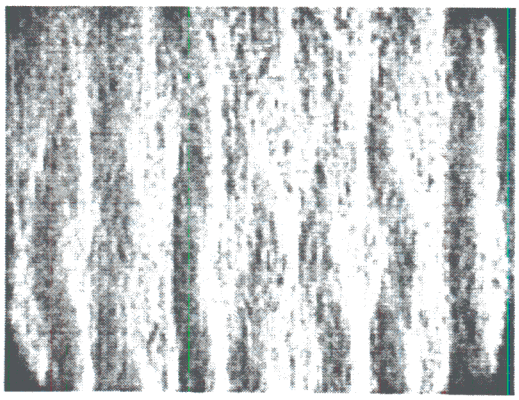

c.
$\psi = 90$

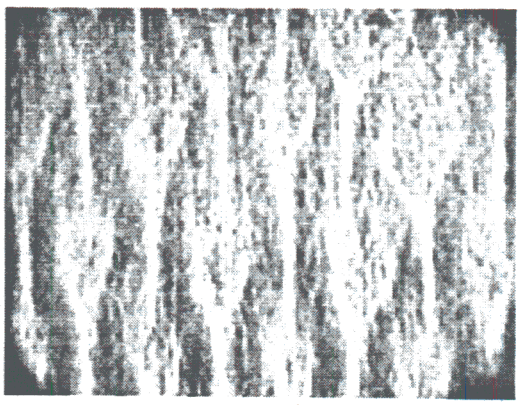

d.
$\psi = 180$

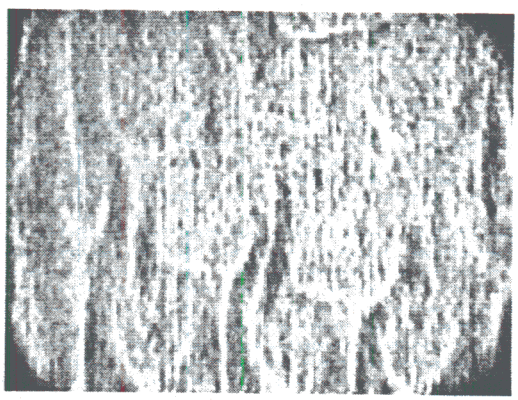

e.
$\psi = 180$ DC offset

Fig. 10

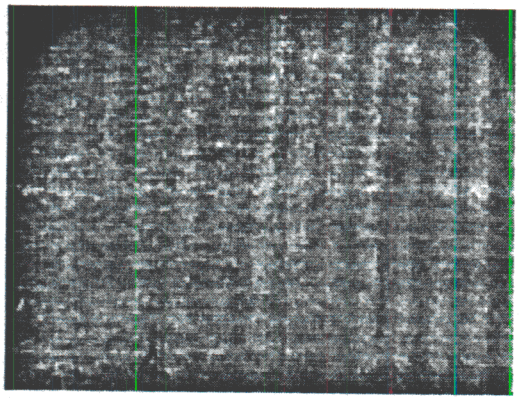

a.
no forcing

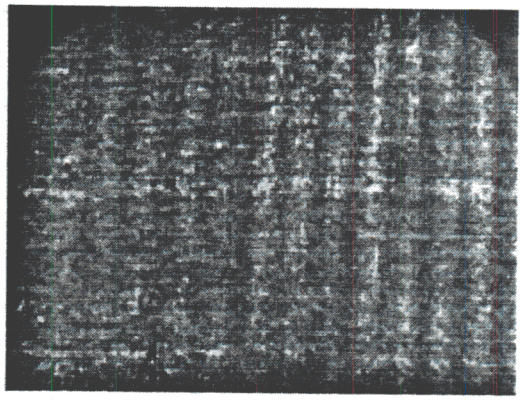

b.
f=0.35

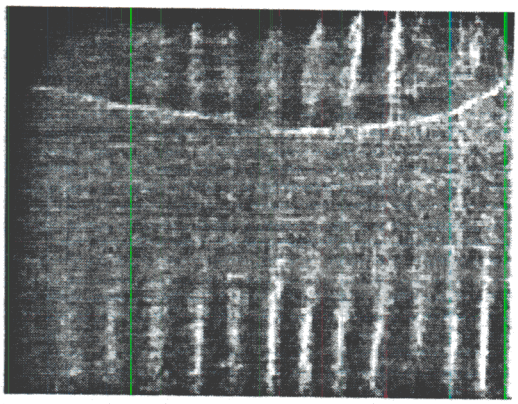

c.
f=0.4

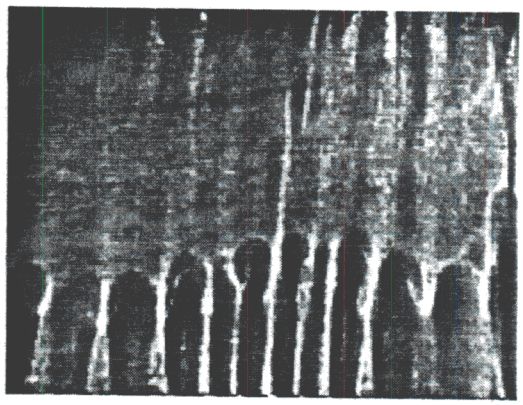

d.
f=0.45

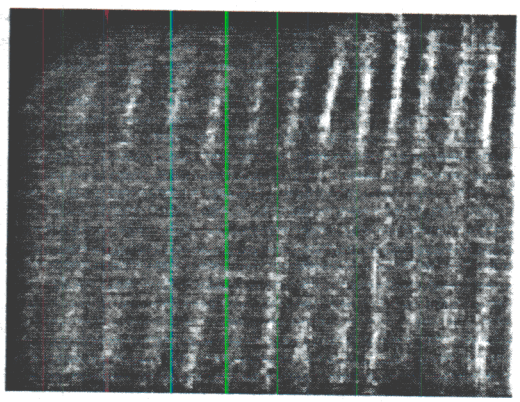

e.
f=0.8

Fig. 11

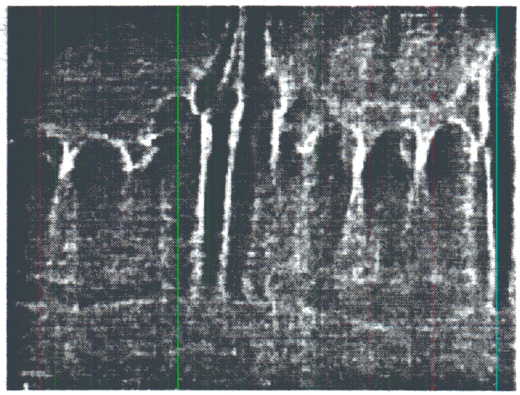

a.

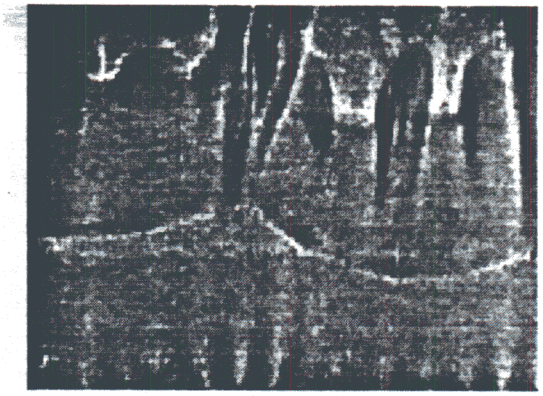

b.

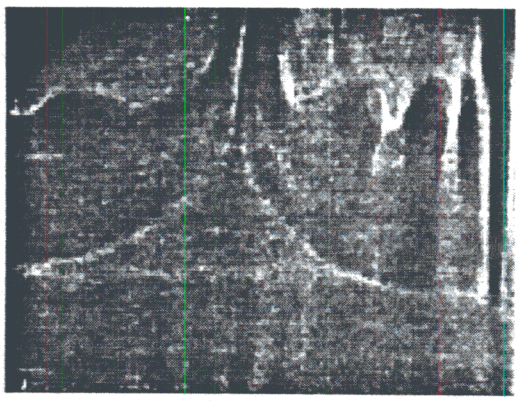

c.

d.

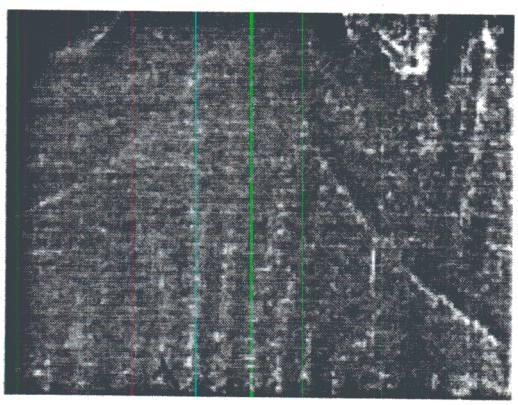

e.

Fig. 12

thermal capacitance (i.e. a thin foil) s'(0)=0 and temperature disturbances can be transferred through the surface into the flow. For intermediate conditions, the general disturbance boundary condition is $s(0) = [i \cdot s'(0)] / [\hat{Q}^2 \beta]$ where $\hat{Q}$ is the relative thermal capacitance parameter such that s(0) = 0 and s'(0)= 0 imply $\hat{Q} = \infty$ and 0, respectively. Even though in the present experiments $\hat{Q}$ is large (effectively ∞), temperature disturbances are forced by surface actuators and thus are nonzero (i.e., $s(0) \neq 0$). In fact, it is the actuator-controlled temperature disturbance at the surface that is exploited for the study the stability of the flow. Furthermore, even though $\hat{Q}$ is large, q" is still constant since the streamwise heat conduction through the surface is approximately 300 times smaller than the heat transfer into the flow.

Because of this rather unique boundary condition it is not possible to match the neutral stability curves of other investigators to the present experimental conditions. The closest data that has been found is that of Knowles and Gebhart (1968). Figure 13 shows the neutral stability curves for a constant heat flux surface with Pr = 0.733, 3.0, 5.0, and 6.9, s'(0) = 0, $\hat{Q} = 0$.

Another important difference between previous and present experimental investigations of the flow stability is the excitation technique. Gebhart used a moveable flap placed near the outer edge of the boundary layer to induce a known temporal velocity disturbance. By contrast, in the present experiments known spatial and temporal temperature disturbances are introduced *directly* at the surface of the plate and thus are fundamentally different from those of previous researchers. Figure 14 shows the stability plot for the present experiment (q" = const, $\hat{Q} = \infty$, $s(0) \neq 0$ $s'(0) \neq 0$, Pr = 6.1). The open and filled circles represent the respective lower and upper bounds of the generalized frequencies that were amplified by the flow. All of the points showed here would lie within the appropriate curve of Figure 12 ($5.0 < Pr < 6.9$). The differences between the neutral stability curves is ostensibly the result of the differences in experimental boundary conditions discussed above.

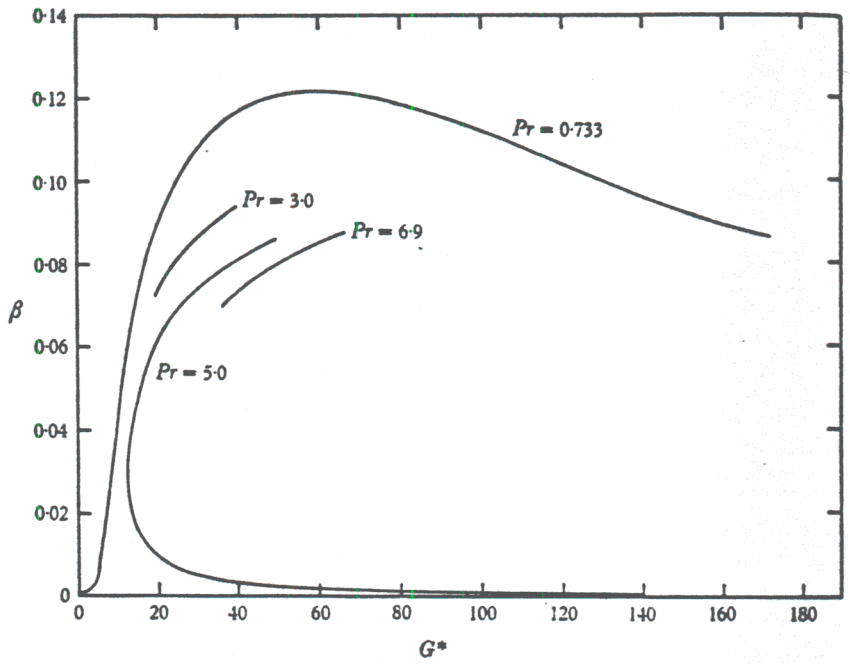
0·14
0·12
0·10
0·08
0·06
0·04
0·02
0
β
Pr = 0·733
Pr = 3·0
Pr = 6·9
Pr = 5·0
0
20
40
60
80
100
120
140
160
180
G*

Fig. 13

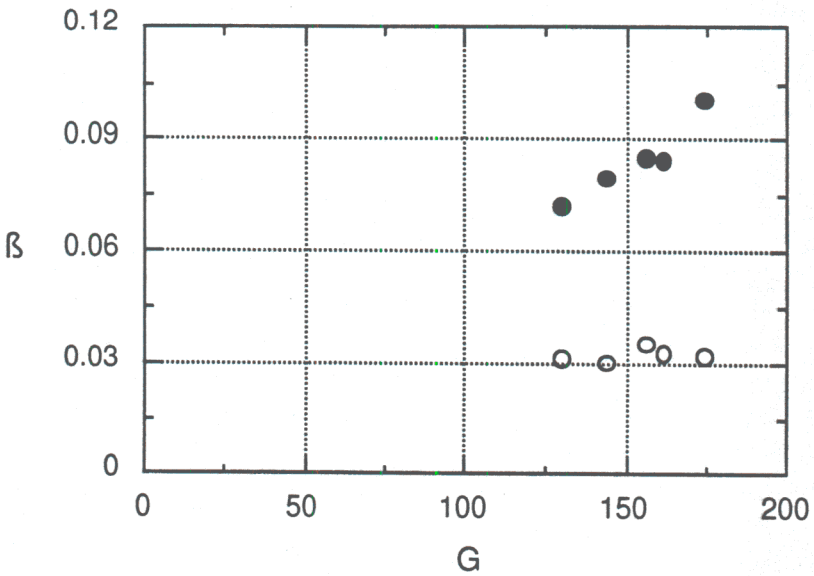
0.12
0.09
0.06
0.03
0
ß
0
50
100
150
200
G

Fig 14

IV. STATEMENT OF WORK FOR YEAR III

- The investigation of the evolution of 2- and 3-D instability modes will be completed with particular emphasis on the effect of inclination angles and surface heat flux.
- Thermochromic Liquid Crystal (TLC) thermometry will be calibrated and used to measure surface temperature distributions for heat transfer calculations.
- The effect of 2-D and 3-D forcing on heat transfer will be quantitatively determined using TLC thermometry.
- Open-loop control configurations will be sought for maximum enhancement of heat transfer. Time-harmonic spanwise-nonuniform excitation waveforms will be studied with emphasis on the onset and evolution of the longitudinal vortices:
    i. Spanwise amplitude-modulated excitation.
    ii. Spanwise phase-modulated excitation.
- Cancellation experiments of controlled disturbances will be attempted. Spanwise arrays of surface heaters will input the control signal with appropriate distributions of gains and delays.
- The streamwise and spanwise velocity components for a selected excitation input will be measured at a number of spanwise and streamwise stations using an LDV system.

References

Farina, D.J. et. al.,"Illuminant invariant calibration of thermochromic liquid crystals," *Experimental Thermal and Fluid Science*, **9**, 1-12, 1994.

Gebhart, B., "Natural convection flow, instability and transition," *J. Heat Transfer,* **18**, 293-309, 1969.

Godaux, F., Gebhart, B. "An experimental study of the transition of natural convection flow adjacent to a vertical surface," *Int. J. Heat Mass Transfer*, **17**, 93-107, 1974.

Görtler, H. "Über eine Analogie zwischen den Instabilitäten laminarer Grenzschichtströmungen an konkaven Wänden und an erwärmten Wänden, " *Ing. Arch.*, **28**, 251-255, 1969.

Haaland, S.E., Sparrow, E.M. "Vortex instability of natural convection flow on inclined surfaces," *J. Heat Mass Transfer*, **16**, 2355-2367, 1973.

Jaluria, Y., Gebhart, B."An experimental study of nonlinear disturbance behavior in natural convection", *J. Fluid Mech,* **61**, 337-365, 1973.
Jaluria, Y., Gebhart, B. "On transition mechanisms in vertical natural convection flow," *J. Fluid Mech,* **66**, 309-337,1974.

Kierkus, W.T. "An analysis of laminar free convection flow and heat transfer about an inclined isothermal plate,", *J. Heat Mass Transfer*, **11**, 241-253, 1968.

Knowles, C.P., Gebhart, B. , "The stability of the laminar natural convection boundary layer," *J. Fluid Mech.*, **34**, 657-686, 1968.

Liepmann, H. W., Brown, G. L. , and Nosenchuck, D. M. "Control of laminar-instability waves using a new technique," *J. Fluid Mech.*, **118**, 187-200, 1982.

Lloyd, J. R., Sparrow, E. M "On the instability of natural convection flow on inclined plates," *J. Fluid Mech.*, **42**, 465-470.

Lloyd, J. R., Sparrow, E. M., and Eckert, E. R. G., "Laminar, transition and turbulent natural convection adjacent to inclined vertical surfaces," *Int. J. Heat Mass Transfer*, **15**, 457-473, 1972.

Merkin, J.H., "The effect of buoyancy forces on the boundary-layer flow over a semi-infinite vertical flat plate in a uniform free stream," *J. Fluid Mech.*, **35**, 439-450, 1969.

Pauley, W.R., Eaton, J.K. "The effect of embedded longitudinal vortex arrays on turbulent boundary layer heat transfer," *J. Heat Transfer*, **116**, 871-879.

Sparrow, E.M., Gregg, J.L., "Laminar free convection from a vertical plate with uniform surface heat flux," *Trans. ASME*, 435-440, 1956.

Sparrow, E.M., Tsou, F.K., Kurtz, E.F., "Stability of laminar free-convection flow on a vertical plate," *Phys. Fluids*, **8**, 1559-1561, 1965.

Shankatullah, E. M. and Gebhart, B., "An experimental investigation of natural convection flow over and inclined surface," *Int. J. Heat Mass Trans.*, **21**, 1481-1490, 1978.

Vliet, G.C., Liu, C.K. "An experimental study of turbulent natural convection boundary layers," *J. Heat Transfer*, 517-531, Nov. 1969.

E-25-W22
#3

CONTROL OF NATURAL CONVECTION ALONG A HEATED, INCLINED PLATE

NSF GRANT CST-9318332
FINAL TECHNICAL REPORT
August 1993 - October 1998

submitted by

Ari Glezer
Woodruff School of Mechanical Engineering
Georgia Institute of Technology

Abstract

Flow instabilities leading to the formation of streamwise vortices in a free convection boundary layer over a heated inclined plate are manipulated using surface mounted film heating elements. The flat plate model (59 cm on the side) is suspended in a water tank measuring one meter on the side. The flow over the plate is driven by a two-ply surface heater comprised of a uniform, constant-heat flux film heater layer and a lower mosaic of 32 x 10 individually-controlled heating elements that are used as control actuators. Temperature distributions on the test surface are measured using a calibrated liquid crystal film and digital image processing. The flow velocity in streamwise planes normal to the surface is measured using particle image velocimetry (PIV). Controlled excitation of two- and three-dimensional instability modes are investigated and it is shown that the receptivity of the flow to the excitation input increases with inclination angle and surface heat flux. Time-invariant spanwise-periodic excitation over a range of spanwise wavelengths leads to the formation of arrays of counter-rotating streamwise vortex pairs and to substantial modification of the surface temperature (and heat transfer). Spanwise-periodic merging of groups of vortices appear to be a precursor to the development of a secondary instability which is followed by breakdown to turbulence. Time-harmonic excitation of plane and oblique instability modes leads to temporal and spatial modulation of the streamwise vortices and to the emergence of vortex loops. Pulsed excitation leads to the formation of wave packets which, following amplification, evolve into patches of vortical structures with temporal modification of the surface temperature.

I. Introduction

The study of thermally-driven boundary layer flows over inclined surfaces owes much of its importance to a number of engineering applications including passive (non-mechanical) surface cooling technologies (e.g., electronic packages), and chemical vapor deposition processes (e.g., in fabrication of microelectronic and optical components). These thermal boundary layers are buoyantly unstable, and the instabilities can lead to the appearance of longitudinal (streamwise) vortices (rolls) which is accompanied by significant changes in transport phenomena near the surface such as heat transfer or surface deposition. Thus, the present research work has focused on the manipulation and control of the flow instabilities that lead to the formation of these streamwise vortices with the objective of enhancing the heat transfer over a heated inclined flat plate.

Spanwise-averaged heat transfer measurements of a free convection boundary layer along a heated inclined surface were made by Rich (1953) over a range of Grashof numbers from 10^6 to 10^9 and inclination angles (measured relative to the vertical position) between 0 and 40^0, using a Mach-Zehnder interferometer. The objective of these experiments was to compare experimental results of laminar 2-D flow to theoretical predictions and the presence of streamwise vortices was not reported. The appearance of streamwise vortices in a flat plate free convection boundary layer was first reported by Sparrow and Husar (1969) who used a Thymol-blue technique for flow visualization. The authors suggested that streamwise instability of these vortices is the first stage of transition to turbulence for plate inclination greater than 15^0. Flow visualization also revealed that the spanwise wavelength of the vortices decreases with increasing temperature difference, and is only weakly affected by the inclination angle of the plate. Furthermore, planform images showed merging of neighboring vortices prior to break up to turbulence.

Lloyd and Sparrow (1970) showed that free convection flat plate boundary layers become unstable in two different modes depending on the vertical inclination angle. When the plate is nearly vertical (i.e., $\theta < 14^0$), the instability is in the form of transverse traveling waves. However, when θ exceeds 17^0, the instability leads to the formation of longitudinal vortices that are similar to the vortices observed by Sparrow and Husar (1969). The critical Rayleigh number for the onset of these instabilities decreases from $Ra = 10^9$ for $\theta = 0^0$ to 10^6 at $\theta = 60^0$.

In a later investigation, Shaukatullah and Gebhart (1978) measured in detail the temperature and velocity along an inclined heated plate operated at constant heat flux. It was determined that for inclination angles exceeding 11^0, the appearance of travelling waves is preceded by streamwise vortices. As for a heated plate that is operated at constant surface temperature, it was confirmed that the wavelength of the spanwise disturbance is independent of the inclination angle, and inversely proportional to the surface heat flux. The authors determined that the onset of the instability depends on the modified Reynolds number ($R=5(Gr^*/5)^{1/5}$, where Gr^* is the Grashof number based on surface heat flux) and the streamwise distance from the leading edge. The dependence on streamwise position was lumped in the dimensionless transition criterion E ($E=R[\nu^2 / gx^3]^{2/15}$) that was originally proposed by Jaluria and Gebhart (1974). This approach yields a measure for the onset of streamwise vortex instability that is given by $E = 88\theta^{-0.65}$.

The stability of flows over heated inclined plates has also been studied numerically. In a linear stability analysis of steady longitudinal disturbances (hereafter denoted S3D disturbances) along an isothermal surface Haaland and Sparrow (1973) found that a non-parallel base flow model yields critical flow conditions (for neutral stability) which differ substantially from what is predicted by the parallel base flow model. The authors report a non zero critical spanwise wavenumber and a critical Reynolds number that is several orders of magnitude larger than for

the parallel base flow model. However, despite the inclusion of a non-parallel base flow in the analysis, the critical Reynolds number for the onset of the instability $\tilde{R}_c$ = 23.5 (Pr = 6.7) was still much smaller than the values observed in the experiments of Lloyd and Sparrow (1970). It was suggested that the Reynolds number is not the only criterion for predicting whether the instability leads to the formation of steady longitudinal vortices or travelling waves. In a linear stability analysis of two-dimensional travelling waves (hereafter denoted T2D disturbances) and stationary longitudinal vortices (S3D) over an inclined constant-temperature plate, Iyer & Kelly (1974) showed that for inclination angles $\theta<4^0$, the critical Reynolds number ($\tilde{R}$) associated with the streamwise position of neutral stability is smaller for T2D than S3D disturbances. For $\theta=4^0$ the streamwise position of neutral stability for both the T2D and S3D disturbances is the same. For $\theta>4^o$ the S3D disturbances are amplified first. These authors also computed the total amplification of the two instability modes between their respective locations of neutral stability and the streamwise stations where they were first observed in various experiments. It was found that the total amplification of both modes is the same at $\theta \approx 16^o$.

Neutral stability curves and heat transfer rates for a laminar free convection flow over isothermal horizontal and inclined surfaces were determined numerically by Chen and Tzuoo (1982) for Grashof numbers of up to 10^7 and inclination angles between 20^0 and 90^0 (relative to the vertical). It was found that as the inclination angle decreases the laminar surface heat transfer rate increases and the flow becomes less susceptible to the S3D disturbances that lead to the formation of streamwise vortices. Lee *et. al.* (1991) used linear theory to investigate the evolution of the S3D instability for surface temperatures that varied like x^n over the same range of inclination angles considered by Chen and Tzuoo (1982). These authors used a non parallel

base flow and considered both streamwise independent and dependent disturbances. Streamwise dependent disturbances stabilized the base flow and yielded critical Grashof numbers that were closer to experimental observations. Merging of the streamwise vortices on a constant temperature surface that was reported by Sparrow and Husar (1969) was investigated by Chen *et. al.* (1991) using a nonlinear stability analysis. This work shows that the vortices are destabilized by a subharmonic mode at a second critical Reynolds number $\widetilde{R}_{1/2} = 41$ for Pr = 5.5.

The onset and evolution of the instability modes of the base flow can be substantially modified by exploiting their receptivity to controlled external disturbances leading to substantial modifications of the base flow. This approach was first tested in a flat plate (momentum) boundary layer by Klebanoff *et. al.* (1961) who used a vibrating spanwise ribbon to introduce controlled three-dimensional disturbances into the two-dimensional base flow in order to study their nonlinear evolution and the onset of transition to turbulence. In a similar experiment in a free convection boundary layer, Jaluria and Gebhart (1972) also used a spanwise non-uniform vibrating ribbon to investigate the nonlinear evolution of controlled time-varying disturbances. Recently, Zuercher *et. al.* (1998) used Schlieren flow visualization and PIV measurements to investigate the onset and merging of streamwise vortices along an inclined isothermal surface. This investigation focused primarily on the linear growth of naturally occurring disturbances in the unforced flow and included some effects of passive forcing using strips of tape on the surface. The present investigation is concerned with the evolution of actively forced spatial and temporal disturbances within the thermal boundary layer over a constant heat flux surface with particular emphasis on surface temperature and the associated heat transfer rates.

II. EXPERIMENTAL APPARATUS AND DIAGNOSTICS

The experiments are conducted in a water tank (measuring 107 cm on the side) using a heated submerged flat test surface (Figure 1). Flow instabilities leading to the formation of streamwise vortices are manipulated using a mosaic of surface heating actuators mounted on a ceramic substrate (66 cm long and 61 cm wide, approximately 50 wavelengths of the spanwise instability that leads to the formation of streamwise vortices), that is attached to metal frame hinged along its span to the sidewalls of the tank. A hoist system is used to adjust the angle of inclination of the test surface. The water tank is connected to a circulation system that is used to either cool or heat the water. Heating and cooling is used to set the water temperature for the calibration procedure of a liquid crystal film that is used to measure the surface temperature.

II.1 Heated Test Surface

The test surface is comprised of a two-layer Kapton insulated foil heater bonded to a 61 cm x 61 cm x 1.27 cm thick mica-glass ceramic sheet (thermal conductivity of 0.42 W/(m*K)). The top layer is a uniform 61 cm x 60 cm x 12.7 μm thick Inconel foil heater connected to streamwise electrodes along the edges on its two sides. The underlying heater is a mosaic of individually controlled heating elements as shown schematically in Figure 2. The mosaic consists of three identical segments each measuring 20 cm x 56 cm in the spanwise (z) and streamwise (x) directions respectively (Figure 2a). Each segment of the mosaic has 32 streamwise-serpentined 40Ω copper-nickel film elements (Figure 2b). Each element is 0.64 cm wide and 56 cm long, and the center-to-center distance between adjacent elements is 0.64 cm. Actuator electrical connections are made in the air cavity beneath the ceramic substrate at each

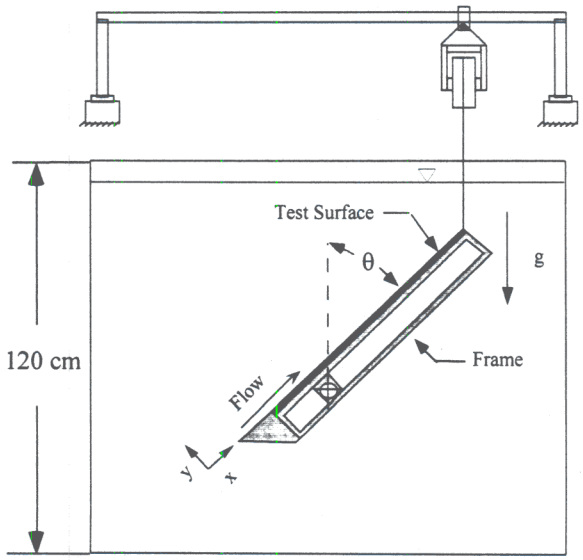

Figure 1. Schematic of the test facility

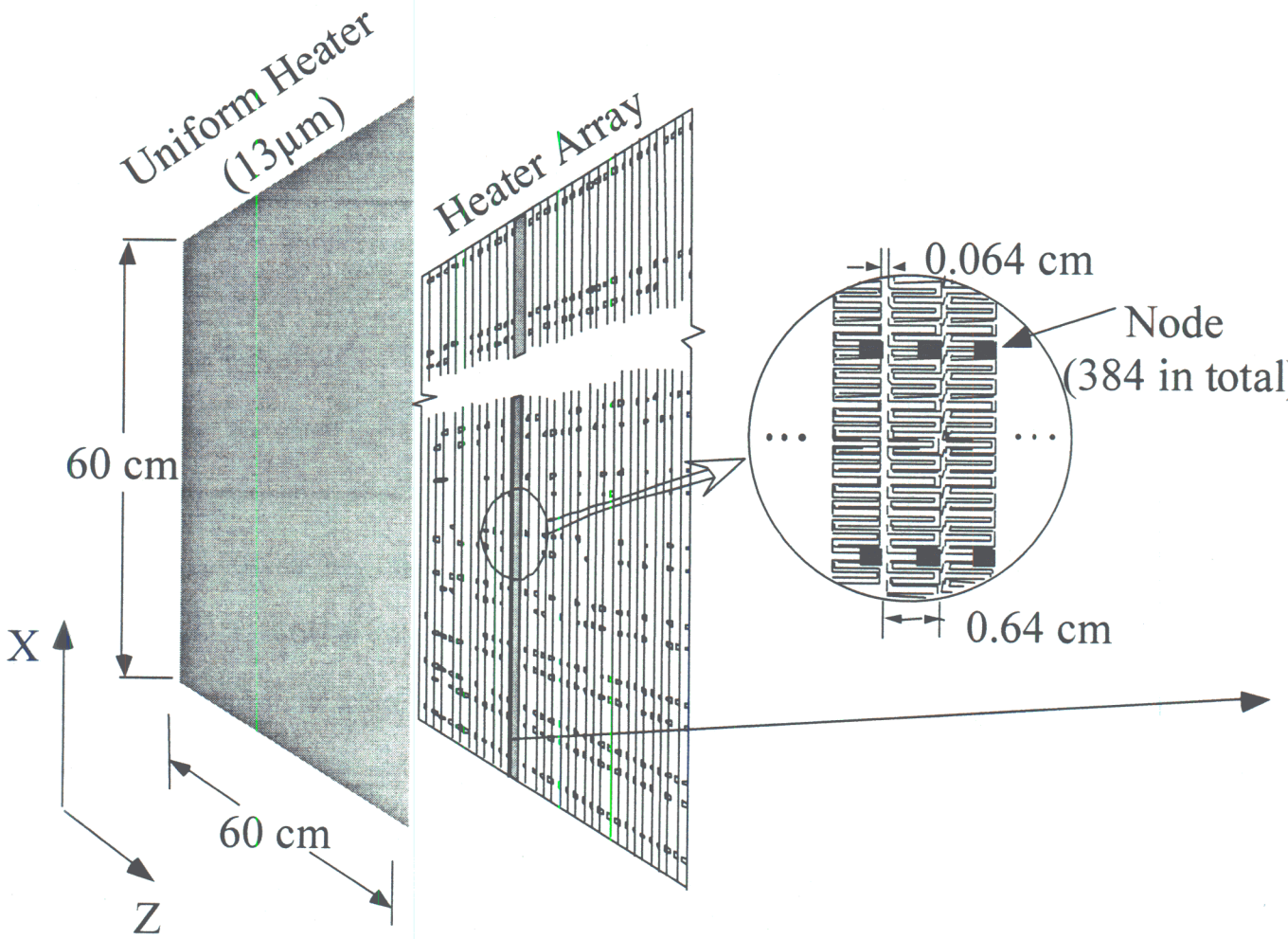

Figure 2a

Figure 2b

reduce surface heating by the spotlights. Images are acquired using a 640x480 pixel array color CCD camera and frame grabber installed in a PC.

During a calibration, the ambient water temperature is slowly increased (< 0.04 °C/min) while 100 images are recorded to a PC computer every 12 seconds. The red, green and blue colors measured are converted into a hue, saturation, intensity color model, and only the hue retained for calibration with temperature. A typical calibration curve is shown in figure 3. The average temperature sensitivity of the liquid crystal is 0.01 °C/Hue (25<Hue<120), and a fifth order polynomial fit to the data is used to extend the usable temperature range. A new liquid crystal sheet has a calibration error of ± 0.06 °C [95% CI] over most of the hue range, but over time water diffuses into the laminate increasing the error to ± 0.1 °C for a 24 hour usage period.

The measured temperature during an experiment is corrected for heat conduction through the 0.12 mm top polyester sheet (having a nominal conductivity of 0.3 W/m°K) and the heat flux is calculated by monitoring the power input to the foil heater. An uncertainty of the polyester conductivity introduces a bias error in the measurement of the surface temperature. However a comparison of the heat transfer rates with the measurements of previous investigators and the theoretical 2-D laminar unforced flow indicates that the value used for the thermal conductivity is reasonable.

Measurements of distributions of the streamwise and cross stream velocity components in cross stream lanes normal to the surface of the test surface are obtained using a cross correlation digital particle image velocimetry (PIV). The light sheet produced by a double pulse Nd:YAG laser is 1mm thick. A 1018x1008 pixel array digital camera is used to image the flow and is capable of capturing 15 image pairs/s. The tank is seeded with nominally 11 μm hollow glass spheres ($\rho = 1.1$ g/cm^3) . A rectangular interrogation spot measuring 128x16 pixels (in the x and

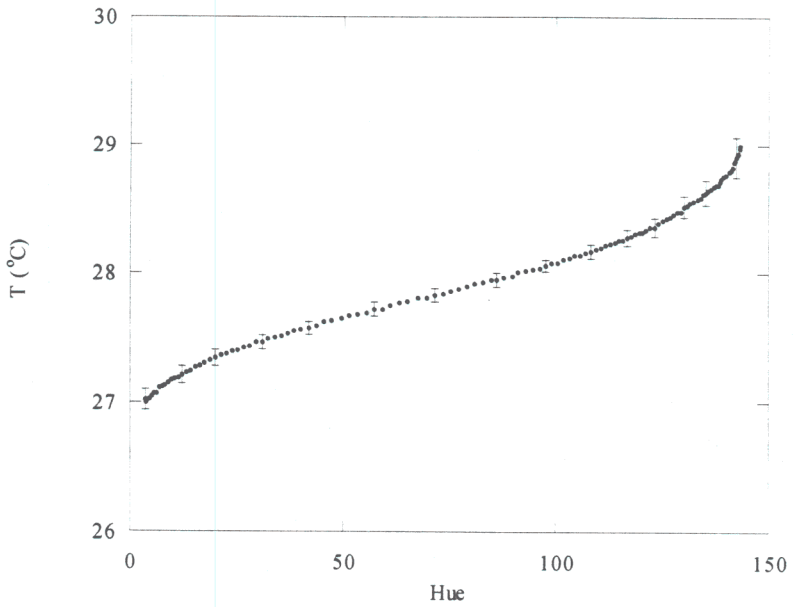

Figure 3. Typical liquid crystal calibration curve

y directions respectively) is used to process the velocity vector, and the image resolution was 25.6 μm/pixel. Spanwise variations were mapped by traversing the laser sheet and camera in the z direction by 1.2mm increments.

III. The Unforced Flow

Section III documents the heat transfer and boundary layer structure for the unforced natural convection boundary layer along a constant heat flux inclined flat plate. The basis of these measurements is to provide a baseline for the impact of time-invariant spanwise periodic forcing of the surface heat flux.

III.1. Thermal Transport

The liquid crystal thermography system was used to record images of surface temperature over a contiguous 16 cm span and 13 cm streamwise extent for a given camera location. Composite maps were created by using images taken at two streamwise locations. Figure 4 shows three normalized temperature Φ composite maps for the unforced flow at inclination angles 14^0, 19^0 and 24^0 and $q"= 2260\ W/m^2$. At $\theta = 14^0$, Φ is relatively constant for all streamwise positions and nearly spanwise uniform. A constant Φ implies that the surface heat transfer is similar to vertical 2-D laminar flow heat transfer, since by definition $\Phi \propto (Gr_x^*)^{1/5}/Nu_x$ and the 2-D laminar flow solution yields that $Nu_x \propto (Gr_x^*)^{1/5}$. Here $Nu_x = hx/k$ is the spanwise averaged Nusselt number and $Gr_x^* = g\beta q" x^4 \cos\theta / k\nu^2$ is the local Grashof number where $h = q"/(T_s - T_\infty)$ is the heat transfer coefficent, $q"$ the surface heat flux, T_s the surface temperature, T_∞ the ambient fluid temperature, x the streamwise distance from the

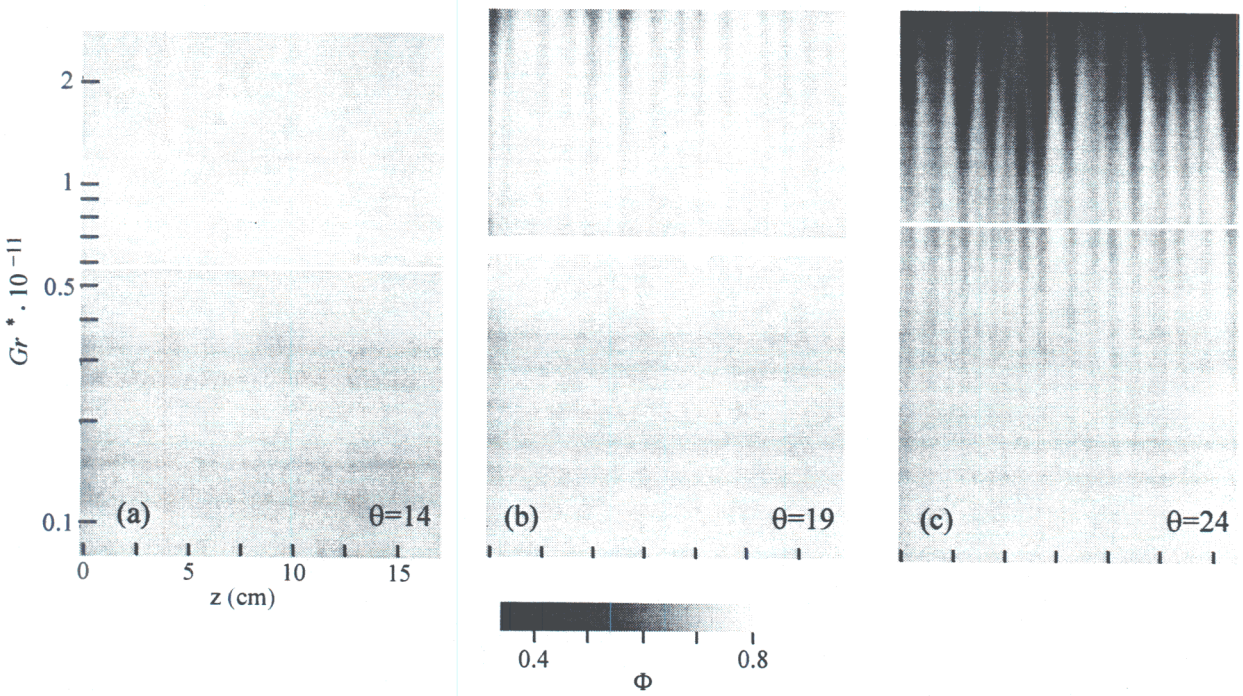

Figure 4. Unforced dimensionless temperature maps for $q'' = 2260$ W/m^2 and $\theta = 14°$ (a), $\theta = 19°$ (b), $\theta = 24°$ (c).

heater origin, k the fluid thermal conductivity, g the acceleration due to gravity, β the coefficient of thermal expansion, θ the plate inclination angle from vertical, and ν the kinematic viscosity. By $Gr_x^*=10^{11}$, small spanwise variations are noticeable for the $\theta=19^0$ case. The darker regions established by $Gr_x^*=2\text{x}10^{11}$ reveal that 3-D effects are causing a local increase in the surface heat transfer relative to a steady 2-D flow. Small spanwise variations are observable in the $\theta=24^0$ case for Gr_x^* as low as$1\text{x}10^{10}$. The general decrease in Φ downstream indicates cooling beyond that provided by a 2-D flow, and the large spanwise variations suggest a well developed 3-D flow field.

The temperature maps were also used to find the correlation between Nu_x and Gr_x^* by computing spanwise averages of the local Nusselt number $Nu_{x,z}$ as a function of Gr_x^*. Figure 5 shows that the correlation $Nu_x = 0.864Gr_x^{*1/5}$ fits the data well based on spanwise averages of the $Nu_{x,z}$ for $\theta=14^0$ and 19^0 over the measured range of Gr_x^*. Although there are observable 3-D structures in figure 4b ($\theta=19^0$ composite map), the spanwise averaged heat transfer follow the 2-D correlation, curve $(q_2",\theta_2)$, implying that in terms of heat transfer, the disturbance is still in a linear growth stage and does not effect the mean flow significantly. However at $\theta=24^0$, the Nu_x curve deviates from the correlation at $Gr_x^* \approx 8\text{x}10^{10}$ and this transition Grashoff number is essentially independent of surface heat flux. This deviation is a result of the 3-D flow effects evident in figure 4c ($\theta=24^0$ composite map). The strength of the streamwise vortices is sufficient to circulate cool fluid from the outer edge of the boundary layer down to the surface, resulting in higher spanwise mean heat transfer and lower surface temperatures. This cooling mechanism is

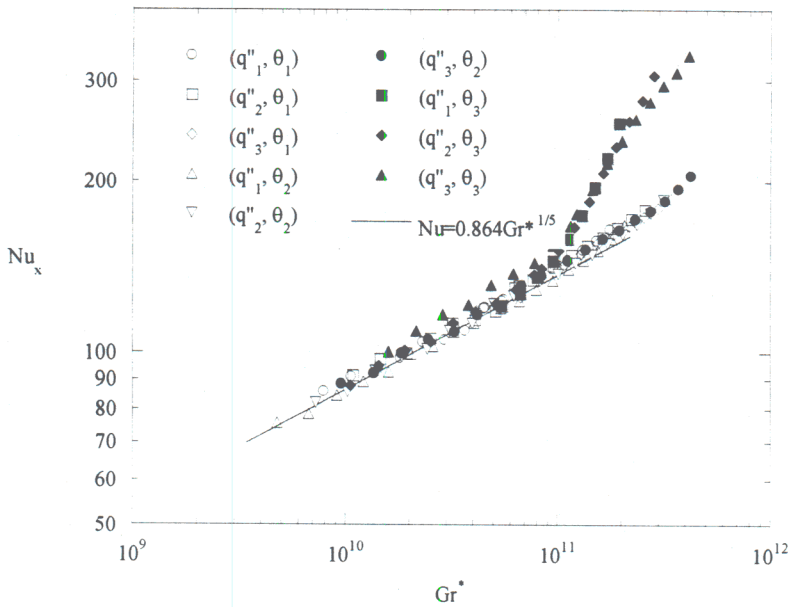

$q_1"=1380\ \ W/m^2 \qquad \theta_1=14^o$

$q_2"=2260\ \ W/m^2 \qquad \theta_2=19^o$

$q_3"=3360\ \ W/m^2 \qquad \theta_3=24^o$

Figure 5. Unforced Nu-Gr curves.

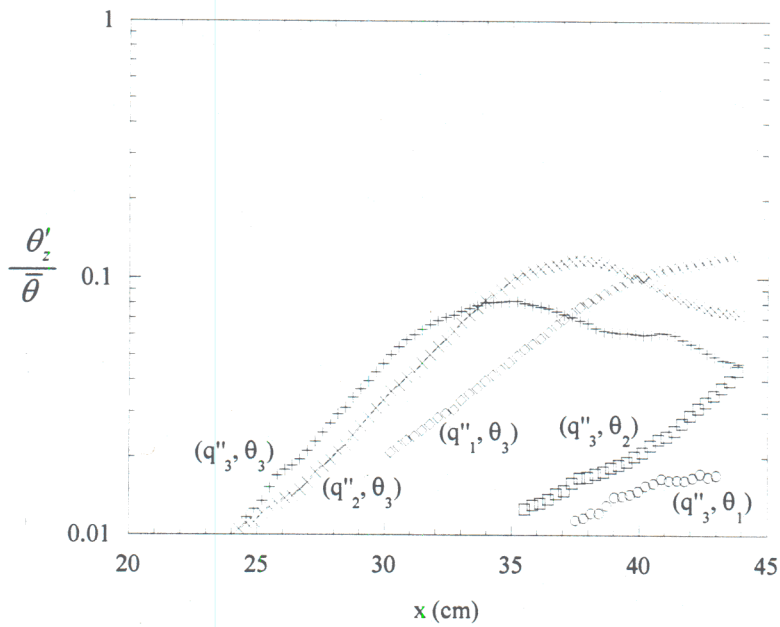

Figure 6. Unforced RMS disturbance growth.

later manipulated through spanwise forcing to dramatically increase the surface heat transfer coefficient.

Growth trends of the streamwise vortices are revealed by computing the spanwise RMS temperature fluctuations Φ_z' (Figure 6). It is clear that initially for all cases, the disturbance growth proceeds exponentially and the streamwise growth rate B increases strongly with increasing θ and weakly with increasing q''. At $\theta=\theta_3=24^o$ for each heat flux condition, the growth rate tapers off at decreasing x locations with increasing heat flux values. Furthermore, it appears that RMS disturbances of more than 0.1 at the surface are not sustainable, with another mechanism checking the growth at the surface.

It is reasonable to expect that test cases with spanwise mean heat transfer coefficients similar to 2-D laminar flow should have spanwise mean velocity profiles similar to 2-D laminar flow. Figure 7 shows u^*, the spanwise averaged streamwise velocity $\bar{u}$ normalized by $\bar{u}_{max}$, the average profile maximum streamwise velocity, plotted against y^*, the wall normal distance divided by the location of y($0.5\bar{u}_{max}$). For all conditions shown except (G^*=540, θ= 24^0), the 2-D steady laminar profile (Pr=5.8) fits the spanwise averaged data quite well. However, at G^*=540 for θ=24^0, the mean profile is slightly thinner then the 2-D profile. This location corresponds to Gr_x^*=7.3x10^{10}, approximately the location where the Nu_x, Gr_x^* correlation begins to deviate from 2-D heat transfer.

The shape of the u^* and v^* velocity profiles at a peak and valley z location (Figure 8 (a) and (b)) reveal the reason for the spanwise variations in surface temperature (or heat transfer coefficient) as seen in figure 4c. Compared to a 2-D profile, the v^* velocities are primarily positive at a peak, and primarily negative at a valley. The net effect of the v^* velocity is similar

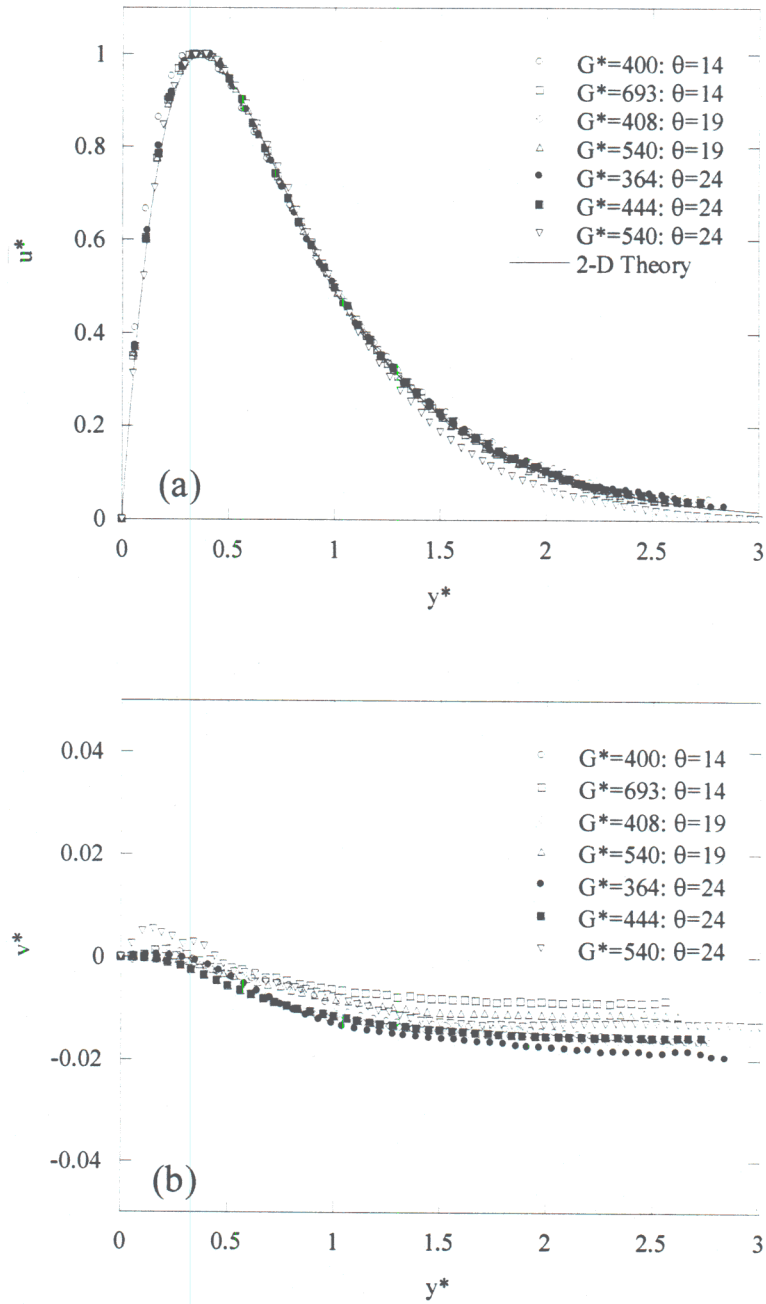

Figure 7. Unforced spanwise averaged (a) streamwise and (b) wall normal velocity.

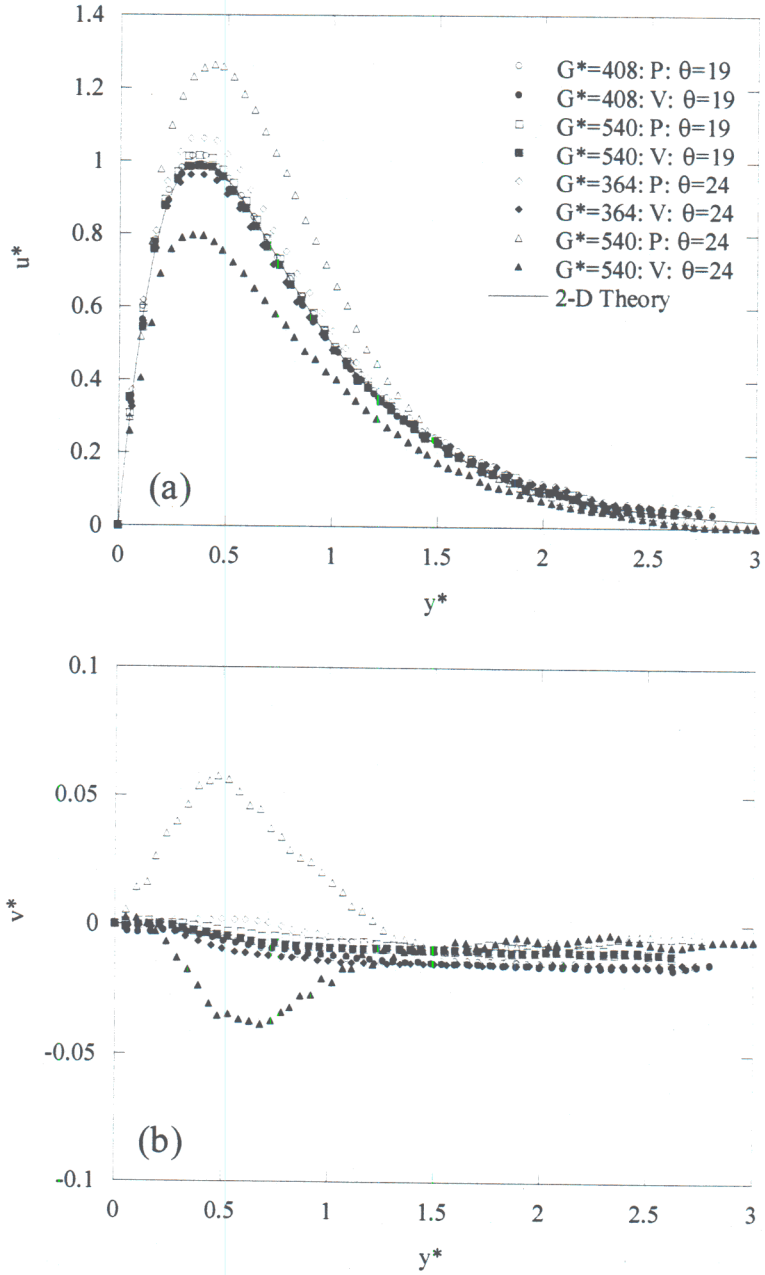

Figure 8. Unforced (a) streamwise and (b) wall normal velocity at both a peak and valley of the spanwise disturbance.

to spanwise periodic blowing and suction at the wall, alternately compressing or stretching the momentum boundary layer. The thermal boundary layer would likewise be compressed and stretched because a negative v^* brings cool ambient fluid toward the wall, while a positive v^* convects warmer fluid away from the wall. This implies that the momentum and thermal boundary layer length scales will follow the same spanwise trend, and therefore higher and lower heat transfer coefficients are expected in the valleys and peaks respectively because of the smaller and larger associated length scales. Furthermore, from linear stability it is known that the fluid T, u and v waveforms have the same spatial phase in the z direction, at least in the linear growth regime, which also implies higher heat transfer coefficients at a disturbance valley than at a peak.

The high resolution of the liquid crystal measurements permits the computation of the spanwise power spectra of the disturbance using fast fourier transforms to reveal energy contribution of a particular wavelength. Figure 9 shows the spectral power A vs spanwise wavenumber k_z for the conditions $\theta = 24^0$ and $q" = 2260\ W/m^2$ for several streamwise postitions, where for clarity the power spectra amplitude for succesive x locations has been multiplied by 1000. At x=19.9cm(curve a) there is significant power contained in a small band about $k_z = 0.93\,cm^{-1}$ with A = 9.2. The power at this wavenumber increases to A=315 by x=28.2 cm and A=1811 by x=35.7 cm before falling to a level of 557 at x=42.8 cm. Curve d also indicates that the energy near the subharmonic ($k_z \approx 0.5$) of the primary peak has become dominant by x= 42.8 cm with A=1370, indicating at this stage the subharmonic mode (a merged or nearly merged streamwise structure) is the dominant wavenumber of the disturbance. These trends will be more apparent when the forced spectra is analyzed later in this paper.

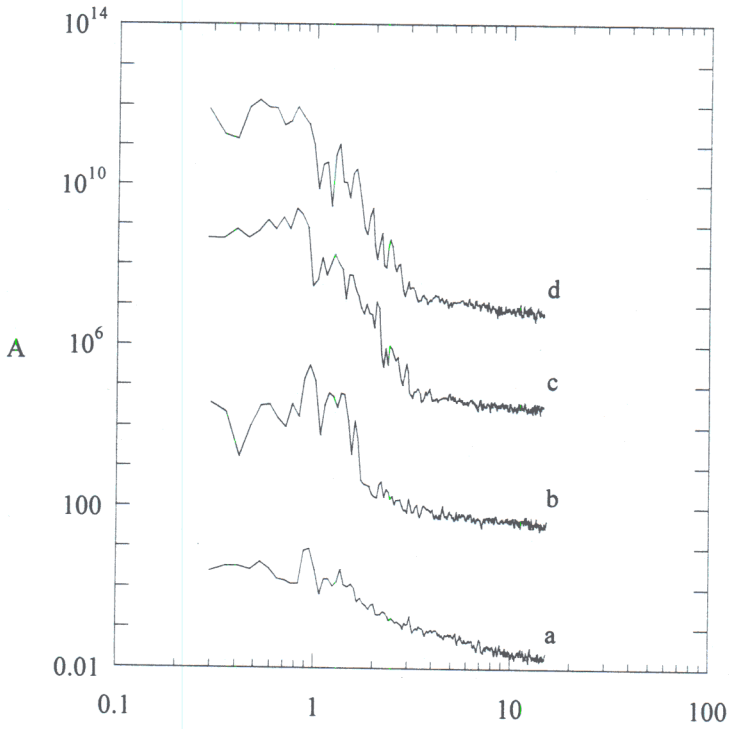

Figure 9. Unforced surface temperature power spectra for q''_2 and θ_3 at x= (a) 19.9, (b) 28.2, (c) 35.7, (d) 42.8 cm.

IV. Time-Invariant Spanwise Forcing

The characteristics of the unforced flow described above are more evident when spanwise patterns of surface heaters are used to force the streamwise instability. For the cases below, a single surface actuator is 0.64 cm wide and extends between 3<x<12.2 cm. A given spanwise waveform is created by driving electrical current through any number of these surface heaters.

IV.1 The Effect of Surface Heaters on Streamwise Vorticity

The streamwise (x) component of the vorticity equation is:

$$\frac{\partial \Omega_x}{\partial t} + u\frac{\partial \Omega_x}{\partial x} + v\frac{\partial \Omega_x}{\partial y} + w\frac{\partial \Omega_x}{\partial z} = \Omega_x \frac{\partial u}{\partial x} + \Omega_y \frac{\partial u}{\partial y} + \Omega_z \frac{\partial u}{\partial z} - g\beta \sin(\theta)\frac{\partial T}{\partial z} + \nu \nabla^2 \Omega_x \quad (1)$$

At the wall (y = 0) for a steady flow this equation becomes:

$$g\beta \sin(\theta)\frac{\partial T_s}{\partial z} = \nu \frac{\partial^2 \Omega_x}{\partial^2 y} \quad (2)$$

Thus, the magnitude and sign of the streamwise vorticity production at the wall depends on the spanwise temperature gradient. Therefore, it is anticipated that streamwise vorticity can be generated (or cancelled) by establishing spanwise temperature gradients along the surface. If the change of viscosity with temperature is significant, then this equation can be modified:

$$g\beta \sin(\theta)\frac{\partial T_s}{\partial z} + \frac{\partial \nu}{\partial T_s}\frac{\partial T_s}{\partial z}\frac{\partial^2 \nu}{\partial y^2} = \nu \frac{\partial^2 \Omega_x}{\partial^2 y} \quad (3)$$

Thus, even without the influence of a wall-normal force, streamwise vorticity can be generated if the change of viscosity with temperature is substantial or the spanwise temperature gradient is large.

IV.2 Forcing Amplitude

To quantify the forcing amplitude of the actuators the variable Q_r is introduced as:

$$Q_r = \frac{\int q''_a(z) L_a dz}{\int q''_s L_{ea} dz}$$

where q''_a and L_a are the actuator heat flux and streamwise length respectively, and q''_s and L_{ea} are the surface heat flux and streamwise location of the downstream edge of the actuator. The integral is taken over one cycle of the spanwise forcing period. Since the actuator heat flux input is nominally a square wave of amplitude q''_a, the above expression evaluates to:

$$Q_r = \frac{q''_a(z) L_a DC}{q''_s L_{ea}}$$

where DC is the forcing waveform spanwise duty cycle. Note that Q_r is a measure of the input disturbance energy relative to the base flow energy at the streamwise location x_{ea} of the actuator. The functional form of Q_r is necessary for scaling the disturbance input energy since the relative forcing amplitude decreases with x relative to the energy in the base flow because of the continuous streamwise heating.

Most measurements were made with a fixed actuator power dissipation of 0.870 W, but because a variety of different heat flux and waveform duty cycles are investigated, the non-dimensional forcing amplitude will vary between cases ($0.12<Q_r<0.3$ for most cases shown).

IV.3 Thermal Transport

As with the unforced flow, composite surface temperature maps were created for the forced flow. Figures 10 a-c show the normalized surface temperature at inclination angles 14, 19 and 24

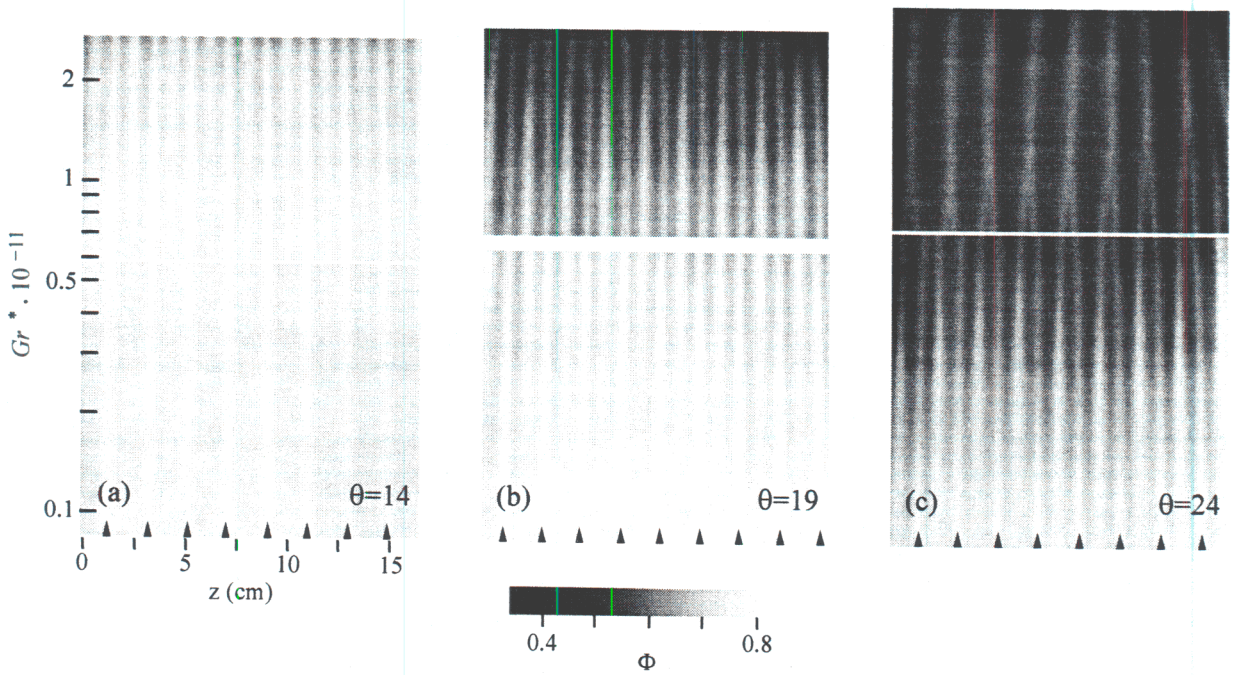

Figure 10. Forced dimensionless temperature maps for $q'' = 2260$ W/m^2 and $\theta = 14°$ (a), $\theta = 19°$ (b) and $\theta = 24°$ (c). Arrows mark the spanwise location of the surface heater actuators.

degrees and $q"= 2260\ W/m^2$ with a spanwise forcing wavelength of λ=1.9 cm , DC = 1/3 and Q_r =0.16. In all three cases, a spanwise periodic waveform is established in the surface temperature, with the magnitude of the variations increasing with inclination angle and streamwise distance. At θ=14^0, only minor changes occur in Φ. For θ=19^0 and θ=24^0 there are large spanwise fluctuations noticeable as well as a general decrease in Φ with increasing x, indicating a higher spanwise averaged Nusselt number Nu_x. Although in each case, the forcing is at λ=1.9 cm (marked by the black arrows), it is clear that a waveform of λ=0.95 cm evolves. This harmonic (in wavenumber) to the forcing wavenumber is not initiated by a temperature gradient at the surface but is an artifact of the flow established by the forced streamwise vortices. The spanwise spectra (Figure 11) of the θ=24^0 case shows the distribution of spectral power A with k_z^*, the disturbance wavenumber multiplied by the forcing wavelength. By defintion $k_z^* = 1$ is the wavenumber being forced. We see from curve (a) that even as far upstream as x=18.6 cm the 1st harmonic of the forced wavenumber contains more power than the forcing wavenumber. However, by x= 35.6 cm (c) the forced wavenumber has become dominant because of the regular merging of the temperature peaks in the θ=24^0 case. The merging phenomenom will be discussed in detail in section IV.5.

The spanwise variations that arise in the aforementioned temperature maps are accompanied by a net increase in the heat transfer coefficient. Figure 12a shows the Nu_x, Gr_x^* correlation for various flow conditions, with λ=1.9 cm for all the forced cases. The unforced curves for θ=14^0 and 24^0 are shown for reference by curves f and g. It is clear that the Nu_x increases (by as much as 100%) when forcing is applied and the change in Nu_x intensifies with larger inclination angles (compare curves a,c and e). From the unforced

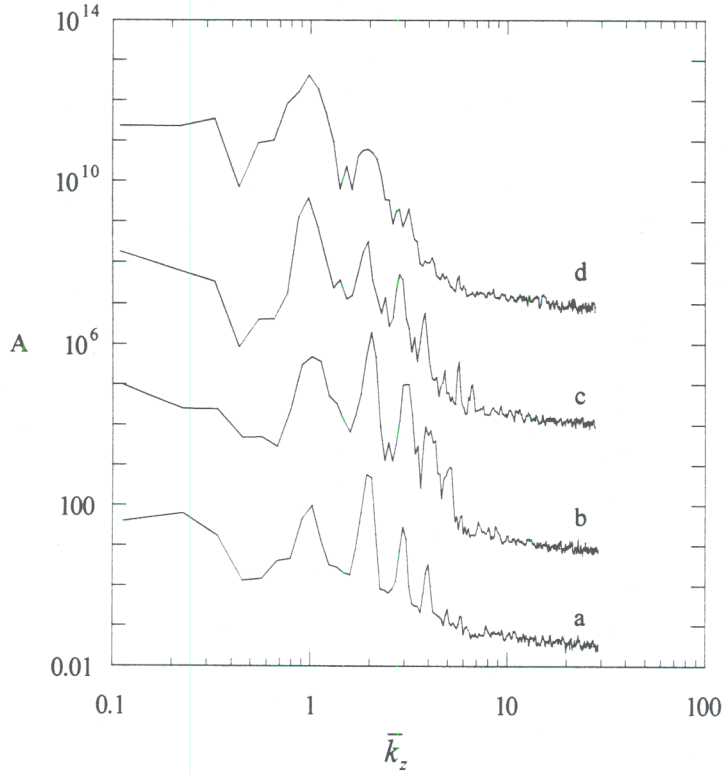

Figure 11. Forced surface temperature power spectra for q''_2 , θ_3 and λ=1.9 cm at x= (a) 18.6, (b) 28.4, (c) 35.6, (d) 42.6 cm.

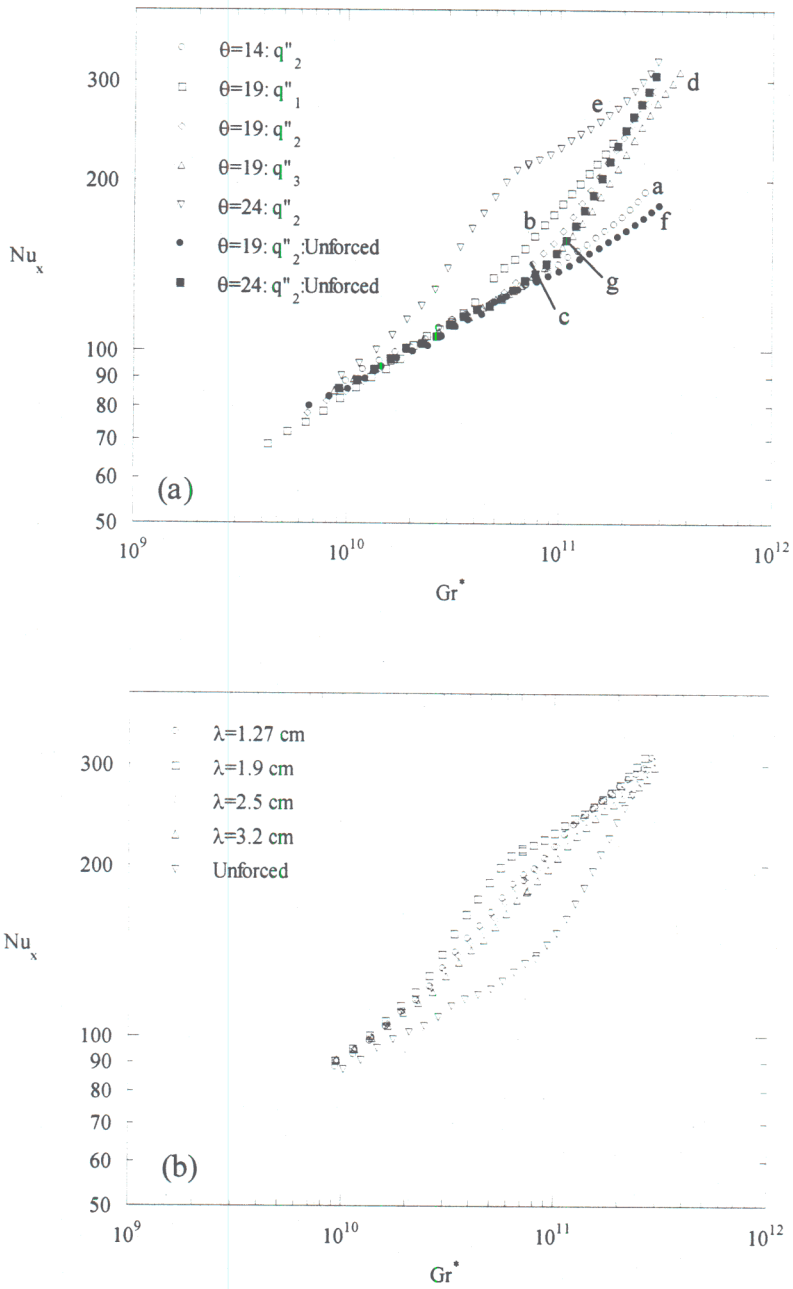

Figure 12. Nu-Gr correlations for (a) fixed λ=1.9 cm, and (b) fixed q"=q"$_2$ and θ=θ$_3$.

data in Figure 5 it was seen that the transition Gr_x^* based on deviations of Nu_x from the 2-D flow does not change substantially with $q"$, but the forced cases (curves b, c and d), show a decrease in the transition Gr_x^* with decreasing heat flux. This is somewhat deceiving since for each experiment the actuator power dissipation was identical, so lower $q"$ cases have higher non-dimensional forcing amplitudes Q_r. Viewed in this way, with all other parameters fixed, the transition Gr_x^* decreases with increasing Q_r. Curves e and g show that the increase in Nu_x of the forced flow relative to the unforced flow is limited to a Gr_x^* range between $1x10^{10}$ and $3x10^{11}$, suggesting that this mode of heat transfer augmentation has a limited range of application.

The dependence of the Nu_x on the forcing wavelength is shown in figure 12b. Even though Q_r for λ=1.9 cm is less than that for λ=1.27 cm (0.16~0.25), the incriment in Nu_x over the unforced flow is maximized by forcing at λ=1.9 cm. This can be partially explained by the larger spanwise RMS surface temperature amplitude and growth rate for the λ=1.9 cm case (Figure 13b).

The variation of the RMS spanwise temperature fluctuations with heat flux and plate inclination angle for a range of spanwise forcing wavelengths is shown in figures 13a and b. Each case exhibits an initial exponential growth indicating that the disturbance amplifies through a linear mechanism. Further downstream, the nonlinear mechanisms dominate causing growth rates to decrease and the disturbance amplitude to decay. From figures 13a it can be seen that the growth rate is strong function of inclination angle but a weak function of heat flux, with the growth rate increasing with $q"$ and θ. However, the characteristic evolution of the disturbance growth, such as the double peak in disturbance amplitude, are retained for different q" at $\theta = 24^0$. This suggests that although the wall heat flux is an important parameter for disturbance growth

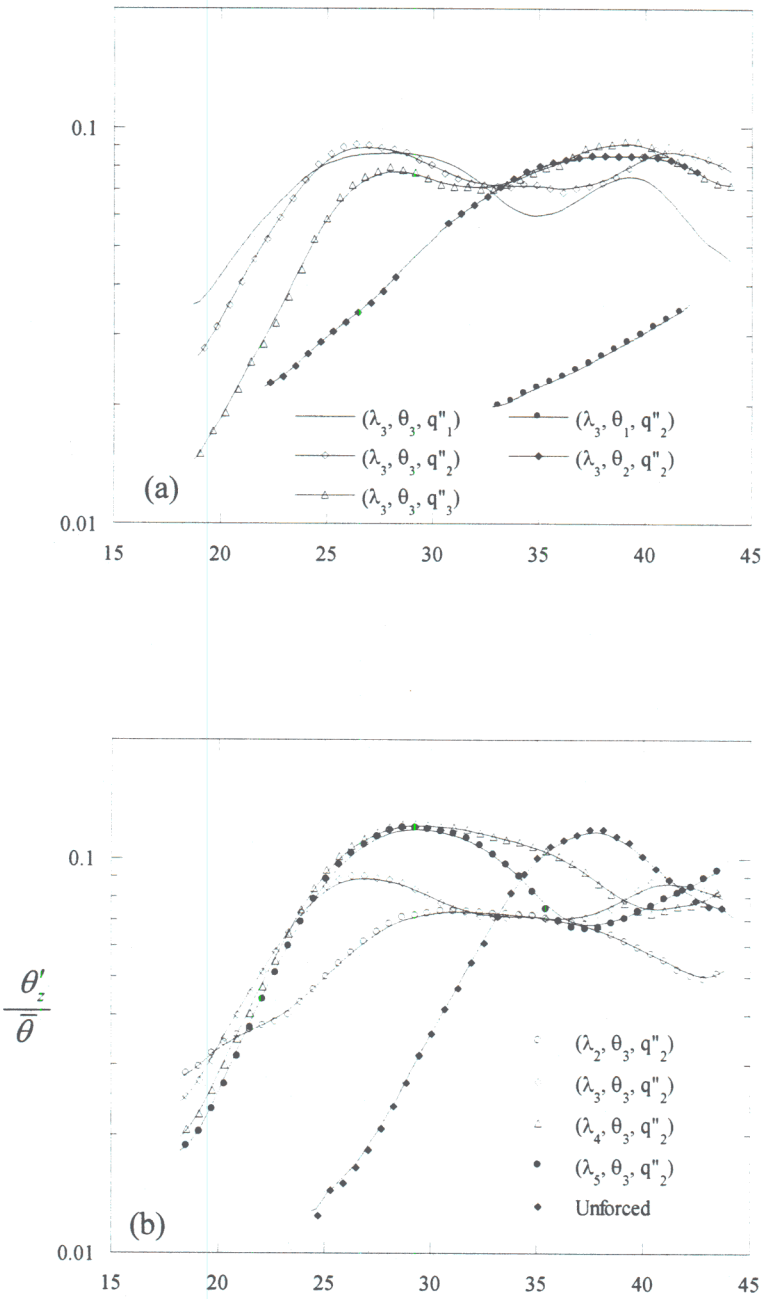

Figure 13. Forced RMS disturbance growth. Change in the disturbance growth rate when (a) inclination angle and (b) forcing wavelength are varied.

(since it drives the flow), it alone does not account for fundamental changes in the transition process (such as vortex merging). Figure 13b shows that, except for λ = 1.27 cm, the growth rates for different spanwise forcing periods are quite similar. The growth rate for the 1.27 cm wavelength case (B=0.08cm^{-1}) is significantly less than for the unforced flow (B =0.21 cm^{-1}), and actually results in an overall smaller peakΦ_z' than the unforced flow (0.075 compared to 0.121). In situations where large spanwise variations in scalar transport are undesirable, (e.g., chemical vapor deposition), passive forcing at an appropriate wavelength could produce more uniform transport than the unforced flow by inducing vortices at a wavelength that undergoes a slower growth rate than the naturally occurring vortices.

The global impact of forcing the instabilities on the streamwise averaged surface heat transfer coefficient can be quantified by defining an average difference Nusselt number:

$$\Delta\overline{Nu}_x \equiv \frac{\overline{Nu}_{xF} - \overline{Nu}_{xUF}}{\overline{Nu}_{xUF}} = \frac{\frac{x}{k}\left[\frac{1}{x}\int_0^x (h_{xF} - h_{xUF})dx\right]}{\frac{x}{k}\left[\frac{1}{x}\int_0^x h_{xUF}dx\right]} = \frac{\int_0^x (h_{xF} - h_{xUF})dx}{\int_0^x h_{xUF}dx}$$

Here h_x indcates an average value across the span, so the bar over the Nusselt number indicates the overall average value for a given streamwis location. By this defintion, $\Delta\overline{Nu}_x$ represents the percentage increase of the forced streamwise averaged Nusselt number relative to unforced average Nusslet number. Figure 14 shows how $\Delta\overline{Nu}_x$ varies with Gr_x^* for several forcing conditions. As seen in curve b, the forced average Nusselt number can be over 20% larger than the unforced average Nusselt number. In each case, $\Delta\overline{Nu}_x$ is zero until the strength of the forced streamwise vortices is sufficient to augment the thermal resistance of the flow. The increase of $\Delta\overline{Nu}_x$ eventually halts at downstream locations where the strength of unforced SWV produces

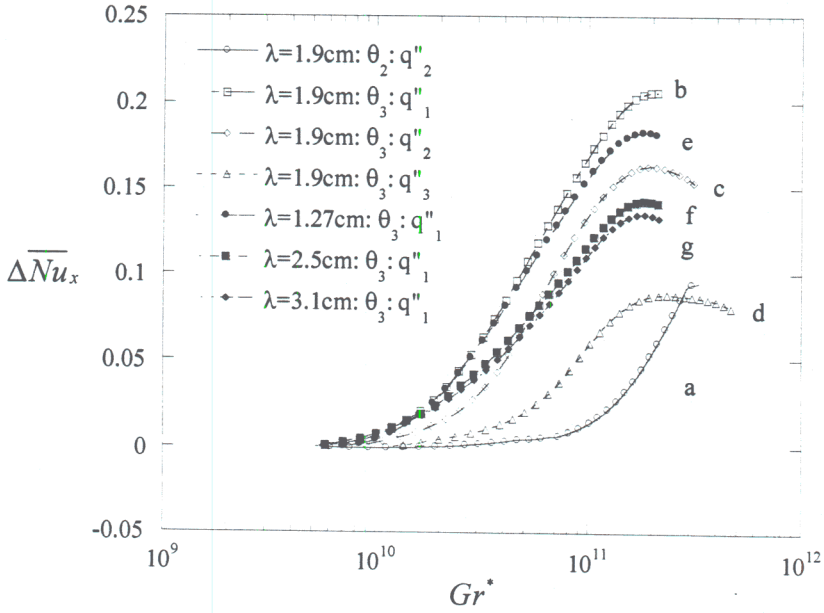

Figure 14. Variation of $\Delta\overline{Nu}_x$ with Gr^* for several forcing conditions.

unforced thermal transport at an equivalent level of the forced flow. It appears from curves b, c and d that $\Delta\overline{Nu}_x$ decreases with increasing surface heat flux, but this is actually an artifact of forcing at a single actuator power. As shown earlier, the unforced Nu_x, Gr_x^* curves for $\theta = 24^0$ are the same for each value of surface heat flux, so the increase in Q_r (Q_r=0.27, 0.17,0.11 for curves b,c and d respectively) produces the increase in $\Delta\overline{Nu}_x$ between surface heat flux conditions. The different forcing wavelengths of curves b, e, f and g reveal that forcing at λ=1.9 cm produces the largest increase in the total average Nusselt number.

It should also be emphasized that the average increase in the heat transfer coefficient depicted in figure 14 is created by dumping additional energy (spanwise periodically) into the flow. This additional energy input is not wasted, however, since it is typically the design goal to remove as much heat as possible at the lowest temperature. In the forced cases, more power is removed from the surface, and at a lower average surface temperature relative to the unforced flow.

The mechanism for the reduction in thermal resistance is the same for both the unforced and forced flow although more graphic in the forced cases. Figure 15a show the spanwise averaged streamwise velocity profile. The similarity to the 2-D profile holds for smaller G^* and θ (curves a,b,d and f), but at higher G^* and θ the profiles lose the similarity with the 2-D verticle solution (curves c,e g and h). The normalized v velocity v^* is shown in figure 15b and indicates that the average entrainment velocity is dramatically increased for cases h, g, and e, and this additional entrainment of lower temperature ambient fluid into the boundary layer raises the Nu_x. The spanwise average dimensionless flowrate $Q^* = Q/(\nu G^*)$ shown in figure 17a depicts the enhanced mixing that can occur. A constant Q^* implies a flowrate similar to vertical

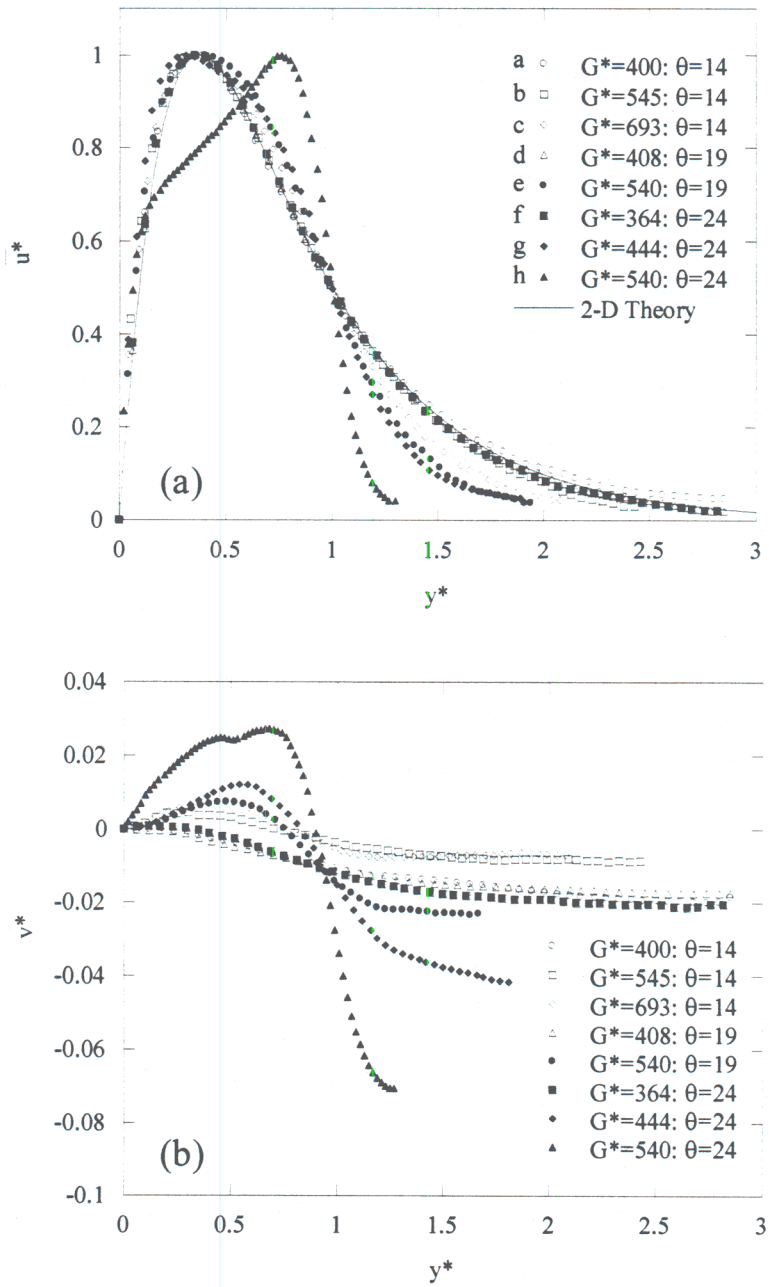

Figure 15. Forced spanwise averaged (a) streamwise and (b) wall normal velocity.

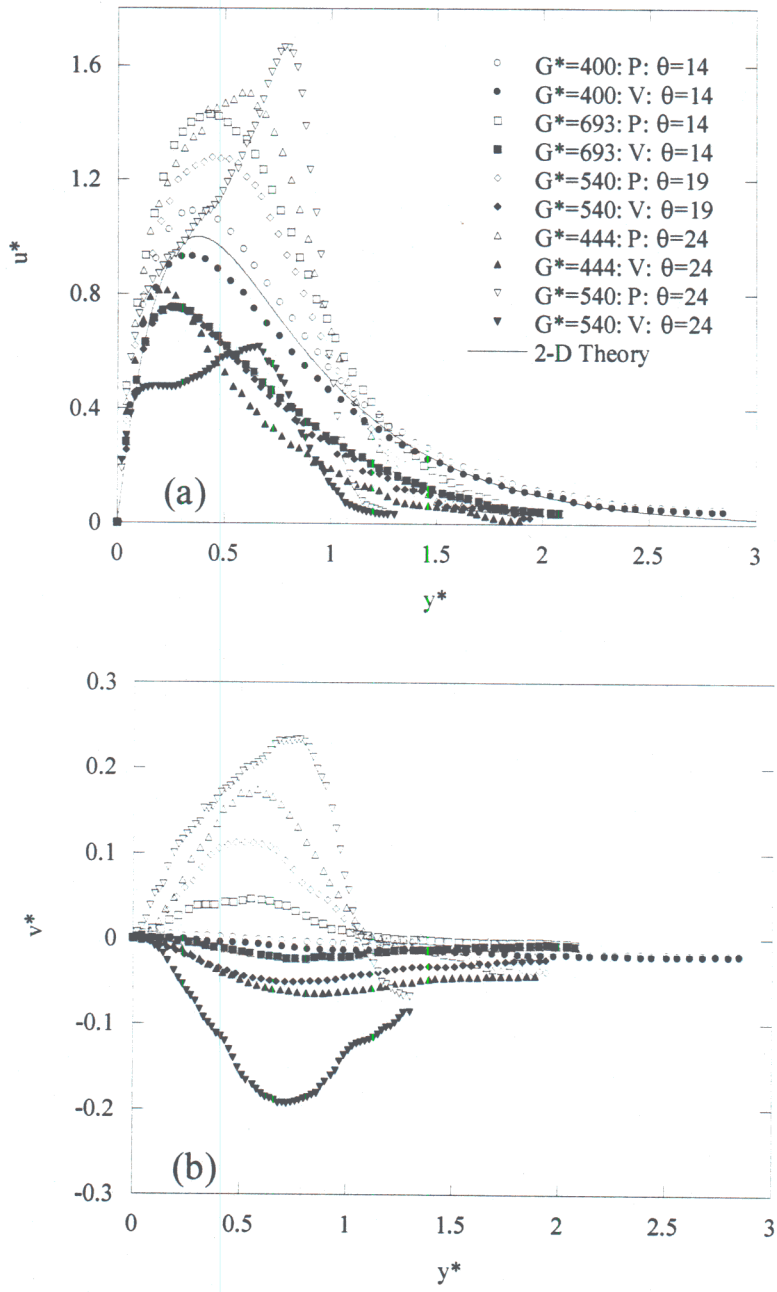

Figure 16. Forced (a) streamwise and (b) wall normal velocity at both a peak and valley of the spanwise disturbance.

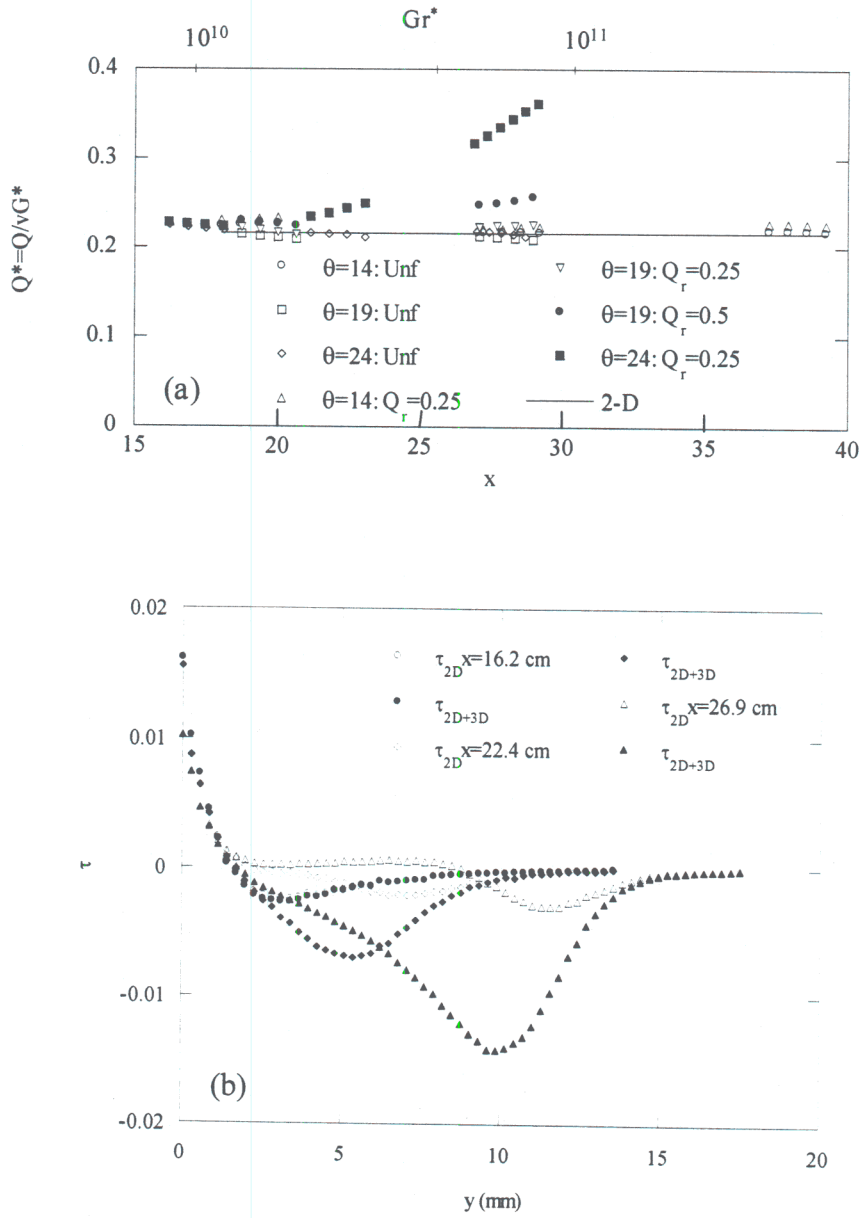

Figure 17. (a) The spanwise averaged dimensionless flowrate Q^* vs. x cm. (b) The 2-D and 3-D shear stress distribution across the boundary layer.

2-D flow (Q^{*}=0.216 for Pr=5.8). For the range of Gr_x^* measured, only the forced flow at $\theta=24^0$, Qr=0.25 and $\theta = 19^0$, Qr=0.5 show appreciable departure from the 2-D flowrate. Note that Q^* for curve (g) begins to deviate from the laminar 2-D solution around Gr_x^* of 1 to $2x10^{10}$, the same location where the heat transfer increases relative to the 2-D flow (see figure 12b). The remaining curves have essentially 2-D heat transfer because additional entrainment of cooler ambient fluid does not occur in this range of Gr_x^*.

The mechanism for the increased mixing, or increased Q^*, can be explained by performing an analysis analogous to Reynolds averaging of the Navier Stokes (RANS) equations, but averaging over the span rather than time. The result is a shear stress $-\rho\overline{u'v'}$ appearing in the viscous diffusion term (u' and v' are spatial not temporal variations). Interpereted this way we can look at the relative importance of the 2-D shear $\mu\,\partial u/\partial y$ and the additional "stress" $-\rho\overline{u'v'}$ induced by the 3-D steady motions. Figure 17b shows both $\tau_{2D} \equiv \mu\,\partial u/\partial y$ and $\tau_{3D} \equiv \mu\,\partial u/\partial y - \rho\overline{u'v'}$ for the λ=1.27cm forcing condition at $\theta=24^0$. In the early stages of the disturbance evoulution, x= 16.7 cm, there is no additional stress created because the v' term is small even though u' levels are significant (~15% , see figure 18 u* rms distribution). But at x=22.4 and 26.9 cm there are large stresses contributed by the 3-D motions at the same level (but opposite sign) as the wall shear stress. This increased stress entrains more ambient fluid into the boundary layer.

The velocity profiles at peak and valley locations of the spanwise variation illuminate how the 3-D stresses are generated (figure 16a and 16b). The u^* values are larger and smaller relative to the average profile at the peak and valleys respectively, and the v^* velocities are primarily positive and negative at the peak and valley respectively. In a valley the v^* velocity drags

relatively low speed fluid toward the wall and at peak higher speed fluid (relative to the averge profile) is pushed outward. This motion creates a net outward momentum transfer by convection rather than diffusion, resulting in more ambient fluid entrainment.

The u^* and v^* spanwise RMS of the disturbance are shown in figure 18a and 18b. The y^* location and value of the $u_z^{*'}$ and $v_z^{*'}$ maximum becomes larger with increasing G^* and θ. The shape of the $u_z^{*'}$ distribution is similar for all conditions shown except for the $G^*>500$ cases at $\theta=24^0$ degrees. At this point the flow has become slightly unsteady, and the spanwise disturbance levels are so large that the base flow is significantly altered from the 2-D laminar form, so the form of the RMS is not likely to conform to the same shape as that during linear growth conditions.

A more subtle characteristic of the surface heat transfer is the change in thermal reistance when the merging of adjacent vortex pairs occurs. The surface temperature maps of figures 19b-d show merging occuring for three different heat flux condtions $q"$=1380, 2260, and 3370 w/m^2. Figure 19a shows the associated Nu_x, Gr_x^* curves for each case where the Nu_x values for $q"$=2280 and 3370 have been multiplied by 10 and 100 repectively. The arrows in the figures mark the Gr_x^* number where there is a definitive shift in the slope of the curves. This Gr_x^* value is shown in each temperature map (b-d) by the dashed line. It appears that the vortex merging has a negative influence on the thermal transport. This can be explained by the fact that the circulation of a vortex before and after merging is not significantly changed, with the inner vortices essentially cancelling. Therefore, after merging there is a reduction in the number of vortices that entrain ambient fluid, so a smaller benfit to heat transfer is observed.

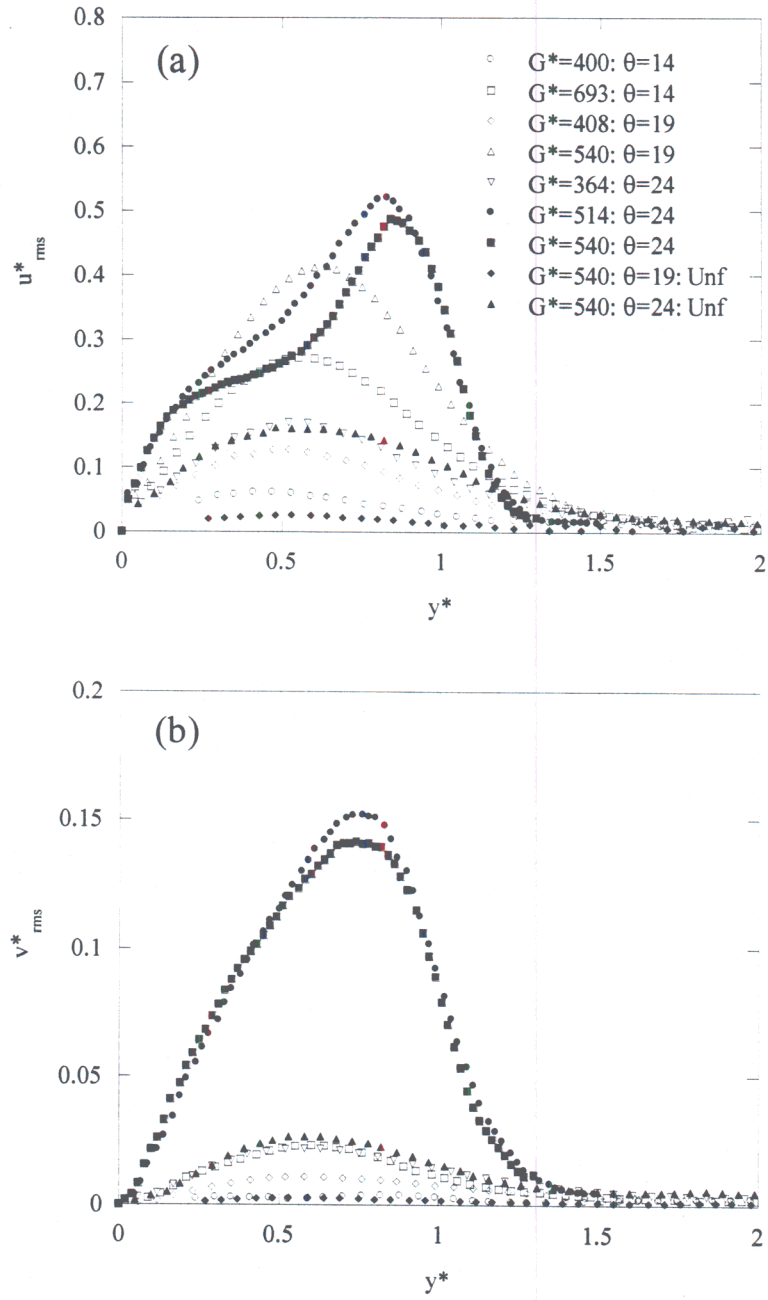

Figure 18. Distribution of the (a) streamwise and (b) wall normal spanwise fluctuating velocity amplitude across the boundary layer.

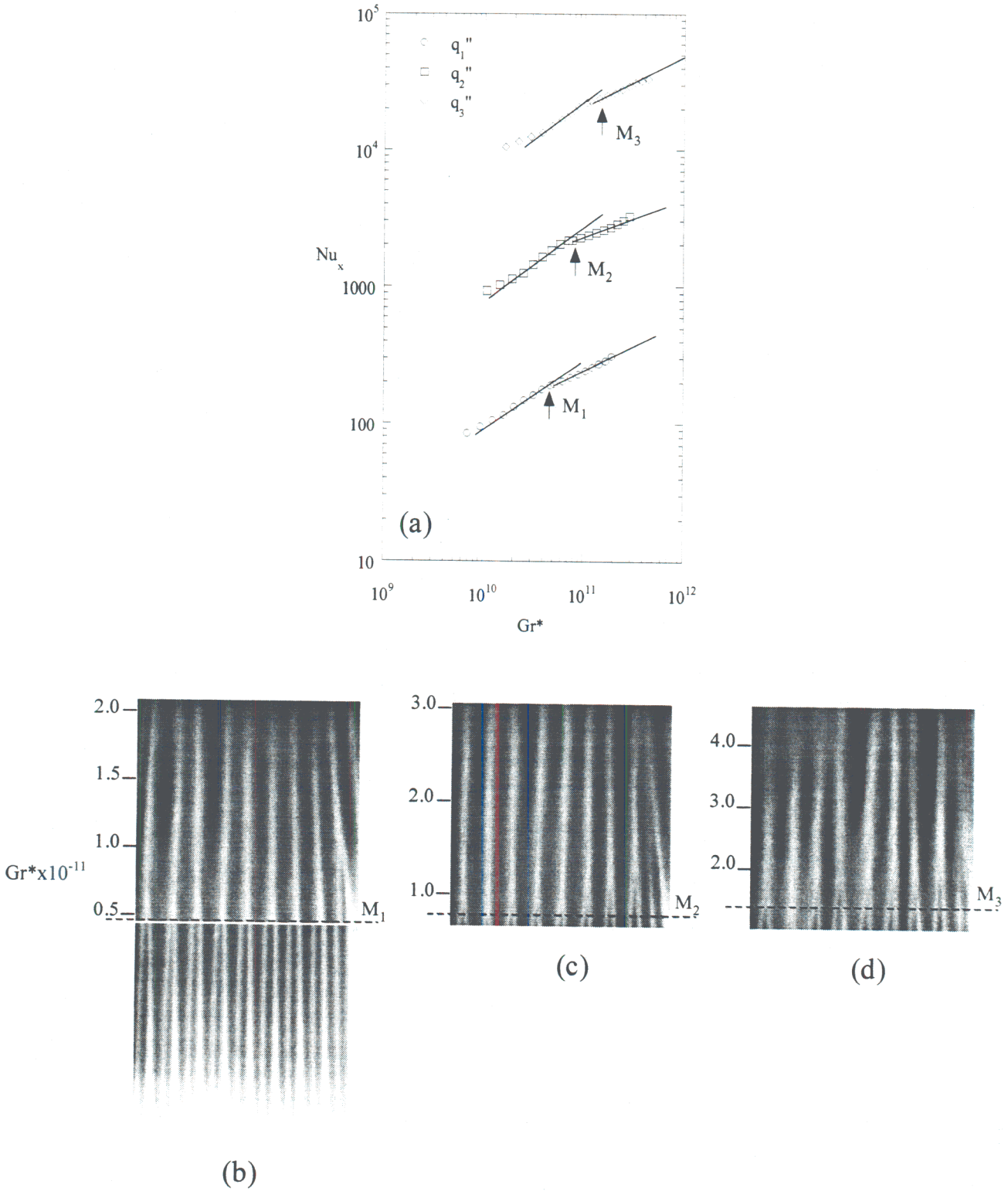

Figure 19. (a) Nu-Gr correlations for θ_3 and λ=1.9cm. Plots (b)-(d) show the associated surface temperature maps with the merging location ($M_{\#}$) indicated by the dashed line.

Since the steady streamwise vortices are reponsible for the augmentation of the thermal transport, it is worthwhile to investigate the evolution and structure of the vortices.

IV.4 Vortex Topology

In order to quantify the strength and growth of the vortices, the circulation of a vortex was calculated using the equation

$$\Gamma = \oint \vec{V} \cdot d\vec{l}$$

where the loop is a rectangle oriented in the y-z plane with the verticle edges of the perimeter constructed of v velocity spanwise peak and valley profiles, and the horizontal edges taken at the wall and outside the boundary layer. The streamwise growth of the vortex circulation is shown in figure 20b for λ=1.27 cm, Q_r=0.25 , θ=14^0 , 19^0 and 24^0 and $q"$=2280 w/m^2. In each case the circulation exhibits exponential growth at upstream stations, and the growth rate of the vortex increases with inclination angle (B=0.121, .207, .328 cm-1 respectively), as did the surface temperature disturbance shown earlier. For the streamwise extent of the data, only the circulation for the θ=24^0 case saturates, starting at approximately x=27 cm. Note that the surface temperature disturbance RMS for this forcing condition begins to saturate at the same location (Fig 13b), indicating the surface temperature yields important information about the state of the 3-D structures in the boundary layer.

The saturation of the circulation effects the thermal transport by fixing the rate that fluid is entrained into the boundary layer relative to the 2-D flow. A constant circulation would cause a linear increase in Q^* with x if the circulation is the only source of additional entrainment over 2-D flow. A closer examination of figure 17a shows that Q^* of curve g is proportional to x for x >

27 cm, while from figure 20b Γ has leveled off at the same location, implying that the circulation is responsible for the increased entrainment at this stage in the flow development.

As the boundary layer thickness is the length scale for the 2-D flow, the height of the vortex from the wall is a prominent length scale of the 3-D flow. Figure 21a shows the distance of the vortex center from the wall y_Γ and $\delta_{1/2}$ as a function of streamwise distance. The center location y_Γ was determined two different ways, firstly by finding the centroid of the $\partial v/\partial z$ distribution, and secondly by using the y location of the v_z^* maximum. The conditions are $\theta=24^0$, $\lambda=1.27$ cm, $Q_r=0.25$ and $q"=2280$ w/m^2. It is seen that initially $\delta_{1/2}$ and y_Γ grow slowly, but at approximately 22 cm there is a distinct change in the growth of both length scales. As the circulation of each vortex grows, the counter-rotating vortex pair lifts from the surface because of the self induced velocity of a vortex pair near a wall. The lifting of the vortex is accompanied by an increase in $\delta_{1/2}$, which in turn is associated with the additional entrainment which also begins at $x \approx 22$ cm. The center of the vortex is between 0.65 and 0.75 of $\delta_{1/2}$ for all x locations, indicating the position of the vortex inside the boundary layer is relatively constant.

The associated slip velocity, $V_s=\Gamma/y_\Gamma$, at the wall is plotted in figure 21b. Clearly there must be an induced sublayer near the wall that cancells the induced velocity, but this layer was too thin to resolve in the current measuremnets. What is of interest is that the slip velocity V_s increases until approximately x=27cm for the conditions above. This implies that the growth of the vortex strength outshadows the lifting of the vortex from the surface until the vortex strength begins to saturate. This slip velocity is another indicator of the heat transfer improvement. As the slip velocity increases, a lower thermal resistance relative to 2-D flow is anticipated, but as V_s saturates, no additional reductions in the thermal resistance are expected. Note that the

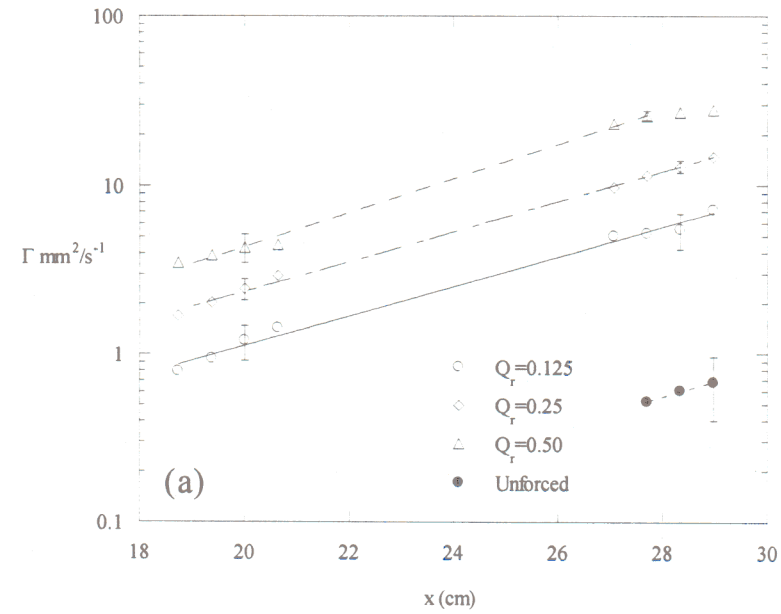

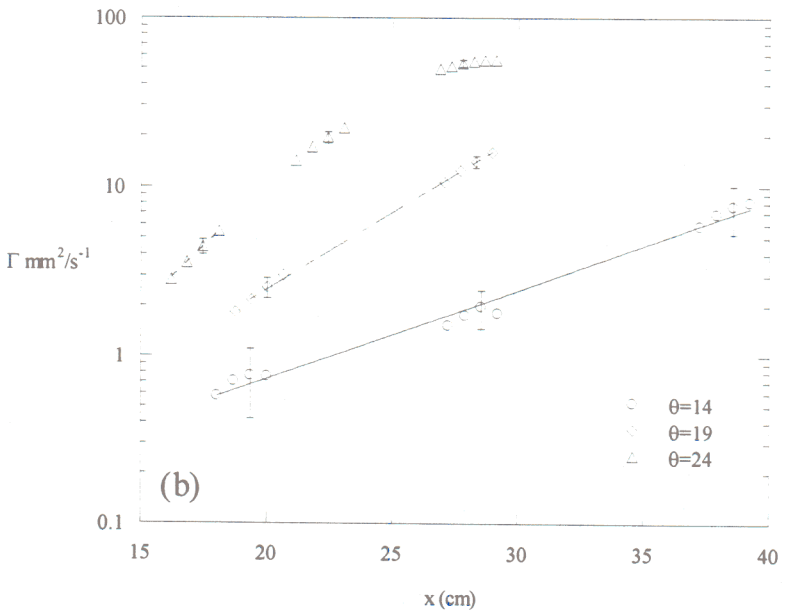

Figure 20. (a) Circulation around a streamwise vortex for q''_2, θ_2 and λ=1.27 cm. (b) Vortex circulation for λ=1.27 cm, q''_2, and Qr=0.25.

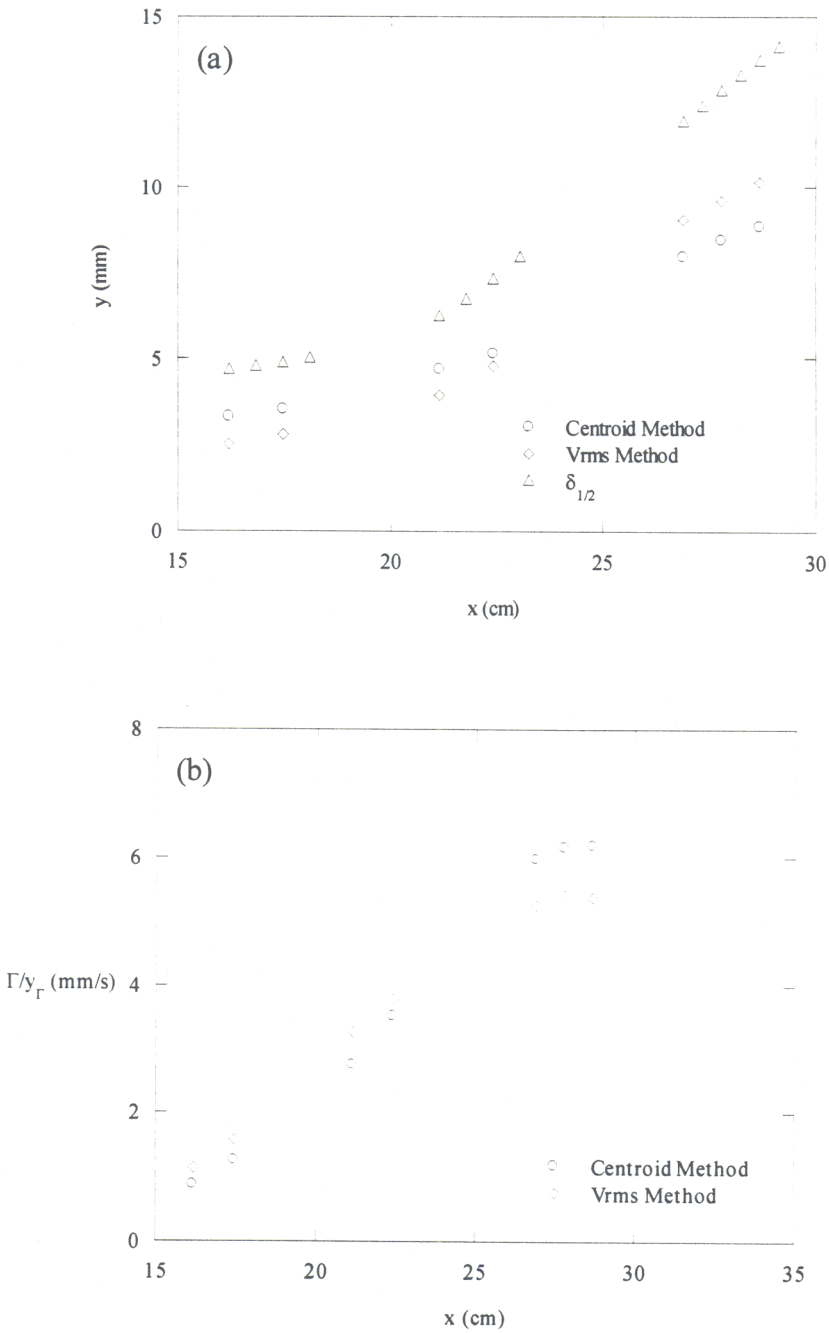

Figure 21. (a) Distance of the vortex center from the wall for conditions $\theta = 24^0$, $\lambda = 1.27$ cm, $Q_r = 0.25$ and $q'' = 2280$ w/m^2. (b) Effective "slip" velocity at the wall induced by the embedded vortex.

location where V_s levels off is the same as when Q^* of figure 17a begins a linear increase with x (at $x \approx 27$ cm).

Vortex circulation also depends on the nondimensional forcing amplitude Q_r. The three curves in figure 20a represent the vortex circulation for three Q_r values. At each streamwise position, increasing Q_r by a factor of 2 likewise increases the circulation by 2, so the magnitude of the circulation input to a given vortex can be written as $|\Gamma| = Q_r A_0 e^{Bx}$, where A_0 and are constant for a given heat flux, inclination angle and actuator location. From Eq. 2, the sign of Γ is dependent on the sign of $\partial T/\partial z$ at the surface. So a vortex of a given amplitude and sign can be created at a specific streamwise location through the proper selection of actuator amplitude and spanwise position (spanwise position determines vortex sign since each actuator produces both positive and negative vorticity). This output relation for the actuator input could be used for the cancellation or enhancement of the streamwise vortices. The vortex enhancement has previously been discussed, and the cancellation discussion is left to section IV.6.

It was found that the contribution of the $\partial w/\partial y$ term to the streamwise vorticity was small compared to the $-\partial v/\partial z$ term. The w velocity is not actually measured, but the importance of the $\partial w/\partial y$ term is found by looking at the expression $(\oint \vec{V} \cdot d\vec{l} - \int_A (-\partial v/\partial z) dA) / \oint \vec{V} \cdot d\vec{l}$. The contour integral about a y-z plane rectangle is completely measurable since the w velocity is zero at the walls and in the ambient fluid. So the above ratio is the fraction of circulation contributed by the w velocity component. It was found that this fraction was between 10-20%, suggesting that the structure of $-\partial v/\partial z$ is likely very similar to that of the streamwise vorticty Ω_x. By looking at contours of $-\partial v/\partial z$ it was determined that the aspect ratio of the vortices is AR=height/width=1.7 ± 0.2, and is relatively insensitive to inclination angle. An AR greater

than 1 suggests that the $-\partial v/\partial z$ term is more significant than the $\partial w/\partial y$ term. For these reasons, contours of $-\partial v/\partial z$ are henceforth used to represent the structure of the spanwise vorticies.

IV.5 Vortex Merging

Under certain circumstances a number of streamwise vortex pairs will merge together. The importance of the merging event on thermal transport has already been described, so information about the merging process and location is valuable. For the following cases a controlled spanwise periodic disturbance in the surface heat flux is introduced 3.3 cm downstream of the heater origin. Figure 22b-c show the ensuing merging patterns that may occur during a merging event (figure 22b is typical).

In general, merging will be observable when the amplification rate of the streamwise vortices is large enough to promote rapid growth of the vortices before the base flow is overcome by temporal disturbances. A nonlinear stability analysis for a natural convection flow over an inclined flat-plate at constant wall temperature (Chen *et al.*1991) predicted that the primary streamwise vortices merge at a fixed Reynolds number $\tilde{R}_{1/2}$, where $\tilde{R}$ is defined as $\tilde{R}=GTan(\theta)$. Chen *et al.* claim that merging occurs at a fixed $\tilde{R}_{1/2}$, with $\tilde{R}_{1/2}$=41 for Pr=5.8.

Figure 22 shows the merging location $\tilde{R}_{1/2}=G^{*}_{1/2}Tan(\theta)$ for two heat flux values $q"$=2130 w/m^2 (closed symbols) and $q"$=2870 w/m^2 (open symbols) at several forcing amplitudes as a function of inclination angle for λ=1.9 cm and a waveform duty cycle of 2/3. For each forcing amplitude, $\tilde{R}_{1/2}$ is approximated well by a horizontal line, indicating that constant $\tilde{R}_{1/2}$ predicts the merging event well for a fixed Q_r. As Q_r decreases, the $\tilde{R}_{1/2}$ value increases, and the fit of a horizontal line to the data becomes better. This indicates that the prediction of a constant

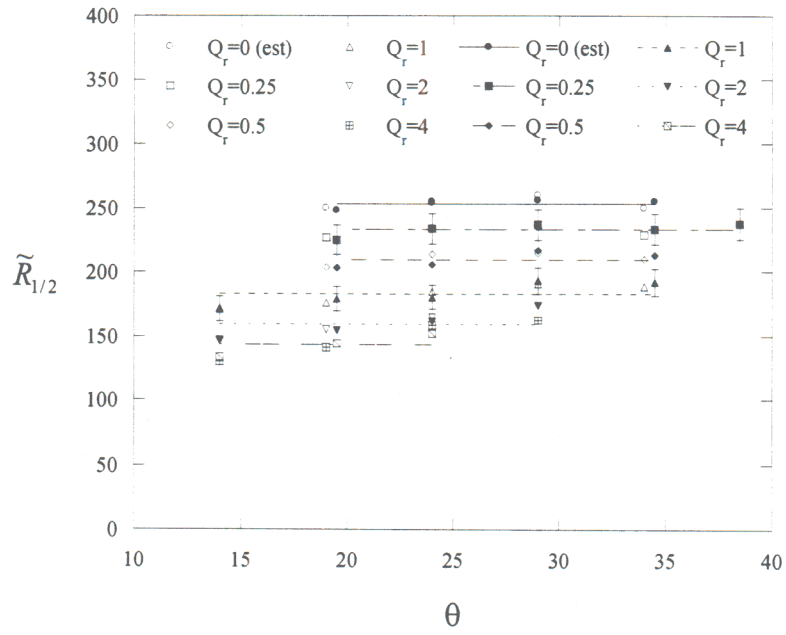

Figure 22. The merging location $\widetilde{R}_{1/2}$ for $q"$=2130 w/m^2 (closed symbols) and $q"$=2870 w/m^2 (open symbols) at several forcing amplitudes as a function of inclination angle for λ=1.9 cm and a waveform duty cylce of 2/3.

merging Reynolds number is more accurate for smaller amplitude disturbances. The $Q_r = 0$ line was extrapolated from the forced data since unforced merging does not occur uniformly, a property not suffered in the forced cases. The $\widetilde{R}_{1/2}$=250 for the $Q_r = 0$ line represents the critical Reynolds number for merging in an unforced, constant heat flux flow. Unfortunately, to the best of this authors knowledge, no theoretical results on merging location have been presented for the constant heat flux plate. At best a comparison can be made to the theory of Chen *et al.* by converting $\widetilde{R}_{1/2}$ of a constant heat flux plate to that for a constant temperature surface. Doing this yields a constant surface temperature $\widetilde{R}_{1/2}$ of 150 (based on merging occurring at Nu_x=200), which is still significantly higher than predicted by theory.

At a merging event, the fundamental streamwise rolls lose their identity. Figure 23a shows the power contained at selected spanwise wavenumbers as a function of $\widetilde{R}$ for λ=1.9 cm (k_z^*=1, k_z=0.53 cm^{-1}). Because the forcing waveform has a duty cycle of 2/3, it contains most of its power at k_z^*=1 (mode 1) but has significant power at k_z^*=2 (mode 2) as well. From figure 23b it can be seen that the merging process does not occur abruptly, but rather over several vortex wavelengths in the streamwise direction. As two vortex pairs approach each other, the spanwise separation decreases, and eventually the mode 2 wavelength rapidly decays. As the separation continues to decrease, the higher wavenumbers also begin to decay abruptly. This process explains the cascade of notches in the spectra at successively higher wavenumbers as the merging event evolves. A good indicator of the completion of merging is the streamwise location of the notch for the largest wavenumber observable above the noise. It should be noted that these notches are not as clear in the unforced flow in general (but do exist) since the vortex merging does not occur uniformly across the span.

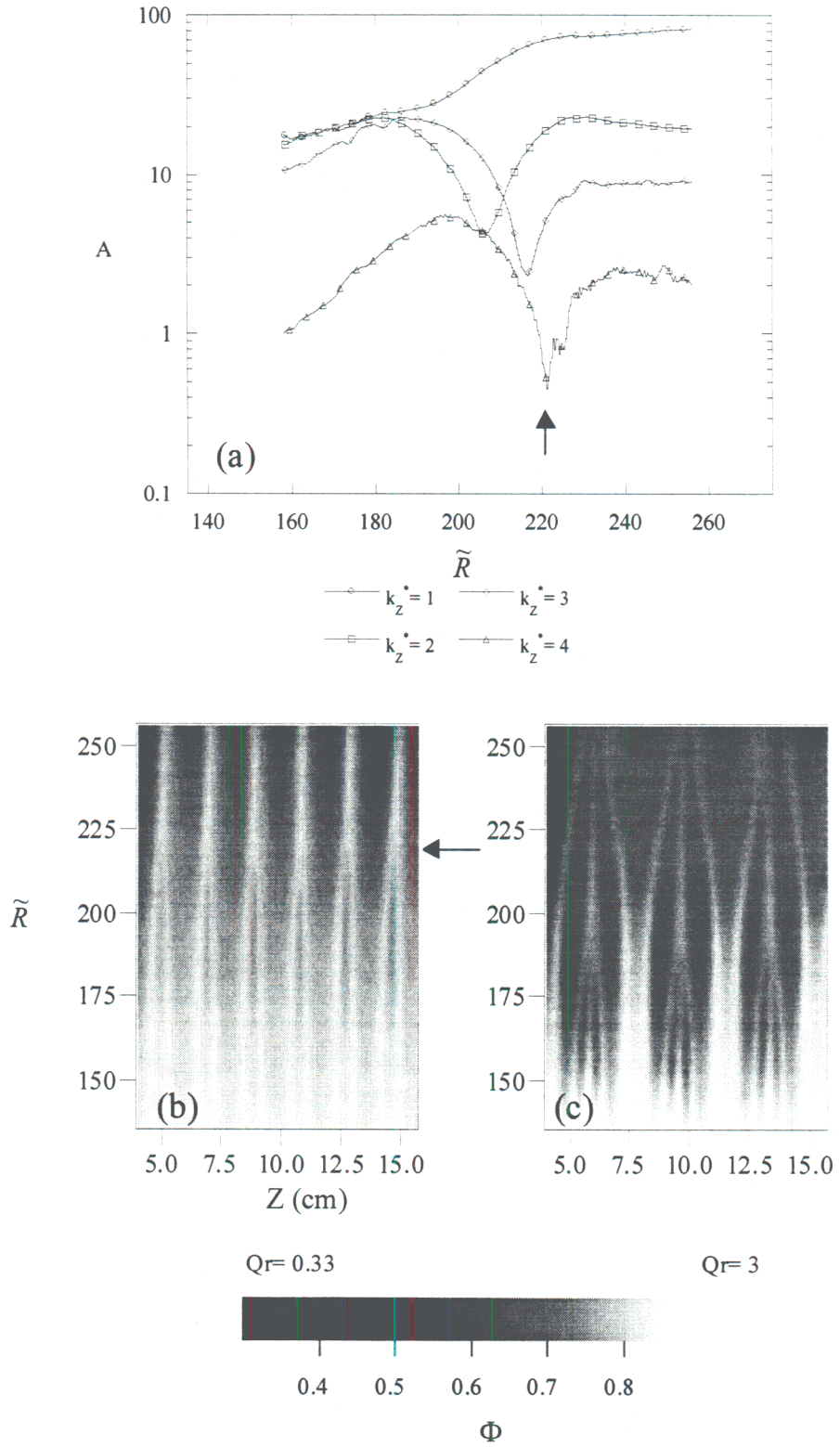

Figure 23. (a) Streamwise dependence of the surface temperature spectral amplitude for $k_z^* = 1,2,3$ and 4. (b) The surface temperature map that generates plot (a). Map (c) is an extreme example of merging patterns possible.

The spectra provide some indication of the transfer in energy between mode 1 and mode 2 during the merging process. For the case shown in figure 23b, both the modes are forced and initially there is growth in the harmonics of the forcing as the streamwise vortices extract energy from the mean flow. But by $\tilde{R}$=185 the fundamental component k_z^*=2 begins to lose energy as the merging process begins. At this stage of development, the growth rate in mode 1 increases since it now gains energy not only from the mean flow but also from mode 2 and higher modes in the flow. The power in the higher modes in turn decreases, as the their power is transferred to mode 1.

The hydrodynamic details of a merging event are revealed through PIV velocity measurements for the conditions $\theta = 24^0$, $q"$=2280 w/m^2, λ=1.9 cm and a waveform duty cycle of 2/3. Figure 24 a-g show contours of $-\partial v/\partial z$ (0.15 s^{-1} increments) before, during, and after a merging event. At $\tilde{R}$=178 (x=23cm) four distinct vortex pairs can be identified. The merging process begins at $\tilde{R}$=190 (x= 24.8 cm) with vortex 3 and 7 being lifted and drawn into vortices 1 and 5 respectively as $\tilde{R}$ varies from 190 to 215 (x=27.8cm). Similarly vortices 2 and 6 are pulled into vortices 4 and 8 respectively, producing a net CCW rotation of the inner pair of each 4 pair vortex group. By $\tilde{R}$=215 (x= 27.8 cm) the merging event is nearly complete. Shortly after merging these vortices begin to break up, proceeding first through a sinuous temporal mode before shredding into small fragments.

Although the mechanism for the vortex breakdown is not clearly known for this flow, there are some similarities in the breakdown with other flow geometries where breakdown is observed. Firstly, the swirl number S=Γ/Q reaches levels of 0.3 to 0.35 before decaying because of the vortex breakdown (figure 25). Secondly , the sinuous (spiral) mode mentioned above occurs in the vortex breakdown on delta wings (Lambourne & Bryer (1961). This mode of breakdown is

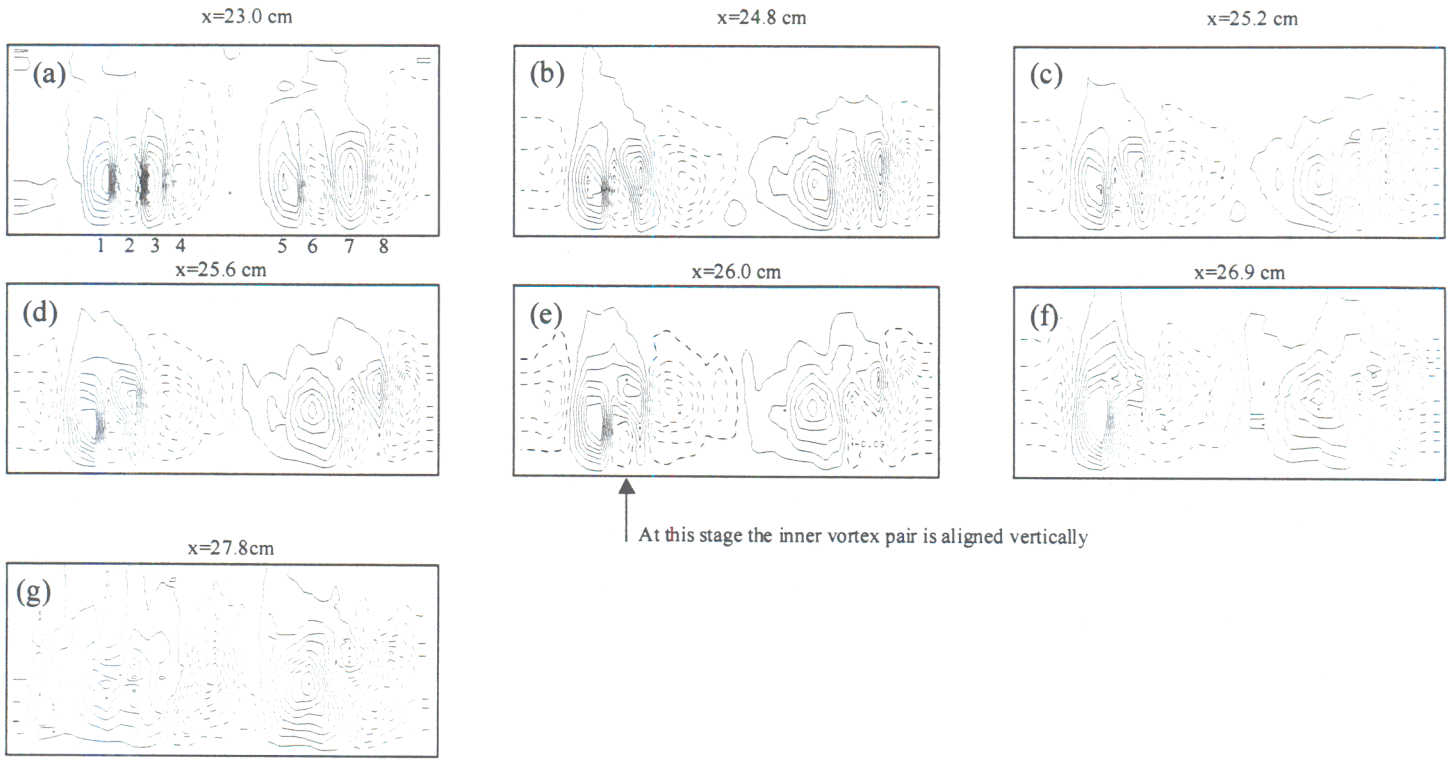

Figure 24. Contours of $-\partial v/\partial z$ (0.15 s^{-1} increments) before, during, and after a merging event. At $\tilde{R}$ = (a) 178, (b) 190, (c) 192, (d) 194, (e) 196, (f) 202, (g) 215 .

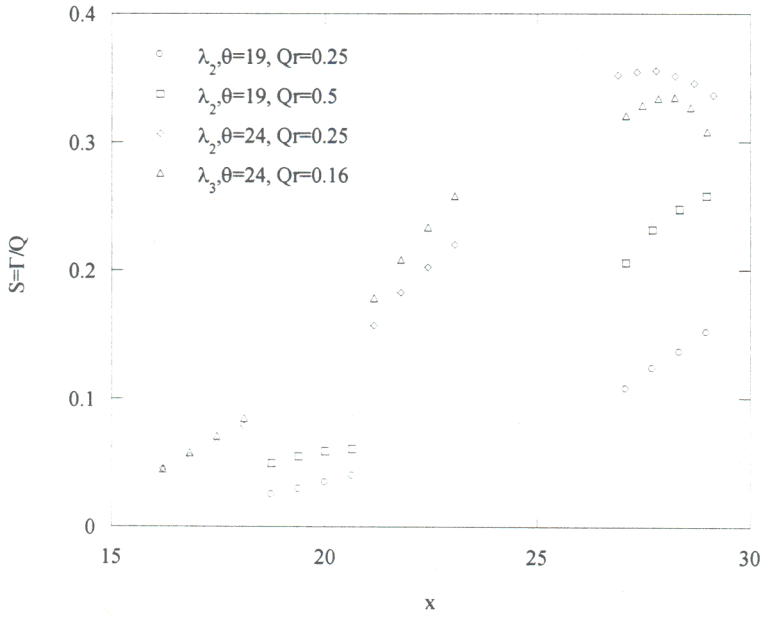

Figure 25. Streamwise dependence of swirl number at several inclination angles and forcing amplitudes.

anticipated since the swirl increases continuously from zero with streamwise distance, and since a spiral breakdown pattern is associated with the minimum swirl necessary for breakdown (Sarpkaya (1971)). It has furthermore been noted (Hall (1972)) that flows containing unsteady disturbances breakdown in a spiral pattern. The mechanisms and additional details on vortex breakdown will be discussed in more detail in an upcoming paper involving time-dependent 3-D forcing of the boundary layer

IV.6 Controlled Cancellation of Flow Instabilities

As mentioned in section **I**, one of the goals of the present research is to implement a control scheme that can be used to stabilize the flow and delay the evolution of the streamwise instability. As a proof of concept for using the surface actuators as control actuators for suppressing streamwise vortices, a system of streamwise vortices having a spanwise wavelength of 1.27 cm was forced into the boundary layer with an upstream row of actuator elements (x=3.3 cm). The corresponding surface temperature distribution for this case is shown in Figure 26a. Because the origin of the disturbance was known *a priori*, a second row of actuators fixed in space could be used to cancel the input disturbance. The cancellation actuators were activated 4.26 cm downstream spatially out of phase from the disturbance actuators. This open loop cancellation showed very promising results as can be seen in figure 26b. The spanwise variations are almost entirely cancelled along the entire measurement area starting at 25 cm downstream from the cancellation actuators. A plot of the spanwise variations is shown in figure 26c at x = 39 cm. The peak to peak spanwise variations in temperature are decreased by a factor of four with the cancellation actuators activated.

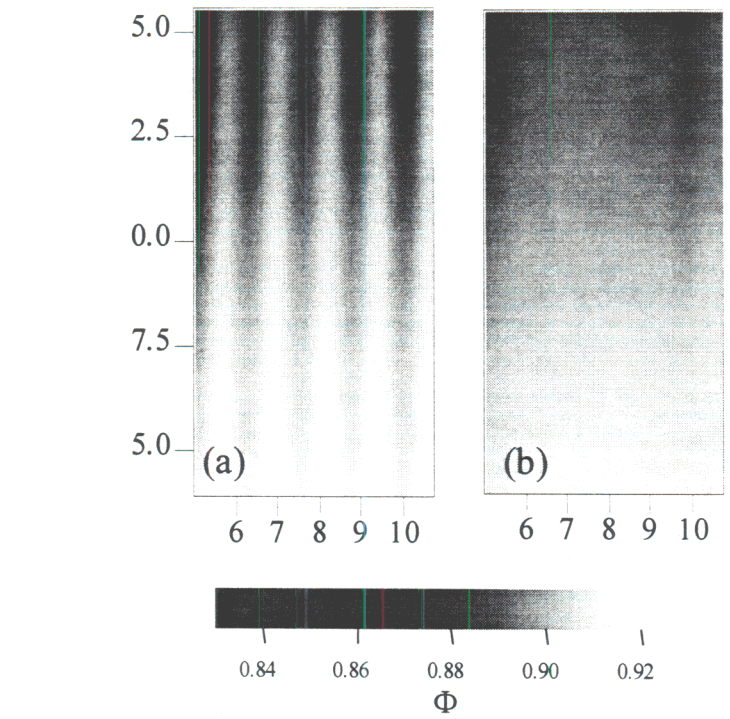

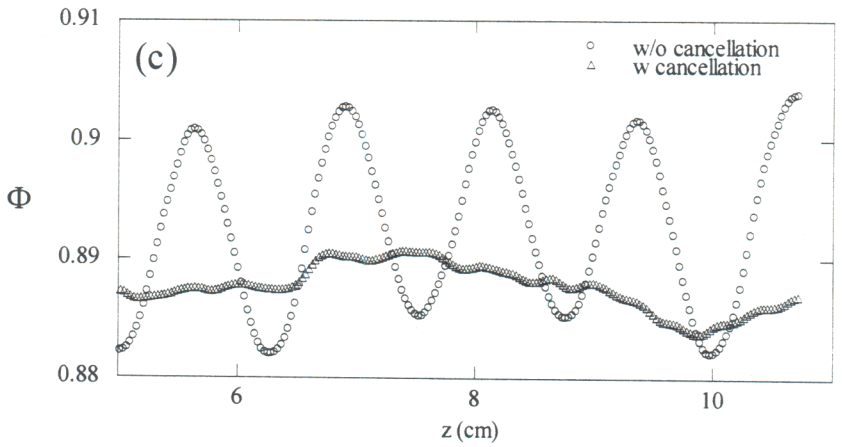

Figure 26. Surface temperature maps for flow (a) without and (b) with cancellation actuators activated. Plot (c) shows the spanwise distribution of surface temperature with and without cancellation at x = 39 cm.

A more practical control scheme would be to control spanwise variations on the average. The problem then becomes a stochastic control problem. The idea is to not be concerned about the instantaneous variations in spanwise transport, but to use the actuators to reduce time-averaged spanwise variations measured over an appropriate time period. The surface actuators could be quite effective in this type of control approach. The present research has demonstrated that the actuators can lock the streamwise vortices to the forcing wavelength, and that a broad range of spanwise wavelengths can be introduced. A rather simple control scheme can take advantage of these forcing characteristics. Initially, a periodic array of actuators generates a system of streamwise vortices locked to the spanwise forcing wavelength of the actuators. This creates a non-uniform but predictable spanwise variation of the surface heat transfer. The actuators then shift 180° spatially out of phase from the original forcing program locking the streamwise vortices 180° out of phase from the initial system. This would have the effect of reducing spanwise heat transfer non-uniformity in the mean. Furthermore, other wavelengths could be introduced in order to remove residual spanwise variations.

V. Time-Dependent Excitation

Previous work by other investigators has demonstrated that for inclination angles smaller than 11°, the base flow is primarily dominated by a 2-D instability while for inclination angles larger than 17° the primary instability mode is three-dimensional and leads to the evolution of streamwise vortices. Because both modes of instability are present when the inclination angle is between 11° and 17° this range is exploited to study the evolution of a pulsed, 3-D disturbance with and without the presence of streamwise vortices.

V.1 Wave-Packets at Shallow Inclination Angles

A wave-packet is introduced into the natural convection boundary layer by generating a short pulse from a single surface actuator. The disturbance generated in this manner contains energy in a broad band of frequencies and spanwise wavenumbers, however, the base flow is only receptive within a relatively narrow band and, as a result, frequencies and wavenumbers outside of this band are attenuated. The most unstable modes can be identified from the spectral content of the wave-packet.

Figure 27a shows surface plots of the spanwise temperature (at three streamwise position) as a function of time during the passage of the wave packet at a plate inclination angle of 1^{o} and surface heat flux q" = $1870 W/m^2$. The upstream plot (x = 38 cm) shows approximately 4 periods of small amplitude oscillations, where the wave fronts are nearly normal to the downstream coordinate. At x = 46 cm, the disturbance is amplified significantly and its duration in time is increased by a full period. At the last streamwise station (x = 54 cm), the amplification of the disturbance leads to spanwise distortion of the wavefront, with two distinct symmetrical structures about the centerline.

Corresponding time traces of the surface temperature at the spanwise position of the side peaks (in the x = 54 cm surface plot) and the disturbances centerline are shown in Figure 27b for the same three streamwise locations. At x = 38 and 46 cm the traces at the two spanwise positions are nearly identical indicating only small spanwise variations in the disturbance. However, at x = 54cm, the two traces show drastic differences. The amplitude of the centerline trace is diminished, and is mostly negative, while the trace measured off-centerline exhibits larger peaks and is also shifted in phase relative to the centerline. The phase change suggests that different parts of the packet are moving with different phase velocities. In particular, similar

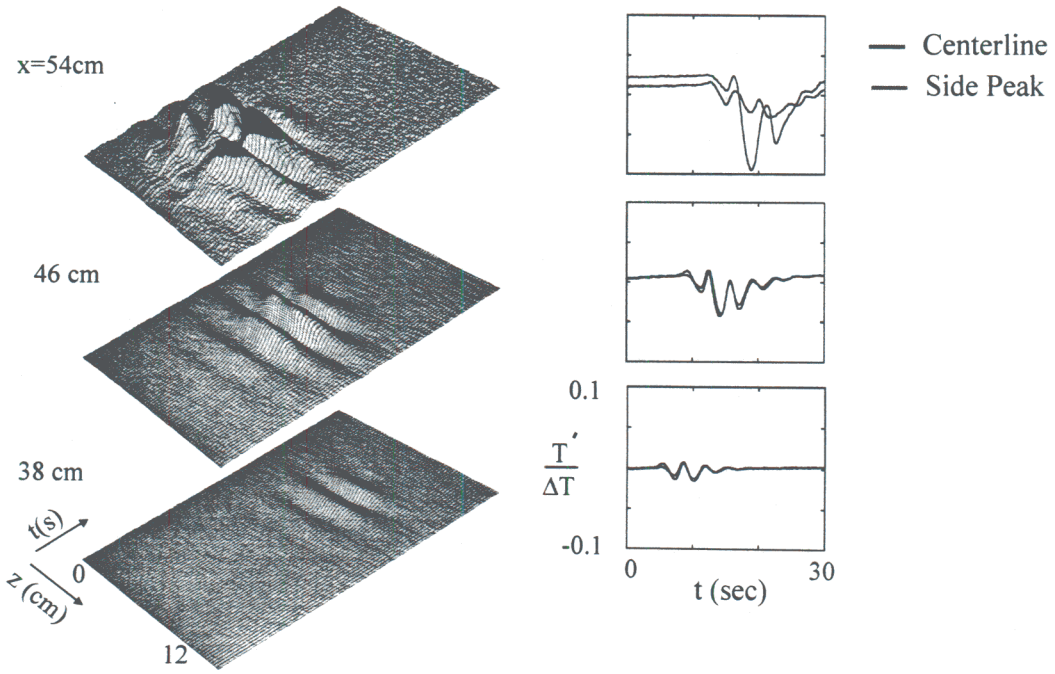

Figure 27. (a). z-t surface temperature map during the propagation of a wave packet at three streamwise locations. (b) Individual time traces at the centerline and off-center of the disturbances in the three cases shown in figure (a).

to a wave packet in a momentum boundary layer, the leading edge of the thermal wave-packet propagates faster than the trailing edge. To quantify the edge velocities, the centerline time traces were plotted at several streamwise positions, as shown in Figure 28. The slope of the lines drawn through the beginning and end of the disturbances approximate the leading and trailing edge velocities respectively. As shown, the leading and trailing edge disturbance velocities are V_{LE} = 2.5 cm/s and V_{TE} = 1.0 cm/s. The ratio of these velocities V_{LE}/ V_{TE} = 2.5 may be thought of as a dimensionless dispersion rate for the wave-packet in a free convection boundary layer. Gaster and Grant (1975) performed a similar measurement for a momentum boundary layer and found V_{LE}/ V_{TE} = 1.2. This implies that the dispersion of the wave-packet in a free convection boundary layer is larger than that in a momentum boundary layer. The increased dispersion may be attributed to the buoyancy force which accelerates the fluid in the free convection boundary layer.

An important feature of the wave-packet evolution is the emergence of spanwise nonuniform structure. Figure 29 shows the spanwise phase variation of the largest spectral (frequency) component of the wave-packet at three streamwise stations. While at x = 38 cm the maximum phase variation across the span of the wave-packet is only 0.5 rad, at x = 51 cm the phase varies by 3.6 rad. This phase variation is a result of the interaction of equal and opposite oblique waves that form the wave-packet. The slope of each curve in figure 29 is equal to the angle of the corresponding oblique waves and it is evident from the increase in slope that the waves angle steepens with downstream distance. The double peak at 51cm curve indicates a split of the single wave-packet into two wave-packets. It appears that at this stage, the large structures on each side of the centerline (e.g., Figure 27) begin to behave like separate wave-packets suggesting a mechanism for spanwise spreading of the instability.

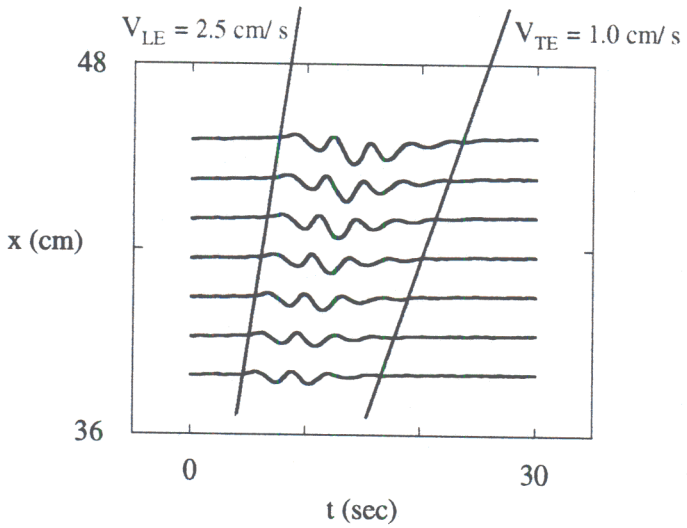

Figure 28. Time traces of a passing wave-packet at several streamwise positions

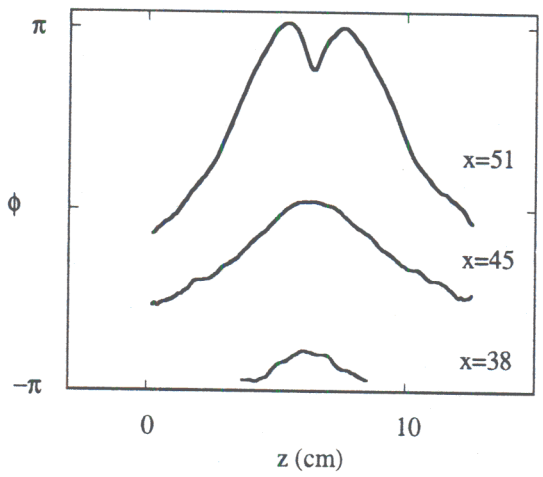

Figure 29. The spanwise variation of the wave-packet temporal phase for the most amplified frequency (f=0.3Hz).

As the wave-packet is advected downstream, energy is transferred to higher spanwise wavenumbers and frequency modes. Figure 30 shows 2-D frequency-wavenumber spectral maps for the wave-packet at three streamwise stations. At x = 38 cm the wave-packet is characterized by a zero spanwise wavenumber and frequency peak of 0.3 Hz, implying that the wave-packet at this stage is nominally two dimensional. At x = 45 cm, there is a transfer of energy to the second harmonic of the primary frequency f_p, and energy is transferred to small non-zero wavenumbers. The second harmonic disappears by x = 51 cm, and lower frequencies emerge as a result of the dispersive nature of the disturbance. Significant levels of energy at nonzero wavenumbers at x = 51 cm, indicate the beginning of breakdown of the wave-packet. The emergence of the subharmonic of f_p at wavenumber $0.3cm^{-1}$ may be attributed to a subharmonic resonance mechanism between f_p and low frequencies which produce the subharmonic ($f_{p1/2}$,+-α_z=$0.3cm^{-1}$). This resonance can only occur if f_p and the subharmonic have the same phase speed ($C=f/\alpha_x$). The measured phase speeds of f_p and its subharmonic were C_{fp} = 1.9 cm/s and C_s = 1.8 cm/s, which strongly supports the existence of the subharmonic resonance mechanism.

V.2 Wave-Packets at Intermediate Inclination Angles

As noted in §V, for inclination angles between 11° and 17°, streamwise vortices and time varying waves can coexist. The objective of the experiments described in this section is to investigate the interactions between these two instability modes and to determine their impact on heat transfer from the plate. Specifically, the effect of a wave packet propagating into a "natural" base flow is compared with that of a wave packet propagating into a base flow that is seeded with a stationary array of counter-rotating streamwise vortex pairs for $\theta = 12°$ and q" = 1870 w/m^2. The spanwise extent of the wave-packet disturbance is measured by considering

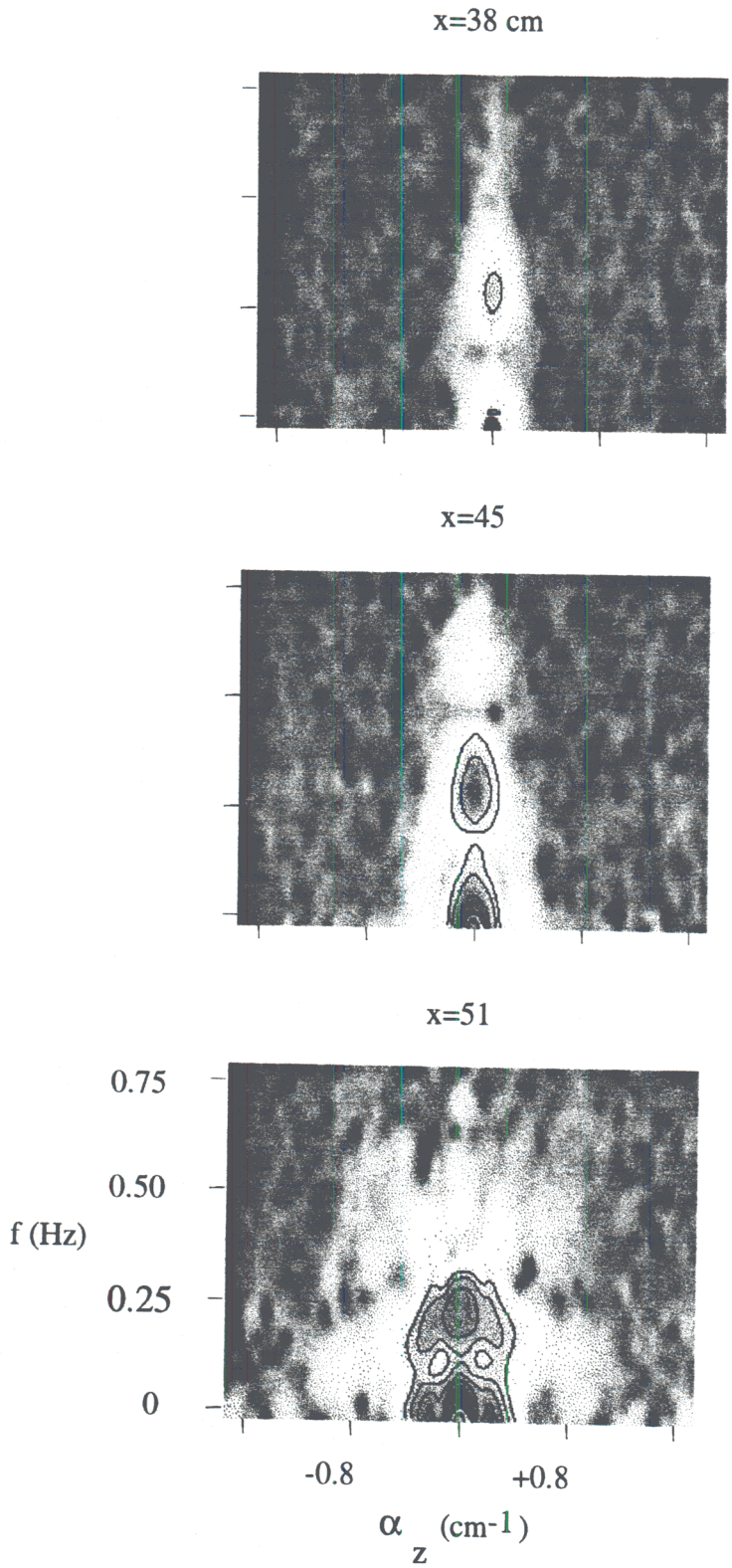

Figure 30. 2-D frequency-wavenumber spectral maps for the wave-packet at x= 38, 45 and 51 cm.

maps of RMS surface temperature fluctuations as the packet propagates through the field of view (Figures 31a and b). Figure 31a shows the base flow with a wave-packet, and 31b shows a wave-packet propagating through a base flow seeded with streamwise vortices. The white contours represent RMS fluctuations of 0.05°C and it is evident that temperature fluctuations are present over a larger region of the span in the presence of streamwise vortices. This rapid spreading of the disturbance results from the interaction between the wave packet and the streamwise vortices. As the packet is advected, the streamwise vortices are locally and temporally distorted or bent in the spanwise direction leading to a "sweep" of the temperature field on the surface of the plate and thus to an increase in the temperature fluctuation levels. It is remarkable however, that despite the increased spatial extent of the disturbance in the presence of the streamwise vortices, spanwise spreading rates (as marked by the red lines on each plot) in the absence and presence of the streamwise vortices are virtually identical. This in turn suggests that the spanwise spreading of the oblique waves that form the packet is unchanged by the presence of the streamwise vortices.

The impact of the interaction between the wave-packet and the streamwise vortices on the surface heat transfer was also investigated. Figure 32a shows a planform map of the relative heat transfer coefficient h_r which is the ratio of the coefficients of the forced flow (seeded with streamwise vortices) to the unforced (base) flow. Based on the discussion in §IV.3, it is clear that the streamwise vortices enhance heat transfer and thus the magnitude of h_r is greater than 1 over most of the domain. In Figure 32b h_r is taken to be the ratio between the heat transfer coefficient of the flow seeded with streamwise vortices and with a wave-packet, and the heat transfer coefficient of the flow seeded with streamwise vortices only. The plot shows h_r during

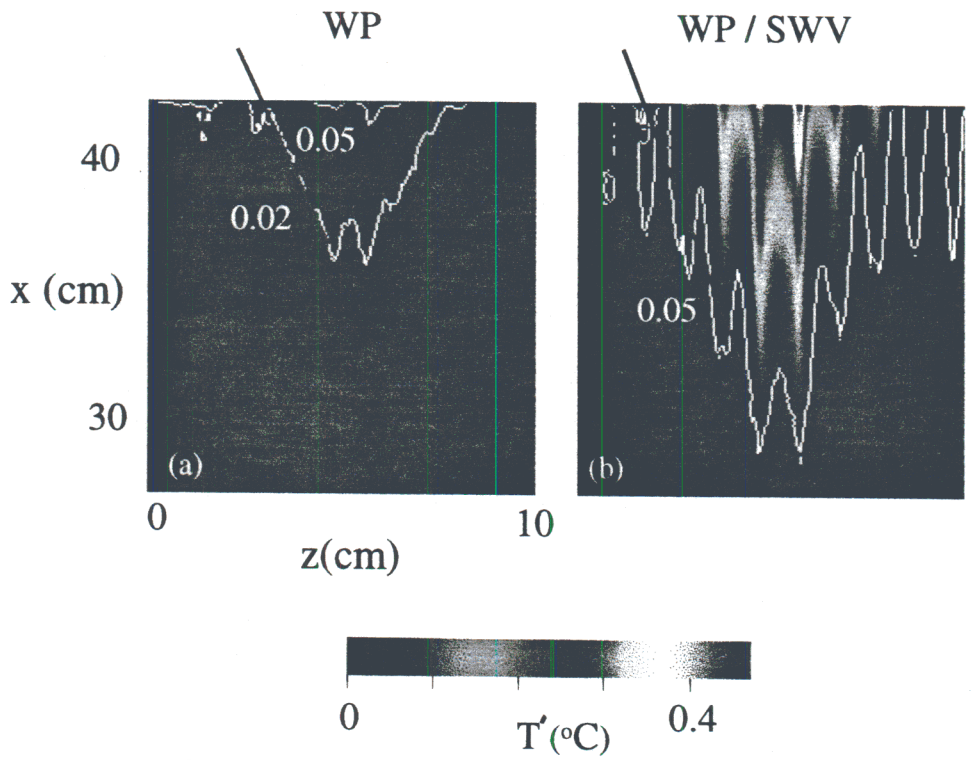

Figure 31. Surface temperature temporal RMS for a wave-packet propagating through (a) no streamwise vortices and (b) streamwise vortices.

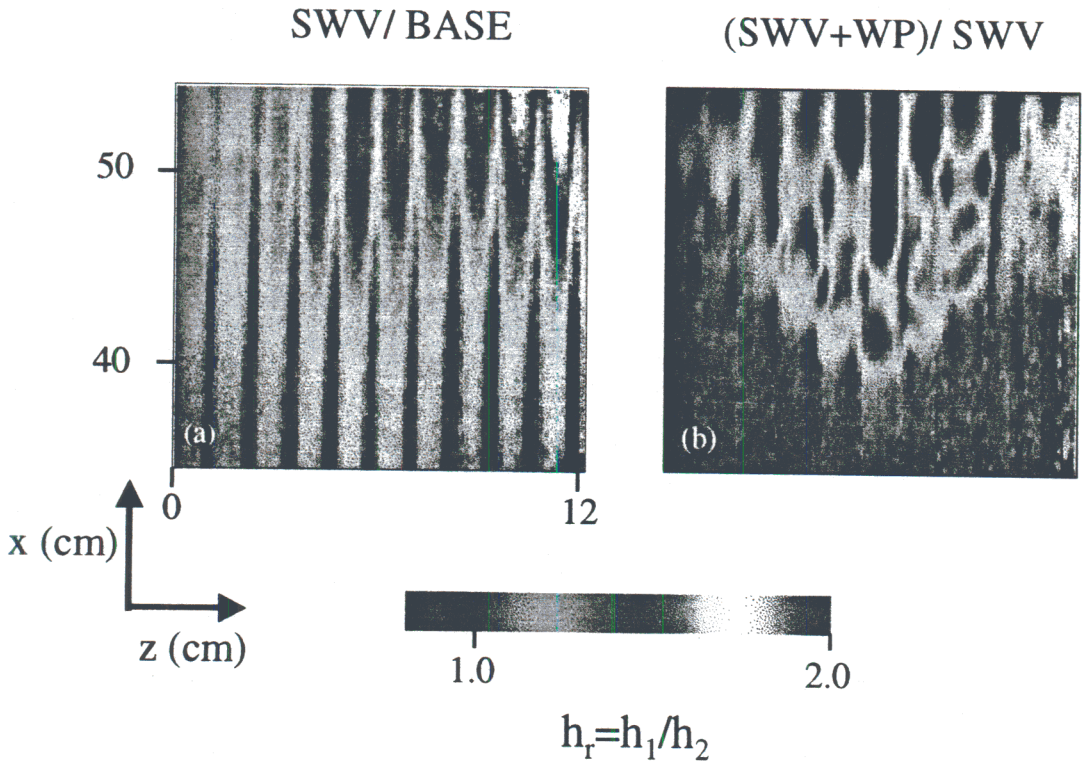

Figure 32. Relative heat transfer ratio h_r for (a) steady streamwise vortices and (b) a wave-packet propagating through the streamwise vortices at a given instant.

one instant in the motion of the wave packet, and the increment in heat transfer induced by its passage is readily evident.

V.3 Streamwise Vortex Cancellation using Wave-Packets

In §IV.6, it is demonstrated that it is possible to cancel spanwise variations in surface temperature that result from stationary streamwise vortices via phased seeding of streamwise vortices. It appears plausible that higher order cancellation can be achieved by combining phased control with propagating wave-packets to exploit the induced spanwise displacement of the streamwise vortices. If this spanwise displacement is on the order of the spanwise wavelength of the streamwise vortices, then "sliding" spanwise-periodic cooling and heating of the surface can be used across the span to achieve uniform surface temperature. Figure 33b shows the average disturbance temperature created by the passage of a single wave-packet through a system of streamwise vortices. The time averaged deficit in surface temperature (T_{ad}) created by the wave-packet is nearly 180° spatially out of phase with respect to the surface temperature established by the streamwise vortices in Figure 33a. This implies that if a wave-packet is used as a control of surface transport, the control input (i.e. change in surface temperature) is the correct sign for canceling the temperature variations imposed by the streamwise vortices. By changing the duty cycle, amplitude, and spanwise distribution of wave-packets, the spanwise variations created by the streamwise vortices could be smoothed in the mean.

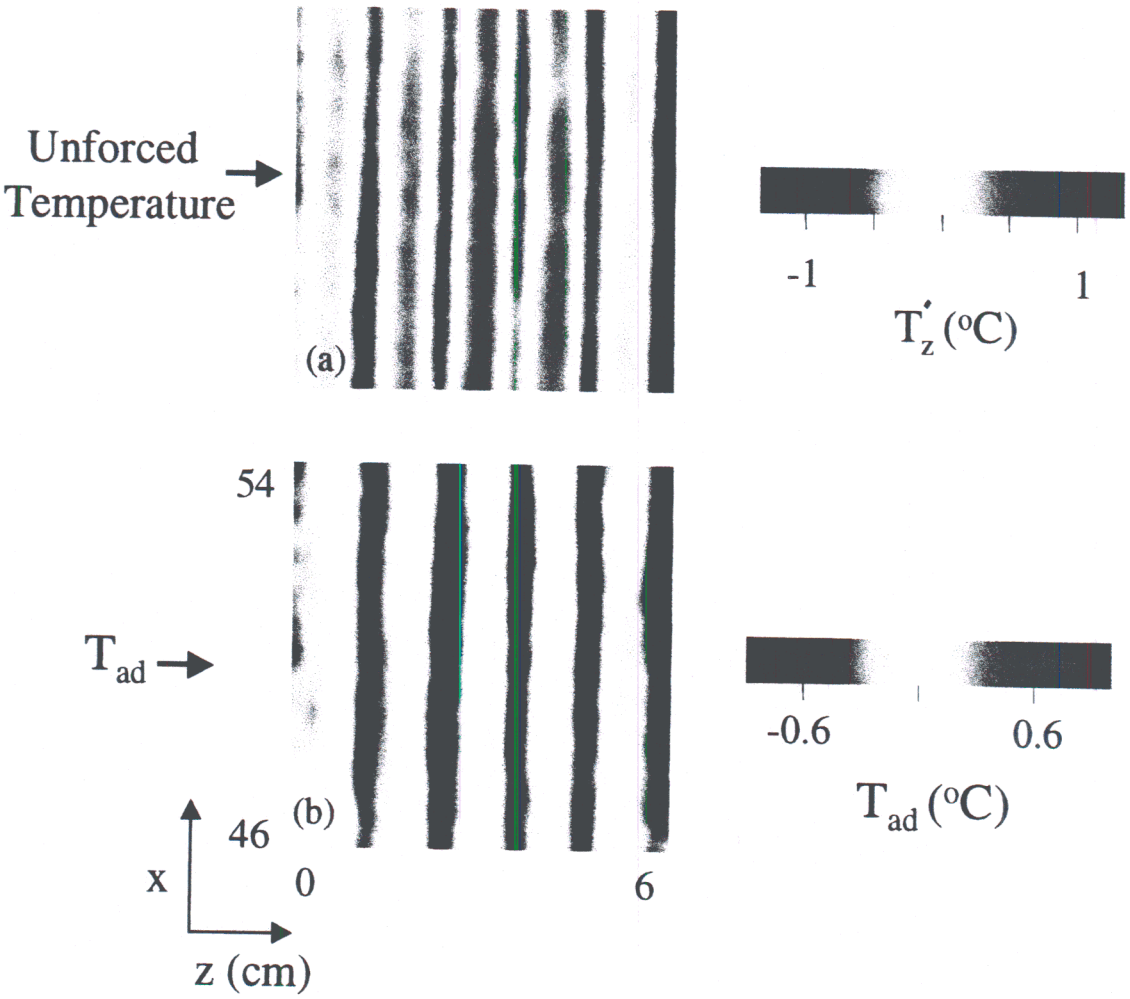

Figure 33. (a) Surface temperature with steady streamwise vortices. (b) The average temperature deficit over the passage of a single wave-packet.

IV Conclusions

Controlled excitation of two-dimensional and spanwise nonuniform instability modes is used to investigate the evolution of streamwise vortices in a free convection boundary layer over an inclined heated plate. It is found that the growth rate of spanwise instabilities depends strongly on plate inclination angle and only weakly on surface heat flux. These instabilities lead to the formation of counter-rotating pairs of streamwise vortices. Measurements of surface temperature and vortex circulation demonstrate that the disturbance growth proceeds initially through linear mechanisms prior to saturation which is followed by breakdown of the streamwise vortices. The appearance of the streamwise vortices leads to a substantial modification of the temperature distribution on the surface and an array of streamwise vortices induced by controlled, spanwise-periodic excitation can lead to a peak increase in the localized heat transfer of 100% and a streamwise averaged increase of up to 20% relative to the unforced flow. Velocity measurements reveal that the appearance of streamwise vortices is accompanied by an increase in the streamwise flowrate over the plate and that the three dimensional motion associated with the vortices leads to a spanwise-averaged "psuedo" shear stress that results in additional entrainment of ambient fluid and therefore increases the rate of heat transfer. Furthermore, the vortices induce spanwise variations in the boundary layer thickness that is in phase (spatially) with the streamwise velocity. Depending on the value of the modified Reynolds number ($R=5(Gr^{*}/5)^{1/5}$ and the initial strength of the spanwise disturbances, the streamwise vortices can merge within the present measurement domain. Vortex merging is accompanied by a reduction in growth of the surface heat transfer rate due to the reduction in the number of vortices across the span of the boundary layer. Particle image velocimetry (PIV) of the merging process reveals that the inner vortex pair is cancelled by the outer stronger pair

resulting in a single counter rotating pair. In the unforced flow for inclination angles between 14° and 40° the critical Reynolds number for vortex merging is $\tilde{R}_{1/2}$=250. This critical Reynolds number decreases as the forcing amplitude is increased. Circulation measurements are used to characterize control inputs of the surface actuators and it was demonstrated that (controlled) open loop excitation can be used to cancel the formation of streamwise vortices resulting in substantial reduction in spanwise variations of the surface temperature.

Time-dependent pulsed excitation that leads to the appearance of isolated wave-packets in a nominally 2-D boundary layer and a boundary layer seeded with streamwise vortices is also investigated. In the 2-D boundary layer, the wave-packet exhibits streamwise stretching that is nearly twice that of a wave-packet in a momentum boundary layer. The packet is comprised of spanwise symmetrical families of equal and opposite oblique waves where the wave angles increase (i.e. they become more oblique) in the streamwise direction indicating the presence of normal vorticity. Farther downstream, the wave-packet undergoes a bifurcation as a result of a subharmonic resonance that is characterized by the development of large side lobes that are symmetric about the spanwise centerline. At this stage the wave-packet is effectively split into two packets with each side lobe consisting of a pair of oblique waves. The spanwise temperature variations induced by the passage of the wave-packet increase substantially when the wave-packet propagates through seeded streamwise vortices thus leading to substantial enhancement in surface heat transfer. The spanwise distribution of the temporal surface temperature fluctuations produced by a wave-packet propagating through seeded streamwise vortices is 180° out of phase (spatially) with respect to the surface temperature induced by the streamwise vortices, suggesting the potential use of the wave-packet to further reduce variations in spanwise transport.

Nomenclature

Φ, non dimensional temperature difference $=\frac{(T-T_\infty)kG^*}{5xq''}$

Φ_z', spanwise rms of Φ relative to $\overline{\Phi}$

Gr_x^*, flux Grashof num $=\frac{g\beta q'' x^4 \cos(\theta)}{kv^2}$

G^*, modified flux Grashof number$=5(Gr_x^*/5)^{1/5}$

Q_r, non-dimensional forcing amplitude

h, heat transfer coefficient$= q''/(T_s - T_\infty)$

k, thermal conductivity of water

v, kinematic viscosity of water

β, coefficient of thermal expansion of water

θ, inclination angle from vertical

g, accelaration due to gravity

x, streamwise coordinate

y, wall normal coordinate

z, spanwise coordinate

u, streamwise velocity component

v, wall normal velocity component

T, temperature in boundary layer

T_s, temperature at the plate surface

T_∞ ambient temperature

$Nu_{x,z}$, local Nusselt number $=h(z)x/k$

Nu_x, Spanwise averaged $Nu_{x,z}$

$\overline{Nu}_x$, Streamwise averaged Nusselt number $=\frac{1}{xW}\int_0^x\int_0^W \frac{hx}{k}\,dzdx$

q'', heat flux from plate

Pr, Prandtl number$=v/\alpha$

$\delta_{1/2}$, Boundary layer thickness (y(1/2Umax))

λ, vortex wavelength

u_{max}, maximum streamwise velocity in a y profile

$\overline{u}_{max}$, maximum streamwise velocity in spanwise averaged y profile

u^*, nondimensional streamwise velocity$=u/u_{max}$

$\overline{u}^*$, spanwise averaged streamwise velocity$=u/\overline{u}_{max}$

v^*, nondimensional wall normal velocity$=$ v/$\overline{u}_{max}$

$\overline{v}^*$, nondimensional wall normal velocity$=$ v/$\overline{u}_{max}$

y^*, nondimensional wall distance=y/ $y(0.5u_{max})$

$\bar{y}^*$, spanwise averaged characteristic wall distance=y/$\bar{y}(0.5u_{max})$

k_z, dimensional spanwise wavenumber

Γ, vortex circulation

$\tilde{R}_{1/2}$, nondimensional distance

Bibliography

1 Rich, B.R., "An investigation of heat transfer from an inclined flat plate in free convection", *Trans. ASME*, **75**, 489-499, 1953.

2 Sparrow, E.M., Husar, R.B., "Longitudinal vortices in natural convection flow on inclined surfaces", *J. Fluid Mech.*, **37**, 251-255, 1969.

3 Lloyd, J. R., Sparrow, E. M "On the instability of natural convection flow on inclined plates," *J. Fluid Mech.*, **42**, 465-470, 1970.

4 Shaukatullah, H., Gebhart, B., "An experimental investigation of natural convection flow over and inclined surface," *Int. J. Heat Mass Trans.*, **21**, 1481-1490, 1978.

5 Jaluria, Y., Gebhart, B. "On transition mechanisms in vertical natural convection flow" *J. Fluid Mech,* **66**, 309-337,1974.

6 Haaland, S.E., Sparrow, E.M. "Vortex instability of natural convection flow on inclined surfaces," *J. Heat Mass Transfer*, **16**, 2355-2367, 1973.

7 Iyer, P.A., Kelly, R.E., "The stability of the laminar free convection flow induced by a heated inclined plate", *Int. J. Heat Mass Trans.*, **17**, 517-525, 1974.

8 Chen, T.S., Tzuoo, K.L., "Vortex instability of free convection flow over horizontal and inclined surfaces", *J. Heat Transfer,* **104**, 637-643, 1982.

9 Lee, H.R., Chen, T.S., Armaly, B.F., "Non-parallel thermal instability of natural convection flow on non-isothermal inclined flat plates", *Int. J. Heat Mass Trans.*, **35**, 207-220, 1992.

10 Chen C.C., Labhabi A., Chang H.-C., Kelly R.E., "Spanwise pairing of finite-amplitude longitudianl vortex rolls in inclined free-convection boundary layers,", *J. Fluid Mech.*, **231**, 73-111, 1991.

11 Klebanoff, P.S., Tidstrom, K.D., Sargent, L.M., "The three-dimensional nature of boundary-layer instability", *J. Fluid Mech,* **12**, 2-34, 1961.

12 Jaluria, Y., Gebhart, B. "An experimental study of nonlinear disturbance behavior in natural convection", *J. Fluid Mech,* **61**, 337-365, 1973.

13 Zuercher, E.J., Jacobs, J.W., Chen, C.F., "Experimental study of the stability of boundary-layer flow along a heated, inclined plate", *J. Fluid Mech,* **367**, 1-25, 1998.

14 Farina, D.J., Hacker, J.M., Moffat, R.J., Eaton, J.K., "Illuminant invariant calibration of thermochromic liquid crystals," *Experimental Thermal and Fluid Science*, **9**, 1-12, 1994.

E-25-W22
n/a

APPENDIX D

ANNUAL NSF GRANT PROGRESS REPORT

NSF Program:	Fluid Particulate and Hydraulic Systems	NSF Award Number:	CTS-9318332
PI Name:	Ari Glezer	Period Covered By this Report:	Sept. 1995-Sept. 1996
PI Organization:	Georgia Institute of Technology School of Mechanical Engineering	Date:	August 9, 1996
PI Address:	Atlanta, GA 30332-0405		

[X] Check if Continued Funding is Requested

Please include the following information:

1. Brief summary of progress, including results obtained to date, and their relationship to the general goals of the grant:
2. A brief summary of work to be performed during the next year of support if changed from the original proposal; an indication of any current problems or favorable or unusual developments; and any other significant information pertinent to the type of project supported by NSF or as specified by the terms and conditions of the grant;
3. Statement of funds estimated to remain unobligated - if more than 20% - at the end of the period for which NSF currently is providing support;
4. Proposed budget for the ensuing year in the NSF format, only if the original award letter did not indicate specific incremental amounts or if adjustments to a planned increment exceeding the greater of 10% or $10,000 are being requested;
5. Information about other current and pending research support of senior personnel, if changed from the previous submission;
6. A statement describing any contribution of the project to the area of education and human-resource development, if changed from any previous submission; and
7. Updated information on animal care and use, Institutional Biohazard Committee and Human Subject Certification, if changed substantially from those originally proposed and approved.

Annual NSF Grant Progress Report
Fluid Mechanics and Mass Transfer of the Rotating Screw Electrode Process for Through-Hole Plating
NSF Grant CTS-9318332

Ari Glezer
School of Mechanical Engineering
Georgia Institute of Technology

Progress

To date we have focused on the construction of the experimental apparatus for the investigation the fluid mechanics of through-hole plating. We now have a flow facility comprised of two 1 m long, concentrically-mounted cylinders (4" and 6" in diameter, made of stainless steel and transparent Plexiglass, respectively). Each of the cylinders can be independently rotated. We are currently in the process of designing the axial through flow hardware. A 20 mW He-Ne laser was purchased for the LDV system that will be used for measurements of the tangential and axial velocity components. We are also developing the software for interfacing the LDV processor to the laboratory data acquisition system.

In the coming year we expect to complete the construction of the experimental apparatus and to begin measurements of the velocity field of the axial flow between a stationary outer cylinder and a rotating inner cylinder.

Because the Grant was awarded in September of last year, we were unable to recruit a permanent graduate student to work full-time on this project and the work to date has been done with the help of temporary research assistants that were supported by the School of Mechanical Engineering. We anticipate that a permanent graduate student will become available for this project beginning in the fall quarter 1996 in mid-October.

Unobligated Funds

Of the first-year funds from NSF ($39,944), $4,058 were expended. The reason for the unobligated balance is that a full-time graduate student could not be recruited owing to the late start date of the grant.

Proposed Budget

Annual increments were specified in the award letter.

Current and Pending Support

Current

"Control of Natural Convection Along a Heated, Inclined Plate," NSF Grant CST-9318332, $169,008, August 12, 1993- August 11, 1996, Sole PI.

"Equipment for Neural Network Determination of Optical Phase Corrections," URI/DOD Grant F49620-95-1-0181, $241,000, January 1, 1995-December 31, 1998 Co-PI (with Professors M. G. Allen, M. A. Brooke, and Nan Marie Jokerst).

"Neural Network Determination of Optical Phase Correction in a Plane Shear Layer using Parallel Optoelectronic Image Processing, Global Optical Flow Diagnostics, and

Micromachined Actuators and Sensors," AFOSR, $935,931, April 15, 1995-April 14, 1998, PI (with Professors M. A. Brooke, and N.- M. Jokerst).

"NSF-ERC Center on Low-Cost Electronic Packaging," NSF Grant EEC-9402723 Principal Investigator Professor R. Tummala, Thrust Area: Thermal Management, annual funding (duration of award 5-10 years) $200,000, Co-PI with Professors W. Z. Black and J. G. Hartley.

"Fluid Mechanics and Mass Transfer of the Rotating Screw Electrode Process for Through-Hole Plating," NSF, $173,118, September 15, 1995- September 15, 1998, Sole PI.

"Control of Particle Laden Jets," McDonnell Douglas Aerospace, $51,100, August 22, 1996-August 22, 1997, Sole PI.

"Microjet Cooling for Missile System Electronics," US Army Missile Command contract DAAH01-92-D-R005-0038, $124,764, June 29, 1995-September 15, 1996, Co-PI (with Professor M. G. Allen)

"Intelligent Turbine Engines," DOD-URI Multidisciplinary Research Program DAAHO4-96-1-0008, $4,001,468, November 1, 1995- October 31, 1998, Co-PI (Professor B. T. Zinn, PI) with an additional option of 2,570,915 for two years.

"The Development of Novel High-Flux Heat Transfer Cells for Thermal Control in Microgravity," NASA, $480,000, June 1, 1996-May 31, 2000, (notified of recommendation for funding in February 1996) Co-PI (with M. K. Smith, PI).

"Shear Flow Control Using Synthetic Jet Fluidic Actuator Technology," AFOSR, $515,872, June 1, 1996-May 31, (notified of recommendation for funding in February 1996), Sole PI.

"The Interaction of Synthetic Jets with Prototypical Embedding Shear Flows," NASA Graduate Student Researcher Program, $66,000, September 1, 1996-August 31, 1999.

Pending

"Synthetic Jets For Thrust Vector Control," McDonnell Douglas Aerospace (MDA), $57,670 September 1, 1996-August 31, 1997.

"Integrated MEMS Flight Manuevering System for Miniature Electromechanical Systems," DARPA/MDA, $2,021,011 October 1, 1996-September 30, 1999.

APPENDIX D

ANNUAL NSF GRANT PROGRESS REPORT

NSF Program:	Fluid Particulate and Hydraulic Systems	NSF Award Number:	CTS-9318332
PI Name:	Ari Glezer	Period Covered By this Report:	Sept. 1995-Sept. 1996
PI Organization:	Georgia Institute of Technology School of Mechanical Engineering	Date:	August 9, 1996
PI Address:	Atlanta, GA 30332-0405		

[X] Check if Continued Funding is Requested

Please include the following information:

1. Brief summary of progress, including results obtained to date, and their relationship to the general goals of the grant:
2. A brief summary of work to be performed during the next year of support if changed from the original proposal; an indication of any current problems or favorable or unusual developments; and any other significant information pertinent to the type of project supported by NSF or as specified by the terms and conditions of the grant;
3. Statement of funds estimated to remain unobligated - if more than 20% - at the end of the period for which NSF currently is providing support;
4. Proposed budget for the ensuing year in the NSF format, only if the original award letter did not indicate specific incremental amounts or if adjustments to a planned increment exceeding the greater of 10% or $10,000 are being requested;
5. Information about other current and pending research support of senior personnel, if changed from the previous submission;
6. A statement describing any contribution of the project to the area of education and human-resource development, if changed from any previous submission; and
7. Updated information on animal care and use, Institutional Biohazard Committee and Human Subject Certification, if changed substantially from those originally proposed and approved.

Annual NSF Grant Progress Report
Fluid Mechanics and Mass Transfer of the Rotating Screw Electrode Process for Through-Hole Plating
NSF Grant CTS-9318332

Ari Glezer
School of Mechanical Engineering
Georgia Institute of Technology

Progress

To date we have focused on the construction of the experimental apparatus for the investigation the fluid mechanics of through-hole plating. We now have a flow facility comprised of two 1 m long, concentrically-mounted cylinders (4" and 6" in diameter, made of stainless steel and transparent Plexiglass, respectively). Each of the cylinders can be independently rotated. We are currently in the process of designing the axial through flow hardware. A 20 mW He-Ne laser was purchased for the LDV system that will be used for measurements of the tangential and axial velocity components. We are also developing the software for interfacing the LDV processor to the laboratory data acquisition system.

In the coming year we expect to complete the construction of the experimental apparatus and to begin measurements of the velocity field of the axial flow between a stationary outer cylinder and a rotating inner cylinder.

Because the Grant was awarded in September of last year, we were unable to recruit a permanent graduate student to work full-time on this project and the work to date has been done with the help of temporary research assistants that were supported by the School of Mechanical Engineering. We anticipate that a permanent graduate student will become available for this project beginning in the fall quarter 1996 in mid-October.

Unobligated Funds

Of the first-year funds from NSF ($39,944), $4,058 were expended. The reason for the unobligated balance is that a full-time graduate student could not be recruited owing to the late start date of the grant.

Proposed Budget

Annual increments were specified in the award letter.

Current and Pending Support

Current

"Control of Natural Convection Along a Heated, Inclined Plate," NSF Grant CST-9318332, $169,008, August 12, 1993- August 11, 1996, Sole PI.

"Equipment for Neural Network Determination of Optical Phase Corrections," URI/DOD Grant F49620-95-1-0181, $241,000, January 1, 1995-December 31, 1998 Co-PI (with Professors M. G. Allen, M. A. Brooke, and Nan Marie Jokerst).

"Neural Network Determination of Optical Phase Correction in a Plane Shear Layer using Parallel Optoelectronic Image Processing, Global Optical Flow Diagnostics, and

Micromachined Actuators and Sensors," AFOSR, $935,931, April 15, 1995-April 14, 1998, PI (with Professors M. A. Brooke, and N.- M. Jokerst).

"NSF-ERC Center on Low-Cost Electronic Packaging," NSF Grant EEC-9402723 Principal Investigator Professor R. Tummala, Thrust Area: Thermal Management, annual funding (duration of award 5-10 years) $200,000, Co-PI with Professors W. Z. Black and J. G. Hartley.

"Fluid Mechanics and Mass Transfer of the Rotating Screw Electrode Process for Through-Hole Plating," NSF, $173,118, September 15, 1995- September 15, 1998, Sole PI.

"Control of Particle Laden Jets," McDonnell Douglas Aerospace, $51,100, August 22, 1996-August 22, 1997, Sole PI.

"Microjet Cooling for Missile System Electronics," US Army Missile Command contract DAAH01-92-D-R005-0038, $124,764, June 29, 1995-September 15, 1996, Co-PI (with Professor M. G. Allen)

"Intelligent Turbine Engines," DOD-URI Multidisciplinary Research Program DAAHO4-96-1-0008, $4,001,468, November 1, 1995- October 31, 1998, Co-PI (Professor B. T. Zinn, PI) with an additional option of 2,570,915 for two years.

"The Development of Novel High-Flux Heat Transfer Cells for Thermal Control in Microgravity," NASA, $480,000, June 1, 1996-May 31, 2000, (notified of recommendation for funding in February 1996) Co-PI (with M. K. Smith, PI).

"Shear Flow Control Using Synthetic Jet Fluidic Actuator Technology," AFOSR, $515,872, June 1, 1996-May 31, (notified of recommendation for funding in February 1996), Sole PI.

"The Interaction of Synthetic Jets with Prototypical Embedding Shear Flows," NASA Graduate Student Researcher Program, $66,000, September 1, 1996-August 31, 1999.

Pending

"Synthetic Jets For Thrust Vector Control," McDonnell Douglas Aerospace (MDA), $57,670 September 1, 1996-August 31, 1997.

"Integrated MEMS Flight Manuevering System for Miniature Electromechanical Systems," DARPA/MDA, $2,021,011 October 1, 1996-September 30, 1999.

E-25-W22

N/A

Georgia Institute of Technology

The George W. Woodruff School of Mechanical Engineering

March 26, 1998

Dr. Ashley Emery
National Science Foundation
4201 Wilson Blvd.
Arlington, VA 22230

Dear Dr. Emery,

Following our recent telephone conversation, the purpose of this letter is to request a no-cost extension for nine months (through October 1998) to NSF Grant CTS-9318332. The term date of this grant was January 31, 1998, and, owing to an oversight on my part, I neglected to request an extension ahead of that date. The balance of unused funds at the term date was $14,742.

The work under this grant has focused on the manipulation and control of flow instabilities that lead to the formation of streamwise vortices and heat transfer enhancement in a free convection boundary layer over a heated inclined plate. The experiments are conducted on a flat plate model that is suspended in a water tank (measuring one meter on the side) and actuation is accomplished using surface mounted film heating elements. The entire experimental apparatus including the water tank, the flat plate model, the surface heating actuators and the ancillary electronic hardware was designed and fabricated specifically for the purpose of the present experiments. The investigations so far have included controlled excitation of various two- and three-dimensional instability modes using surface double-pass shadowgraph visualization and liquid crystal measurements of surface temperature distributions. This work has demonstrated that the formation of arrays of counter-rotating streamwise vortex pairs results in substantial modification of the surface temperature (and heat transfer) and, furthermore, that time-harmonic excitation of plane and oblique instability modes leads to temporal and spatial modification of the temperature on the surface. As per your request, I enclose a report that summarizes this work.

We have recently modified the optics of our PIV (particle image velocimetry) system to enable us to measure in detail the velocity field within the thermal boundary layer over the plate. During the requested no-cost extension, we propose to complete these measurements and the related data processing. These data will be correlated to our earlier heat transfer measurements. In particular, we propose to reconstruct the streamwise vorticity field and to determine the evolution, dynamics and merging of the streamwise vortices. We also expect to continue our investigations of open-loop control configurations to maximize surface heat transfer. It is anticipated that this investigation will be completed by the Ph.D. student who has been working on this project since its inception within three quarters from the term date of the grant. The student support will be covered by the remaining funds.

I hope that this request receives your favorable consideration. Your effort on our behalf is greatly appreciated.

Sincerely,

Ari Glezer

Ari Glezer
Professor

Atlanta, Georgia 30332-0405 U.S.A.
Administration Office 404•894•3200
Finance Office 404•894•7400

Graduate Program 404•894•3204
Undergraduate Office 404•894•3203
Fax 404•894•8336 or

web site: http://www.me.gatech.edu/

CONTROL OF NATURAL CONVECTION ALONG A HEATED, INCLINED PLATE

NSF GRANT CST-9318332
PROGRESS REPORT
March 1998

submitted by

Ari Glezer
Woodruff School of Mechanical Engineering
Georgia Institute of Technology

Abstract

Flow instabilities leading to the formation of streamwise vortices and heat transfer enhancement in a free convection boundary layer over a heated inclined plate are manipulated using surface mounted film heating elements. The flat plate model (59 cm on the side) is suspended in a water tank measuring one meter on the side. The flow over the plate is driven by a two-ply surface heater comprised of a uniform, constant-heat flux film heater layer and a lower mosaic of 32 x 10 individually-controlled heating elements that are used as control actuators. The flow in planes parallel to the test surface is visualized using a double-pass shadowgraph system and the planform temperature distribution on the surface is measured using a calibrated liquid crystal film. Controlled excitation of two- and three-dimensional instability modes have been investigated and it is shown that the receptivity of the flow to the excitation input increases with inclination angle and surface heat flux. Time-invariant spanwise-periodic excitation over a range of spanwise wavelengths leads to the formation of arrays of counter-rotating streamwise vortex pairs and to substantial modification of the surface temperature (and heat transfer). Spanwise-periodic merging of groups of vortices appear to be a precursor to the development of a secondary instability which is followed by breakdown to turbulence. Time-harmonic excitation of plane and oblique instability modes leads to temporal and spatial modulation of the streamwise vortices and to the emergence of vortex loops. Pulsed excitation leads to the formation of wave packets which, following amplification, evolve into patches of vortical structures with temporal modification of the temperature on the surface.

I. BRIEF OVERVIEW

The study of thermally-driven boundary layer flows over inclined surfaces owes much of its importance in a number of engineering applications including passive (nonmechanical) surface cooling technologies (e.g., electronic packages), and chemical vapor deposition processes (e.g., in fabrication of microelectronic and optical components). These thermal boundary layers are buoyantly unstable, and the instabilities can lead to the appearance of longitudinal (streamwise) vortices (rolls) which is accompanied by significant changes in transport phenomena near the surface such as heat transfer or surface deposition. Thus, the present research work has focused on the manipulation and control of the flow instabilities that lead to the formation of these streamwise vortices with the objective of enhancing the heat transfer over a heated inclined flat plate.

The onset and development of free convection boundary layers along heated inclined surfaces was studied experimentally both for constant-temperature surfaces by Sparrow and Husar (1969) and Lloyd and Sparrow (1970), and for constant heat flux surfaces by Shaukatullah and Gebhart (1978). The appearance of streamwise vortices was first observed by Sparrow and Husar who used a Thymol-blue technique for flow visualization. Sparrow and Husar also showed that at large angles of inclination, neighboring vortices merge prior to break up to turbulence. Lloyd and Sparrow (1970) showed that free convection flat plate boundary layers become unstable in two different modes depending on the vertical inclination angle α. When the plate is nearly vertical (i.e., $\alpha < 14^{o}$), the instability is in the form of transverse traveling waves. However, when α exceeds 17° the instability leads to the formation of the longitudinal vortices previously observed by Sparrow and Husar. The critical Rayleigh number for the onset of these instabilities decreases from $Ra = 10^{9}$ for $\alpha = 0^{\circ}$ to 10^{6} at $\alpha = 60^{\circ}$. Lloyd (1974) found that the critical spanwise wavelength of the vortices is independent of the angle of inclination, but that it varies with the temperature difference between the plate and the bulk fluid. Shaukatullah and Gebhart (1978) carried out detailed temperature and velocity surveys along an inclined constant heat flux plate.

The present experiments differ substantially from previous work in this area in that instability modes are *externally excited and controlled* thus allowing for control of the flow instabilities and, in particular, for their suppression or enhancement as demonstrated, for example, by Liepmann et al. (1982) for Tollmien-Schlichting waves in a flat plate Blasius boundary layer. While the suppression of flow instabilities is important in applications such as surface deposition in order to achieve deposition uniformity, the enhancement of flow instabilities is important in applications where it is desirable to enhance heat transfer by promoting three-dimensional motions.

II. EXPERIMENTAL APPARATUS AND DIAGNOSTICS

The experiments are conducted in a water tank using a submerged flat plate model (Figure 1). Flow instabilities leading to the formation of streamwise vortices are manipulated using a mosaic of novel surface heating actuators. The experimental hardware was specifically designed and constructed for the purpose of the present investigation. The water tank measures 107 cm on the side and the test surface is 66 cm long and 61 cm wide (i.e., approximately 100 wavelengths of the spanwise instability that leads to the formation of streamwise vortices), and is attached to an insulated substrate, hinged along its span to the sidewalls of the tank.

II.1 Heated Test Surface

The test surface is comprised of a two-layer Kapton insulated Inconel heater measuring 23 x 23cm. The top layer is a uniform foil heater connected to streamwise electrodes along its two side edges. The bottom heater is a mosaic of individually controlled heating elements as shown schematically in Figure 2. The mosaic consists of three identical segments each measuring 20 x 56 cm in the spanwise (z) and streamwise (x) directions, respectively. Each segment of the mosaic has 32 streamwise-serpentined 40 Ω copper-nickel film elements. Each element is 0.64 cm wide and 56 cm long, and the spanwise spacing between adjacent elements is 0.64 cm. All streamwise heating elements are connected to common spanwise electrodes along their upstream and downstream ends. Equally-spaced (0.64 cm apart) node pads for external wiring allow for controlled addition or subtraction of current between any two nodes. The two heater layers are laminated between two 0.007 cm thick Kapton sheets. The heater mosaic is bonded to a 1.25 cm thick mica-glass ceramic substrate plate that is flat to within 0.1 mm and has a thermal conductivity of 0.001 (cal-cm)/(sec-cm^2-°C) and high resistance to water absorption. The mechanical properties of this material are similar to acrylic and it is machinable using standard carbide tooling. Each node is wired from below through the ceramic substrate and any number of nodes can be externally connected to achieve a desired spatial pattern. Current is added or subtracted using a bank of 32 amplifiers that can be directly controlled from the laboratory computer.

II.2 Effect on Streamwise Vorticity

The streamwise (x) component of the vorticity equation is:

$$\frac{D\Omega_x}{Dt} - (\Omega_x \frac{\partial u}{\partial x} + \Omega_y \frac{\partial u}{\partial y} + \Omega_z \frac{\partial u}{\partial z}) = -\beta g \sin\theta \frac{\partial T}{\partial z} + \nu \nabla^2 \Omega_x$$

At the wall (y = 0) this equation becomes:

$$\frac{\partial \Omega_x}{\partial t} = -\beta g \sin\theta \frac{\partial T}{\partial z} + \nu \nabla^2 \Omega_x$$

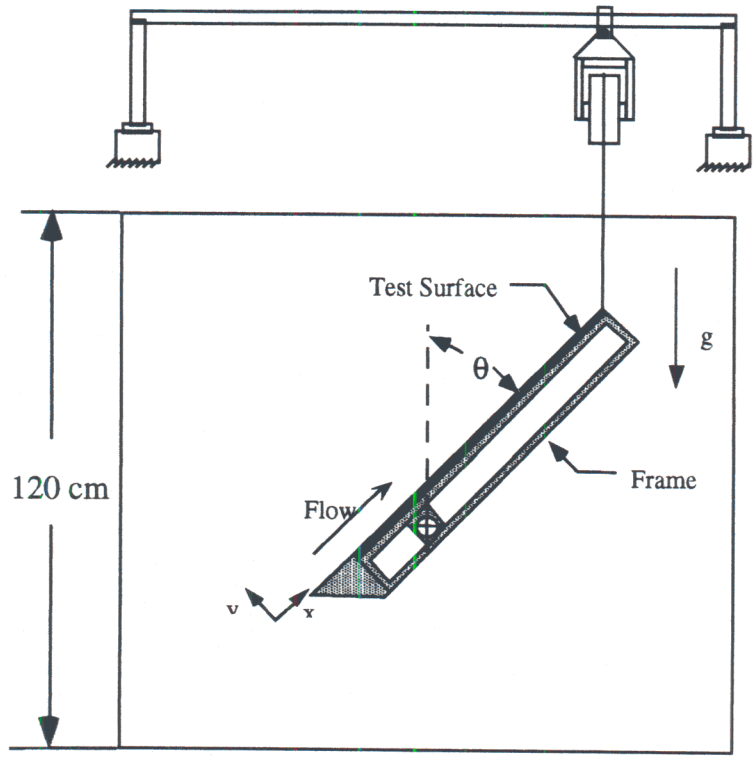

Figure 1

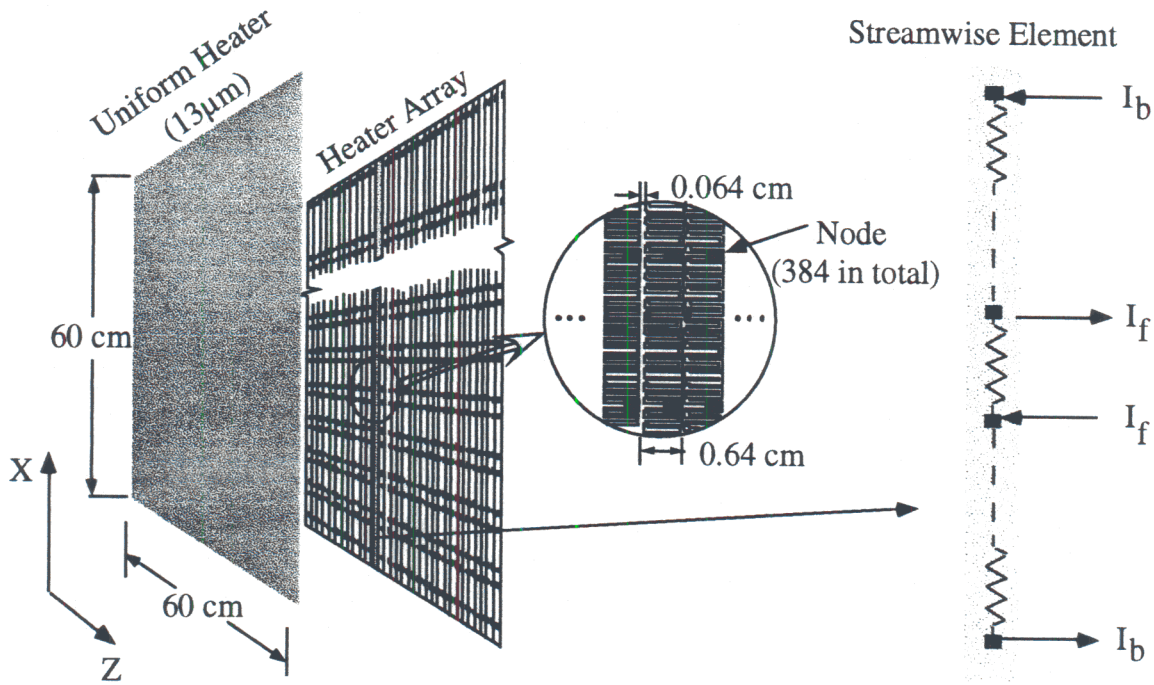

Figure 2

Thus, the magnitude and sign of the streamwise vorticity at the wall depend on the spanwise temperature gradient. Therefore, it is anticipated that naturally occurring or forced streamwise vorticity can be cancelled by generating vorticity of opposite sign at the wall. If the change of viscosity with temperature is significant, then this equation can be modified:

$$\frac{\partial \Omega_x}{\partial t} = -\beta g \sin\theta \frac{\partial T}{\partial z} + \nu \nabla^2 \Omega_x - \frac{\partial \nu}{\partial T}\frac{\partial T}{\partial z}\frac{\partial^2 v}{\partial y^2}$$

Thus, even without the influence of a normal force, streamwise vorticity can be generated if the change of viscosity with temperature is substantial or the spanwise temperature gradient is large enough.

II.3 Temperature Diagnostics

Distributions of surface temperatures are measured using thin encapsulated sheets of Thermochromic Liquid Crystal (TLC) which is attached directly to the heated surface with minimal contact resistance and is calibrated *in situ* at the exact viewing arrangement used in an experiment. During the calibration the temperature in the facility is gradually increased uniformly using a water heater and circulation pump. The dependence of the TLC color on temperature is determined by measuring the surface temperature with a platinum RTD sensor and recording the color image with a CCD camera equipped with a polarizing filter having its optical axis nearly normal to the plane of the TLC sheet. Polarized white light co-aligned with the camera is used to illuminate the TLC sheet. The two polarizing filters create a cross polarized viewing system which enhances the signal to noise ratio by increasing the amount of circularly polarized light that is reflected from the TLC relative to the background light.

The CCD image is digitized using the laboratory computer/frame-grabber and the dependence of color on illumination intensity is removed in software using an HSI color model which consists of hue (H) a measure of the spectral wavelength of the reflected light, saturation (S) related to the purity of the color, and intensity (I) of the light. Since illumination intensity is decoupled from the color components, this color model is well suited for a color based measurement system. The calibration curve in figure 3 is typical for the liquid crystal material used. Using this technique the surface temperature can be measured with an accuracy of +-0.1 °C [95%CI] over most of the color play range.

III RESULTS

In the present experiments, excitation is effected using uniform, time-invariant heat flux from the top heater and by adding or subtracting control current from the nodes of the lower mosaic heater. The localized addition or subtraction of the control current through a rectangular grid of nodes of the streamwise heating elements leads to localized increase or decrease in heat flux and surface temperature. Thus, this technique allows, in effect, for the introduction of three-dimensional vorticity perturbations at the flow boundary by exploiting the dependence of the buoyancy force and viscosity on temperature (e.g., Liepmann et al. 1982). The inherently fast

response time of film heating actuators and current injection coupled with the fact that the current density at each node is controlled by a dedicated amplifier, allows for the synthesis of complex spatial and temporal heat flux distributions at the test surface. Furthermore, heat flux excitation is in essence reconfigurable on the fly from the laboratory computer through a D/A interface to the control amplifiers. Feedback from the system will be obtained from global surface temperature measurements using TLC.

III.2 Time-Invariant forcing

At moderate inclination angles the dominant mode of instability is spatial rather than temporal. The instability appears as a system of counter-rotating streamwise vortices which are nominally steady in time over a large section of the test surface before breaking down. The first part of this work has focused on time-invariant forcing of the streamwise vortices. In these studies, the surface temperature measured with the TLC was used to indicate the effect of forcing the flow with the surface actuators.

III.2.1 Single Actuator

In order to determine the effect of the surface actuators on the base flow, the effect of forcing the flow with a single actuator (0.64 cm W x 2.54 cm L) was monitored while the streamwise location of the actuator x_{ea} and forcing amplitude

$$Q_r = \frac{L_a}{x_{ea}} \frac{\int_w q''_a dz}{\int_w q''_{base} dz}$$

(where L_a is the streamwise length of the actuator and q"$_a$ is the actuator heat flux) were varied. Note that Q_γ is a measure of the input disturbance energy relative to the base flow energy at the streamwise location x_{ea} of the actuator. The functional form of Q_γ is necessary for scaling the disturbance input energy since its relative magnitude decreases relative to the boundary layer of the base flow because of the continuous streamwise heating.

The effects of the forcing level and actuator location were investigated at a plate inclination angle of 14° and heat flux of q" = 1380w/m^2. Under these conditions only weak streamwise vortices were present in the base flow. A single actuator is activated triggering a pair of counter-rotating streamwise vortices that grow downstream. Figure 4 shows the spanwise surface temperature profile for several streamwise stations. The shape of the profile is consistent with the motion of the streamwise vortex pair generated by the actuator. The center peak at z = 10.7 cm represents the upwelling of the center counter-rotating vortex pair, while the two side peaks at z = 9.4 and 12 cm indicate induced vortices on the sides of the primary vortex pair. Thus, two minima in the profile develop where the common downdraft of the vortex pairs entrain cool fluid from the outer

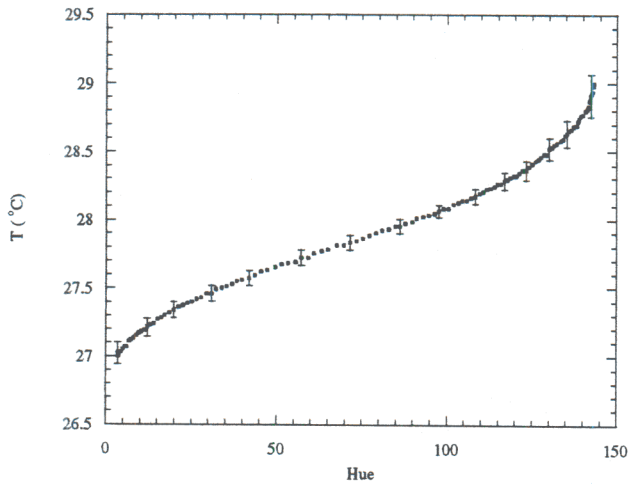

Figure 3

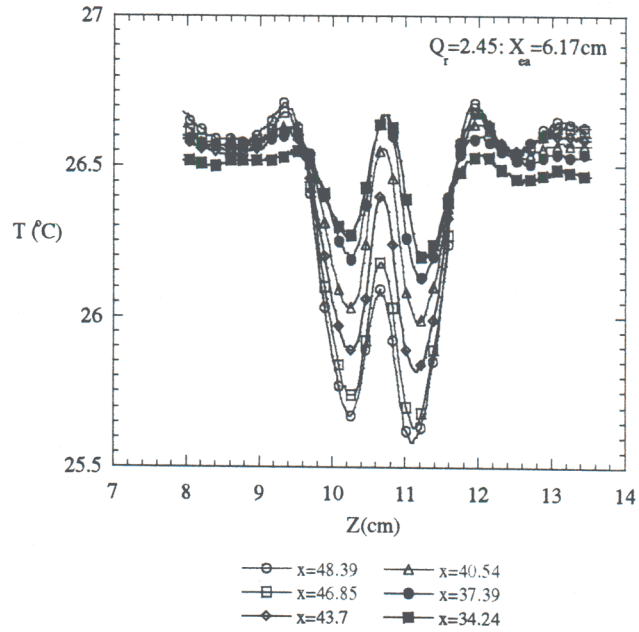

Figure 4

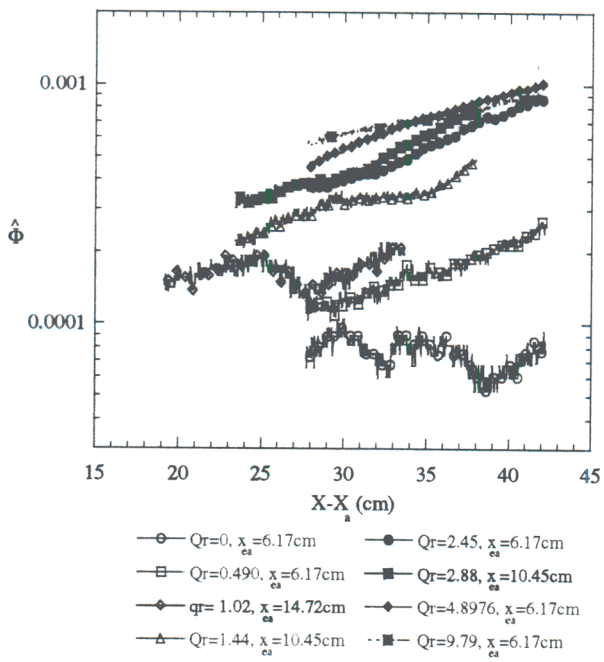

Figure 5a

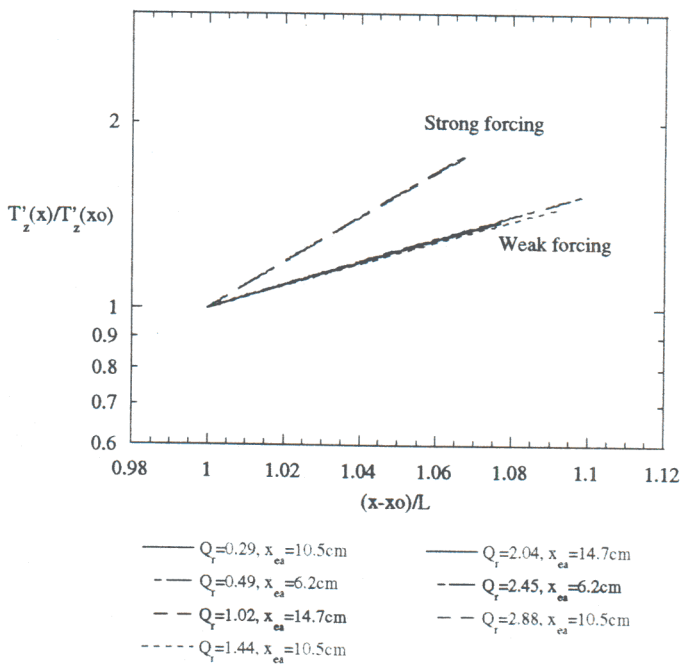

Figure 5b

region of the boundary layer to the surface. As the growth progresses downstream, the center peak temperature decays due to the net cooling of the vortex pair relative to the unforced regions of the surface. The troughs continue to deepen because of the additional cooling provided by the common downwash of the primary and induced vortices. The spanwise averaged strength of the vortex disturbance on the surface was calculated as the normalized temperature difference

$$\hat{\Phi} = \frac{(T_{max} - T_{min})k}{q''_{base}\, L}$$

Figure 5a shows the effect of the forcing amplitude ratio Q_γ for three different streamwise locations x_{ea} of the actuator. These data show that an increase of the forcing amplitude leads to an increase in $\hat{\Phi}$ for each actuator position. However, the effect begins to saturate at large Q_γ as can be seen by the marginal difference in $\hat{\Phi}$ between the curves for Q_γ = 2.88, 4.90 and 9.8 in figure 5a. This indicates that forcing at Q_γ > 2.5 produces nonlinear amplification of the disturbance. Furthermore, as shown in figure 5b, the initial growth rate of the disturbance is exponential and constant for Q_γ < 2, but larger forcing amplitudes generate a distinctly larger growth rate. This is unusual since nonlinear growth rates are typically smaller than linear growth rates due to strong damping of the disturbance.

III.2.2 Spanwise Periodic Forcing

The variation with heat flux and plate angle of the rms spanwise temperature fluctuations T_z' induced by spanwise-periodic forcing was measured over a range of spanwise wavelengths. The streamwise variation q", λ and θ are shown in Figures 6a-c, respectively. Each plot exhibits an initial exponential growth indicating that the disturbance amplifies through a linear mechanism. Further downstream, the nonlinear mechanisms dominate causing growth rates to decrease and the disturbance amplitude to decay. From figure 6a it can be seen that the growth rate is only a weak function of heat flux, with the growth rate increasing slightly with q". However, the characteristic evolution of the disturbance growth, such as the double peak in disturbance amplitude, are retained for different q" at fixed inclination angle. This suggests that although the wall heat flux is an important parameter for disturbance growth (since it drives the flow), it alone does not account for fundamental changes in the transition process (such as vortex merging). Figure 6b shows that, except for λ = 1.27cm, the growth rates for different spanwise forcing periods are quite similar. The growth rate for the 1.27cm wavelength case is significantly less than for the other wavelengths, and actually results in an overall smaller T_z' than the unforced flow. In situations where large spanwise variations in scalar transport are undesirable, (e.g., chemical vapor deposition), passive forcing at an appropriate wavelength could produce more uniform transport than the unforced flow by inducing vortices at a wavelength that undergoe a slower growth rate than the naturally occurring vortices.

The growth rate increases with the surface inclination angle (Figure 6c) although at lower angles ($\approx 11°$) the occurrence of streamwise vortices is superceded by a preferred 2-D wave instability. Each curve in figure 6a (at 24° inclination) has an initial region of exponential growth in T_z. This

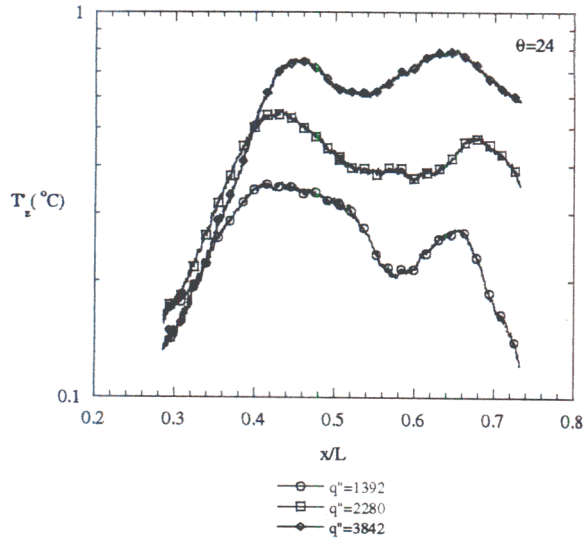

Figure 6a

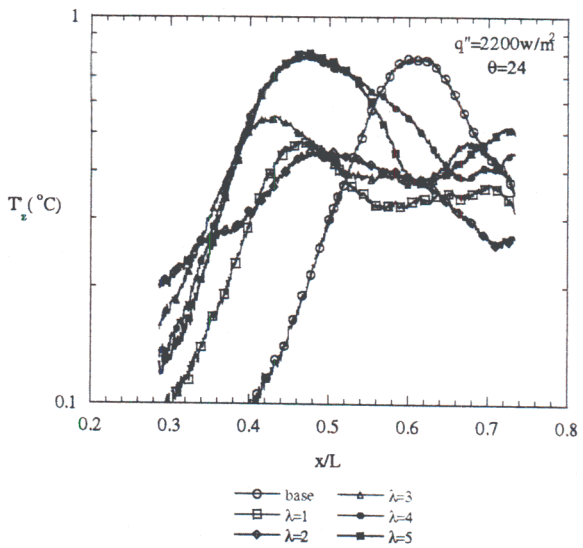

Figure 6b

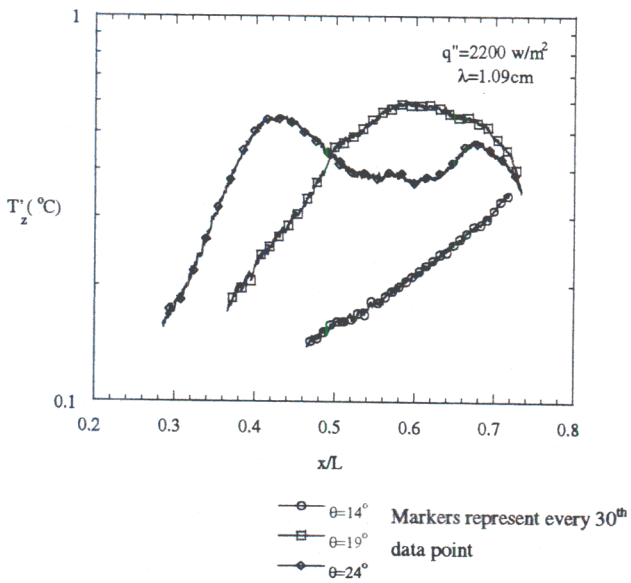

Figure 6c

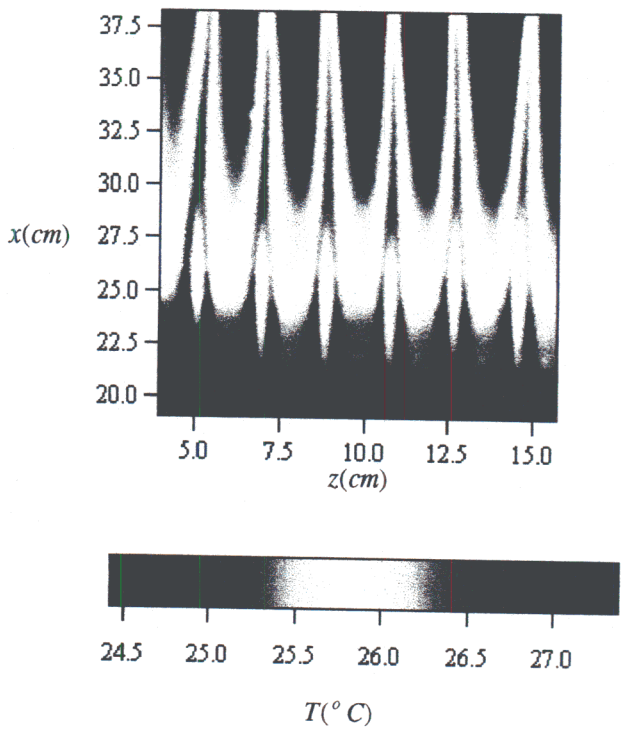

Figure 7

growth tapers off and decays followed by an additional growth and decay cycle. It is believed that the first T_z' peak value corresponds to the streamwise location where the increased circulation of the streamwise vortices is countered by the increased distance between the vortex pair and the surface. The vortices apparently are lifted off the surface as a result of their self-induced velocities. After the peak disturbance level is reached, the lifting of the vortices from the surface causes T_z' to decay until merging occurs. The merged vortex pair, now identified by twice the wavelength of the original pair, is large enough to drive cool fluid from the boundary layer across the surface, thus increasing further the spanwise temperature variations. The second decay cycle corresponds to the merged pair lifting off the surface. At the lower inclination angles (θ = 14° and 19°) in figure 6c, no merging is evident at the last measurement station and the data do not exhibit a double peak in the temperature distributions.

III.2.3 Vortex Merging

The initial disturbance that appears at inclination angles greater than 11° is a spanwise periodic system of streamwise vortices. Downstream these streamwise vortices merge and the spanwise wavelength is effectively doubled. To the best of our knowledge, the experiments described in this section have yielded the first measurements of the conditions that lead to vortex merging. A controlled spanwise periodic disturbance in the surface heat flux was introduced 2.54 cm downstream of the leading edge of the heated surface at a spanwise wavelength corresponding to two of the three heating elements (each element measures 2.54 cm in the streamwise direction and is 0.635 cm wide) are active. The resulting surface temperature distribution leading to a typical merging process is shown in Figure 7.

In general, merging occurs when the amplification rate of the streamwise vortices is large enough to promote rapid growth of the vortices before the base flow becomes susceptible to the temporal disturbances which lead to vortex breakdown. Since the growth rate increases with inclination angle, it is anticipated that the merging location x_m should move upstream at larger plate inclination angles and, as shown in Figure 8, this is indeed the case. A nonlinear stability analysis for a natural convection flow over an inclined flat-plate at constant wall temperature (Chen *et al.*1991) predicted that the primary streamwise vortices become destabilized by a subharmonic mode at a critical Reynolds number $R_{c1/2}$. It was argued that the dependence of the critical Reynolds number $R_{c1/2}$ on inclination angle could be removed by normalizing the Reynolds number with the inclination angle ($R_{c1/2}\tan\theta$) and it was numerically predicted that merging would occur when $R_{c1/2}\tan\theta = 43.5$. Because in the present work the plate is operated at constant heat flux, the Reynolds number is defined as $R = 3.62(Gr)^{1/5}$ and therfore it is not possible to have a direct comparison with the theory. However, the data shown in Figure 8b support the predicted merging behavior where the normalized critical Reynolds number is found to be essentially constant (for fixed Q_γ) over a wide range of inclination angles. It should be noted that for small inclination angles (less than 14°) merging is not possible due a temporal instability that destabilizes the organized structure of the streamwise vortices before the conditions for merging can be reached.

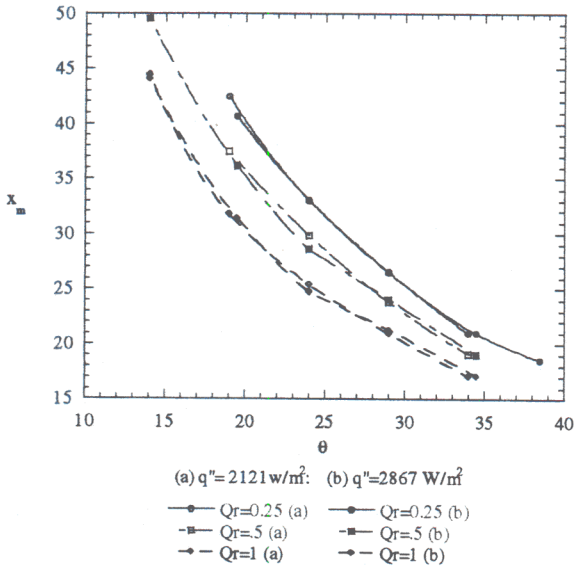

Figure 8a

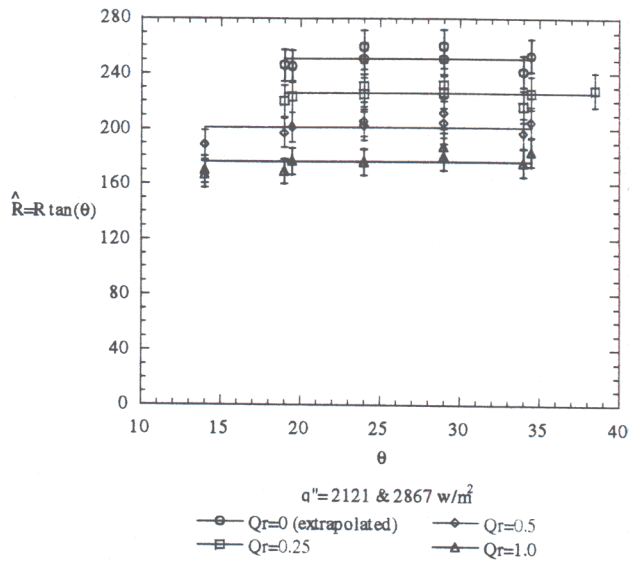

Figure 8b

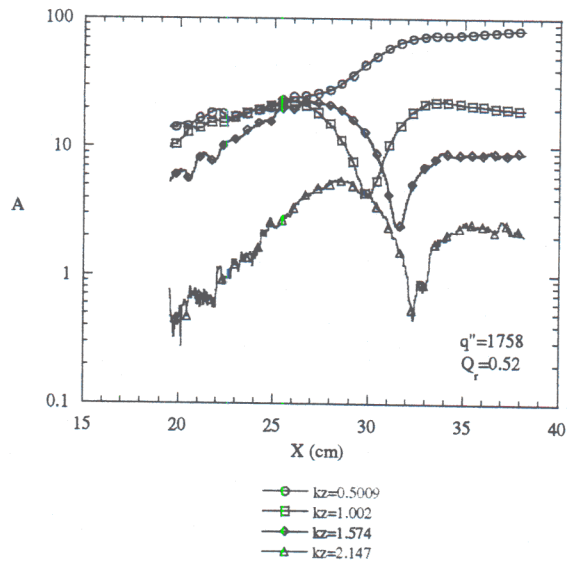

Figure 8c

An increase in the forcing amplitude Q_γ leads to a lower critical Reynolds number for merging (Figure 8b) due to the increase in the initial amplitude of the disturbance. The line $Q_\gamma = 0$ was extrapolated from the data for Q_γ = 0.25, 0.5, 1, 2, and 4 (2 and 4 are not shown) and represents the predicted normalized critical Reynolds number for naturally occurring streamwise vortices. It is noted that while in the unforced flow it is difficult to measure the critical Reynolds number because the merging locations are highly nonuniform across the span, small amplitude forcing removes this difficulty by locking the disturbance to the forcing wavelength and by establishing a known disturbance level at a fixed streamwise location across the span. When organized merging occurs, the power spectra of the surface temperature develops a characteristic notch at the fundamental and higher harmonic wavenumbers. Figure 8c shows the power at selected spanwise wavenumbers as a function of streamwise coordinate x. The merging process does not occur abruptly, but rather over one to two wavelengths in the streamwise direction. As two vortex pairs approach each other, the spanwise separation decreases, and eventually the fundamental wavelength disappears. As the separation continues to decrease, the higher wavenumbers also begin to disappear. This process explains the cascade of notches in the spectra at successively higher wavenumbers as the merging process evolves. A good indicator of the completion of merging is the streamwise location of the notch for the largest wavenumber observable above the noise. However, for simplicity we define incipient merging to be the location of the notch in the energy spectra of the fundamental wavenumber (k = 1.00 cm^{-1} in figure 8c). It should be noted that these notches are not observable in the unforced flow in general since the vortex merging does not occur as uniformly across the span compared to the forced flow.

The spectra provides some indication of the transfer in energy between the fundamental and subharmonic modes during the merging process. For this case, shown in figure 8c, both the subharmonic and fundamental modes are being forced, and initially there is growth in the harmonics of the forcing as the streamwise vortices extract energy from the mean flow, but by x = 25 cm the fundamental component k_z = 1.00 cm^{-1} begins to lose energy as the merging process continues. At this stage of development, the growth rate in the subharmonic increases since it now gains energy not only from the mean flow but also from the fundamental and higher harmonics in the flow which lose energy during the merging process.

III.2.4 Heat Transfer Enhancement

The ability of the surface actuators to directly introduce streamwise vortices into the base flow enables control of the surface heat transfer by exploiting the natural spanwise instabilities of the flow. Forcing of these instabilities results in an organized system of streamwise vortices that are considerably stronger than the naturally-occurring streamwise vortices and thus advect more cool fluid towards the surface thereby increasing the heat transfer.

Figure 9a shows how the Nusselt number varies with the Grashof number for the unforced flow for three inclination angles. For $\theta = 14^0$ and 19^0, the curves for the three heat flux values collapse and are comparable to the laminar solution indicating a relatively small departure from laminar flow heat transfer at all measurement stations. In contrast, at $\theta = 14^0$ the Nusselt number departs

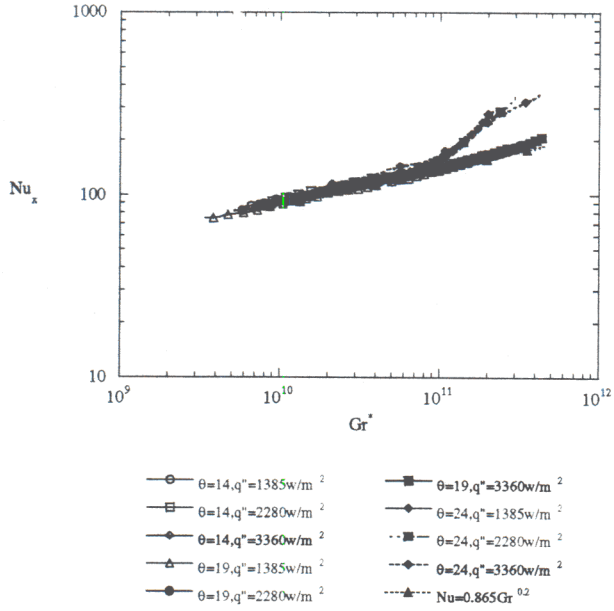

Figure 9a

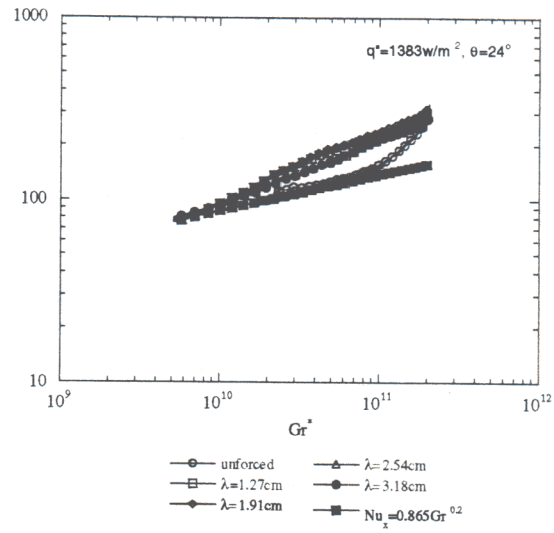

Figure 9b

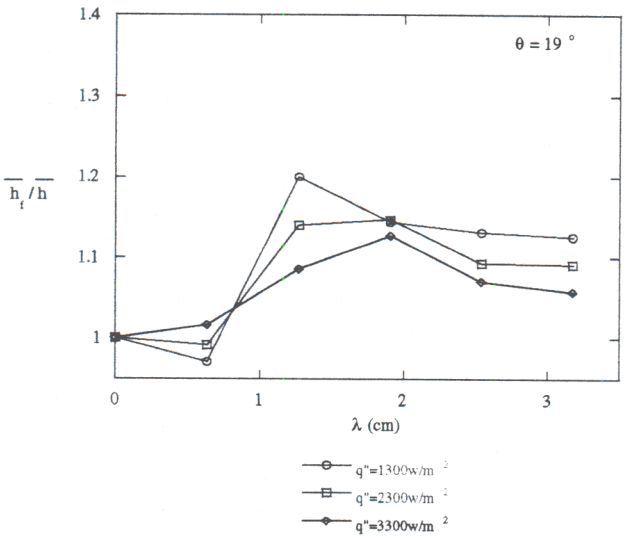

Figure 10a

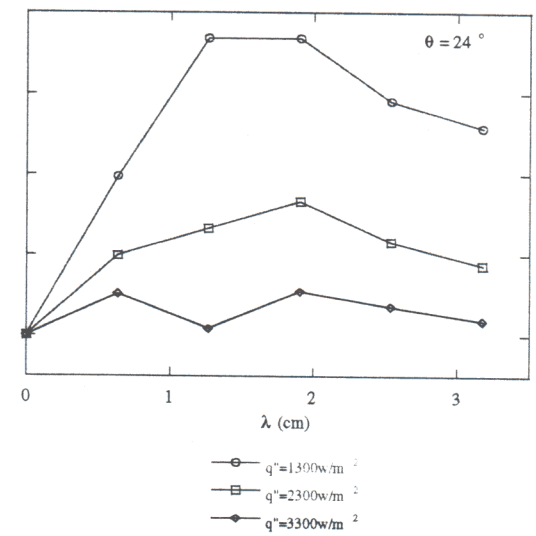

Figure 10b

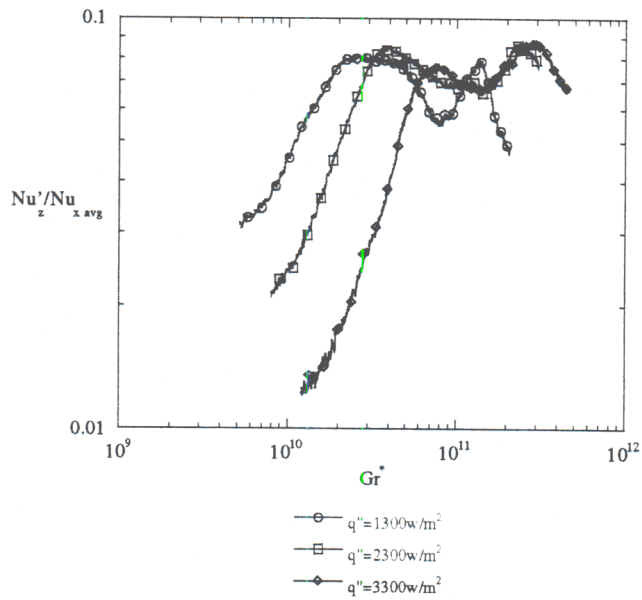

Figure 11

from the laminar solution at $Gr \approx 0.7 \cdot 10^{11}$ due to the presence of naturally occurring streamwise vortices in the boundary layer. Figure 9b illustrate the cooling effect produced by employing a spanwise periodic forcing pattern. The various curves represent different spatial forcing wavelengths. In all cases, forcing increased the Nusselt number relative to the unforced flow, with increases of nearly 200% achieved in the local Nusselt number for a forcing wavelength λ = 1.91 cm. Figure 9b shows that the increase in cooling occurs only in the transition region at moderate angles of inclination. Therefore, this method of control of heat transfer is best suited for the transition regime of the flow. This result is not surprising since this method relies on the natural instabilities in the flow to enhance the heat transfer. It is important to recognize, however, that the increase in heat transfer requires very little additional power from the actuators and can be operated in a controlled manner if temperature regulation is important.

The percentage change in the average Nusselt number between the forced and unforced flows is shown in figures 10a and 10b. For $\theta = 19^0$, a 15-20% increase in the average Nu was achieved by selecting an appropriate spatial forcing period for a given wall heat flux. Figure 10b shows nearly a 40% increase in the Nu for the low heat flux cases, but the effect diminishes markedly with increasing wall heat flux. This decrease in effectiveness results from naturally occurring streamwise vortices pre-existing over a larger portion of the unforced flow for larger inclination angles and higher heat flux values.

It is also noteworthy to look at the spanwise variations in Nu to determine if the forcing produces local hot spots that would actually yield a lower local heat transfer coefficient relative to the unforced flow. The amplitude of the spanwise variations in Nu were entirely under 10% of the spanwise averaged Nusselt number as shown in figure 11. As figure 9b illustrates, local increases in Nu can be of the order of 200%, so a 10% fluctuation would still provide a larger heat transfer coefficient relative to the unforced flow.

III.2.5 Controlled Cancellation of Flow Instabilities

As mentioned in §I, one of the primary goals of the present research is to implement a control scheme that can be used to stabilize the flow and delay the evolution of the streamwise instability. As a proof of concept for using the surface actuators as control actuators for suppressing streamwise vortices, a system of streamwise vortices having a spanwise wavelength of 1.27 cm was forced into the boundary layer with an upstream row of actuator elements. The corresponding surface temperature distribution for this case is shown in Figure 12a. Because the origin of the disturbance was known *a priori*, a second row of actuators fixed in space could be used to cancel the input disturbance. The cancellation actuators were activated 4.26 cm downstream spatially out of phase from the disturbance actuators. This open loop cancellation showed very promising results as can be seen in figure 12b. The spanwise variations are almost entirely cancelled along the entire measurement area which begins 25 cm downstream from the cancellation actuators. A plot of the spanwise variations is shown in figure 12c, for x = 40 cm. The peak rms spanwise variations in temperature are decreased by a factor of three.

Figure 12a

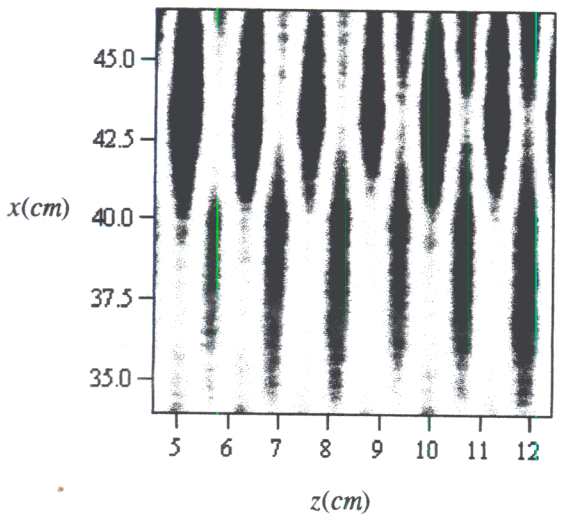

Figure 12b

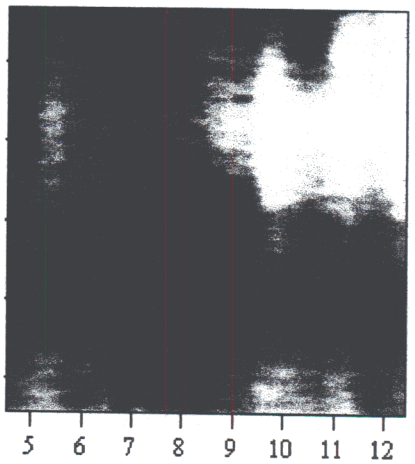

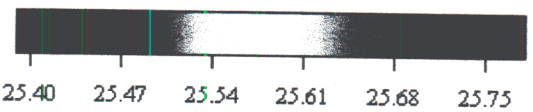

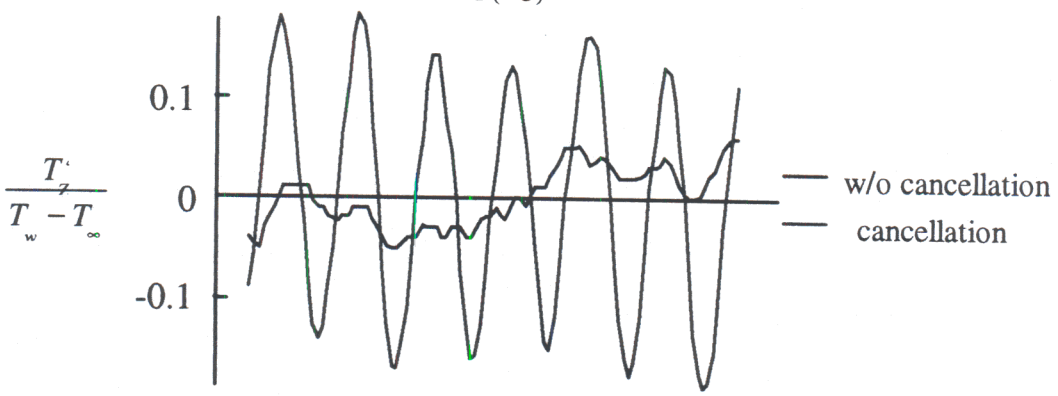

Figure 12c

A more practical control scheme would be to control spanwise variations on the average. The problem then becomes a stochastic control problem. The idea is to not be concerned about the instantaneous variations in spanwise transport, but to use the actuators to reduce time-averaged spanwise variations measured over an appropriate time period. The surface actuators could be quite effective in this type of control approach. The present research has demonstrated that the actuators can lock the streamwise vortices to the forcing wavelength, and that a broad range of spanwise wavelengths can be introduced. A rather simple control scheme can take advantage of these forcing characteristics. Initially, a periodic array of actuators generates a system of streamwise vortices locked to the spanwise forcing wavelength of the actuators. This creates a non-uniform but predictable spanwise variation of the surface heat transfer. The actuators then shift 180° spatially out of phase from the original forcing program locking the streamwise vortices 180° out of phase from the initial system. This would have the effect of reducing spanwise heat transfer non-uniformity in the mean. Furthermore, other wavelengths could be introduced in order to remove residual spanwise variations.

III.3 Time-Dependent Excitation

Previous work by other investigators has demonstrated that for inclination angles smaller than 11°, the base flow is primarily dominated by a 2-D instability while for inclination angles larger than 17° the primary instability mode is three-dimensional and leads to the evolution of streamwise vortices. Because both modes of instability are present when the inclination angle is between 11° and 17° this range is exploited to study the evolution of a pulsed, 3-D disturbance with and without the presence of streamwise vortices.

III.3.1 Wave-Packets at Shallow Inclination Angles

A wave-packet is introduced into the natural convection boundary layer by generating a short pulse from a single surface actuator. The disturbance generated in this manner contains energy in a broad band of frequencies and spanwise wavenumbers, however, the base flow is only receptive within a relatively narrow band and, as a result, frequencies and wavenumbers outside of this band are attenuated. The most unstable modes can be identified from the spectral content of the wave-packet.

Figure 13a shows surface plots of the spanwise temperature (at three streamwise position) as a function of time during the passage of the wave packet at a plate inclination angle of 2° and surface heat flux q" = 1870W/m^2. The upstream plot (x = 38 cm) shows approximately 4 periods of small amplitude oscillations, where the wave fronts are nearly normal to the downstream coordinate. At x = 46 cm, the disturbance is amplified significantly and its duration in time is increased by a full period. At the last streamwise station (x = 54 cm), the amplification of the disturbance leads to spanwise distortion of the wavefront, with two distinct symmetrical structures about the centerline.

Corresponding time traces of the surface temperature at the spanwise position of the side peaks (in the x = 54 cm surface plot) and the disturbances centerline are shown in figure 13b for the same three streamwise locations. At x = 38 and 46 cm the traces at the two spanwise positions

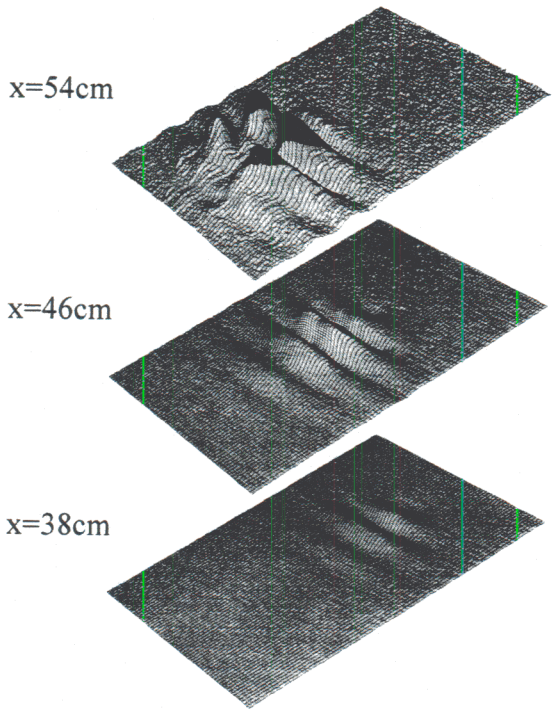

Figure 13a

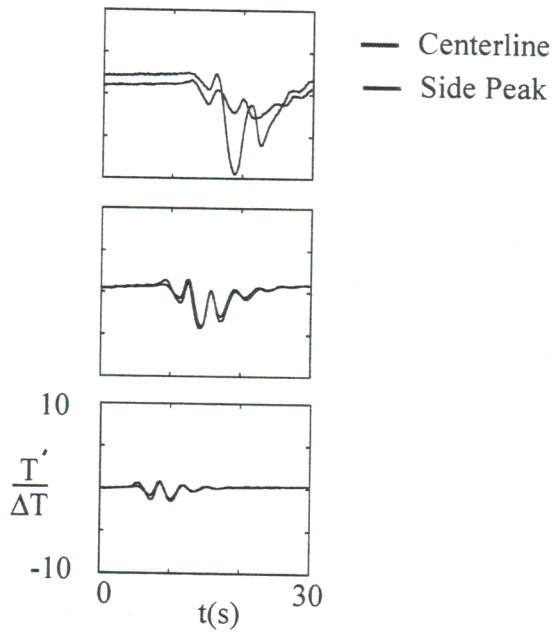

Figure 13b

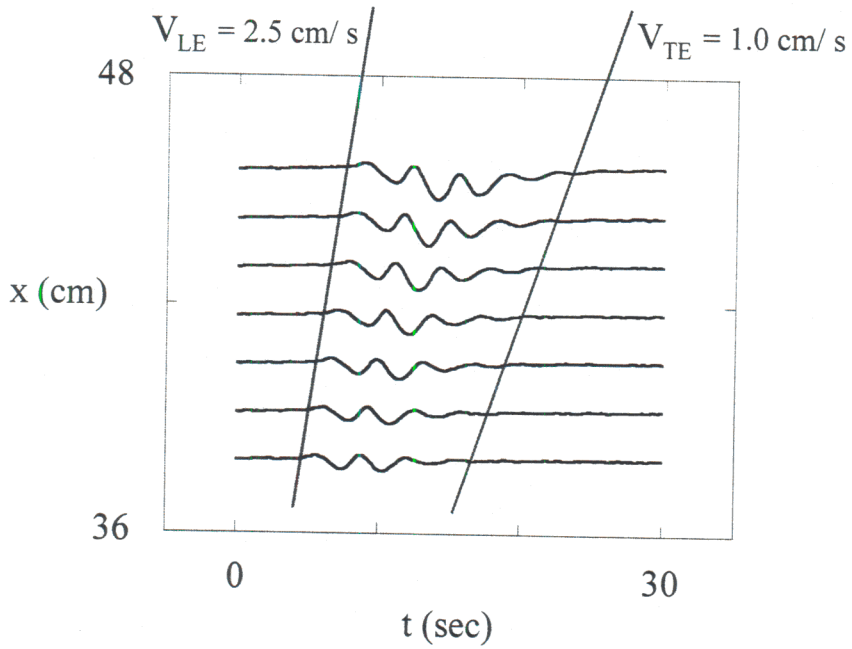

Figure 14

are nearly identical indicating only small spanwise variations in the disturbance. However, at x = 54cm, the two traces show drastic differences. The amplitude of the centerline trace is diminished, and is mostly negative, while the trace measured off-centerline exhibits larger peaks and is also shifted in phase relative to the centerline. The phase change suggests that different parts of the packet are moving with different phase velocities. In particular, similar to a wave packet in a momentum boundary layer, the leading edge of the thermal wave-packet propagates faster than the trailing edge. To quantify the edge velocities, the centerline time traces were plotted at several streamwise positions, as shown in figure 14. The slope of the lines drawn through the beginning and end of the disturbances approximate the leading and trailing edge velocities respectively. As shown, the leading and trailing edge disturbance velocities are V_{LE} = 2.5 cm/s and V_{TE} = 1.0 cm/s. The ratio of these velocities $V_{LE}/ V_{TE} = 2.5$ may be thought of as a dimensionless dispersion rate for the wave-packet in a free convection boundary layer. Gaster and Grant (1975) performed a similar measurement for a momentum boundary layer and found $V_{LE}/ V_{TE} = 1.2$. This implies that the dispersion of the wave-packet in a free convection boundary layer is larger than that in a momentum boundary layer. The increased dispersion may be attributed to the buoyancy force which accelerates the fluid in the free convection boundary layer.

An important feature of the wave-packet evolution is the emergence of spanwise nonuniform structure. Figure 15 shows the spanwise phase variation of the largest spectral (frequency) component of the wave-packet at three streamwise stations. While at x = 38 cm the maximum phase variation across the span of the wave-packet is only 0.5 rad, at x = 51 cm the phase varies by 3.6 rad. This phase variation is a result of the interaction of equal and oppositie oblique waves that form the wave-packet. The slope of each curve in Figure 15 is equal to the angle of the corresponding oblique waves and it is evident from the increase in the slope with streamwise distance that the waves steepen. The double peak at 51cm curve indicates a split of the single wave-packet into two wave-packets. It appears that at this stage, the large structures on each side of the centerline (e.g., Figure 13) begin to behave like separate wave-packets suggesting a mechanism for spanwise spreading of the instability.

As the wave-packet is advected downstream, energy is transferred to higher spanwise wavenumbers and frequency modes. Figure 16 shows 2-D frequency-wavenumber spectral maps for the wave-packet at three streamwise stations. At x = 38 cm the wave-packet is characterized by a zero spanwise wavenumber and frequency peak of 0.3 Hz, implying that the wave-packet at this stage is nominally two dimensional. At x = 45 cm, there is a transfer of energy to the second harmonic of the primary frequency f_p, and energy is transferred to small non-zero wavenumbers. The second harmonic disappears by x = 51 cm, and lower frequencies emerge as a result of the dispersive nature of the disturbance. Significant levels of energy at nonzero wavenumbers at x = 51 cm, indicate the beginning of breakdown of the wave-packet. The emergence of the subharmonic of f_p at wavenumber $0.3cm^{-1}$ may be attributed to a subharmonic resonance mechanism between f_p and low frequencies which produce the subharmonic at ($f_{p1/2}$,+-α_z=$0.3cm^{-1}$). This resonance can only occur if f_p and the subharmonic have the same phase speed ($C=f/\alpha_x$). The measured phase speeds of f_p and its subharmonic were C_{fp} = 1.9 cm/s and C_s = 1.8 cm/s, which strongly supports the existence of the subharmonic resonance mechanism.

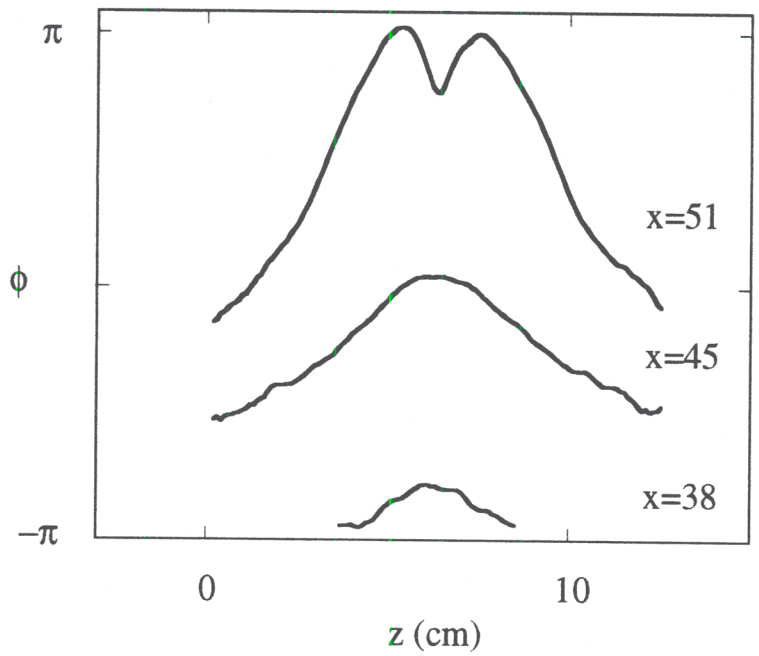

Figure 15

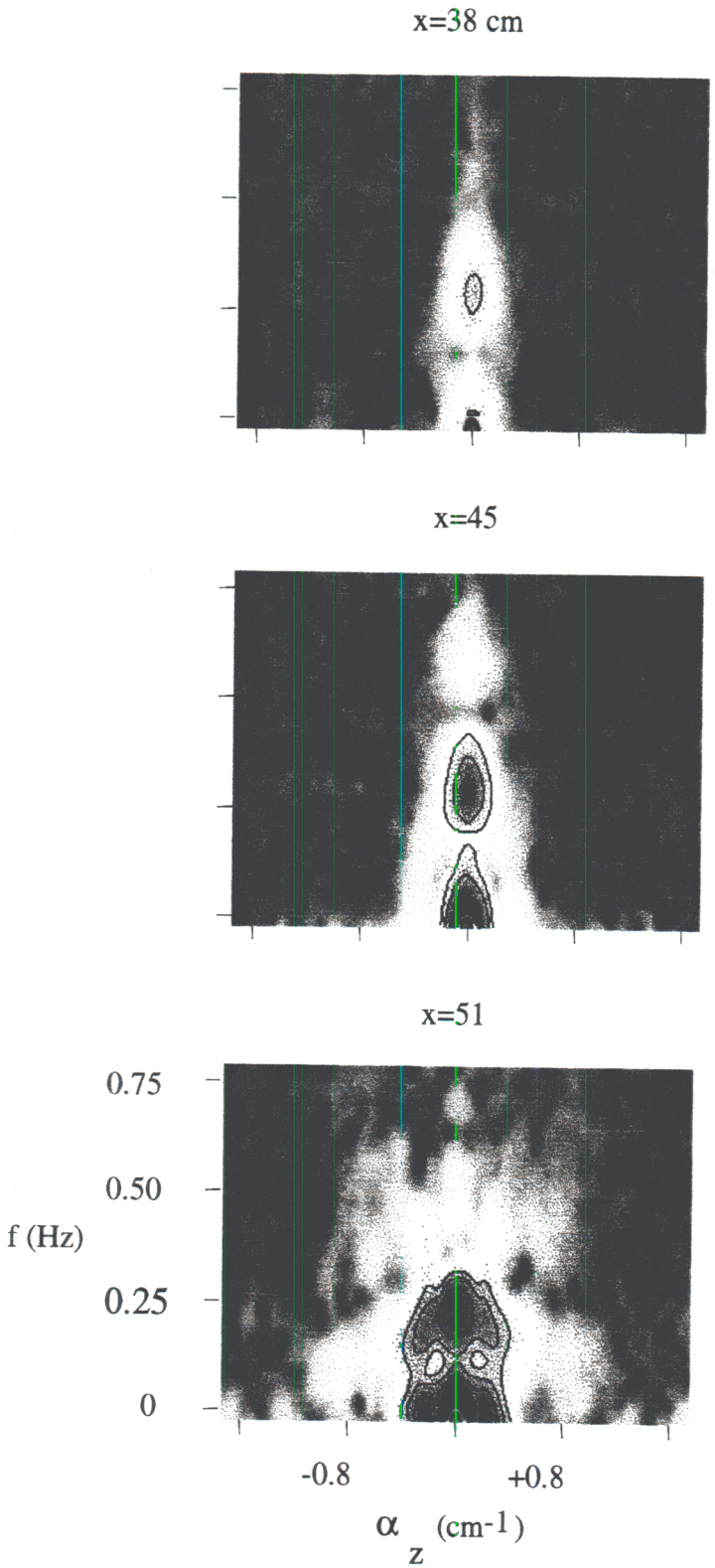

Figure 16

III.3.2 Wave-Packets at Intermediate Inclination Angles

As noted in §III.3, for inclination angles between 11° and 17°, streamwise vortices and time varying waves can coexist. The objective of the experiments described in this section is to investigate the interactions between these two instability modes and to determine their impact on heat transfer from the plate. Specifically, the effect of a wave packet propagating into a "natural" base flow is compared with that of a wave packet propagating into a base flow that is seeded with a stationary array of count-rotating streamwise vortex pairs for $\theta = 12°$ and $q'' = 1870$ w/m^2. The spanwise extent of the wave-packet disturbance is measured by considering maps of rms surface temperature fluctuations as the packet propagates through the field of view (Figures 17a and b). Figure 17a shows the base flow with a wave-packet, and 17b shows a wave-packet propagating through a base flow seeded with streamwise vortices. The white contours represent rms fluctuations of 0.05°C and it is evident that temperature fluctuations are present over a larger region of the span in the presence of streamwise vortices. This rapid spreading of the disturbance results from the interaction between the wave packet and the streamwise vortices. As the packet is advected, the streamwise vortices are locally and temporally distorted or bent in the spanwise direction leading to a "sweep" of the temperature field on the surface of the plate and thus to an increase in the temperature fluctuation levels. It is remarkable however, that despite the increased spatial extent of the disturbance in the presence of the streamwise vortices, spanwise spreading rates (as marked by the red lines on each plot) in the absence and presence of the streamwise vortices are virtually identical. This in turn suggests that the spanwise spreading of the oblique waves that form the packet is unchanged by the presence of the streamwise vortices.

The impact of the interaction between the wave-packet and the streamwise vortices on the surface heat transfer was also investigated. Figures 18a shows a planform map of the relative heat transfer coefficient h_r which is the ratio of the coefficients of the forced flow (seeded with streamwise vortices) to the unforced (base) flow. Based on the discussion in §III.2.4, it is clear that the streamwise vortices enhance heat transfer and thus the magnitude of h_r is greater than 1 over most of the domain. In Figure 18b h_r is taken to be the ratio between the heat transfer coefficient of the flow seeded with streamwise vortices and with a wave-packet, and the heat transfer coefficient of the flow seeded with streamwise vortices only. The plot shows h_r during one instant in the motion of the wave packet, and the increment in heat transfer induced by its passage is readily evident.

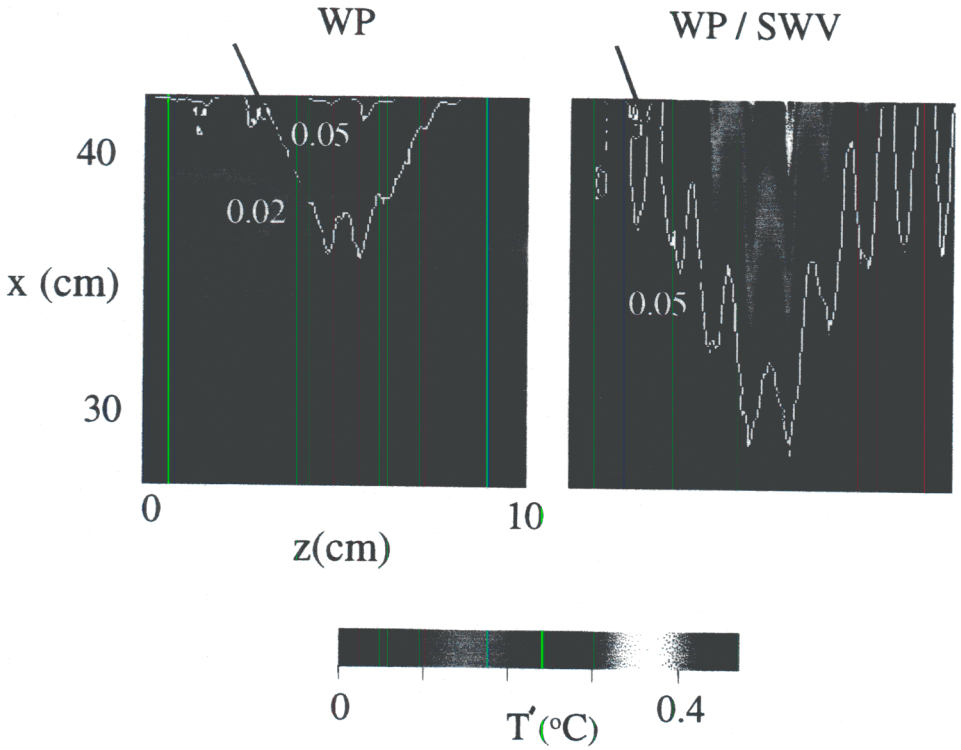

Figure 17a

Figure 17b

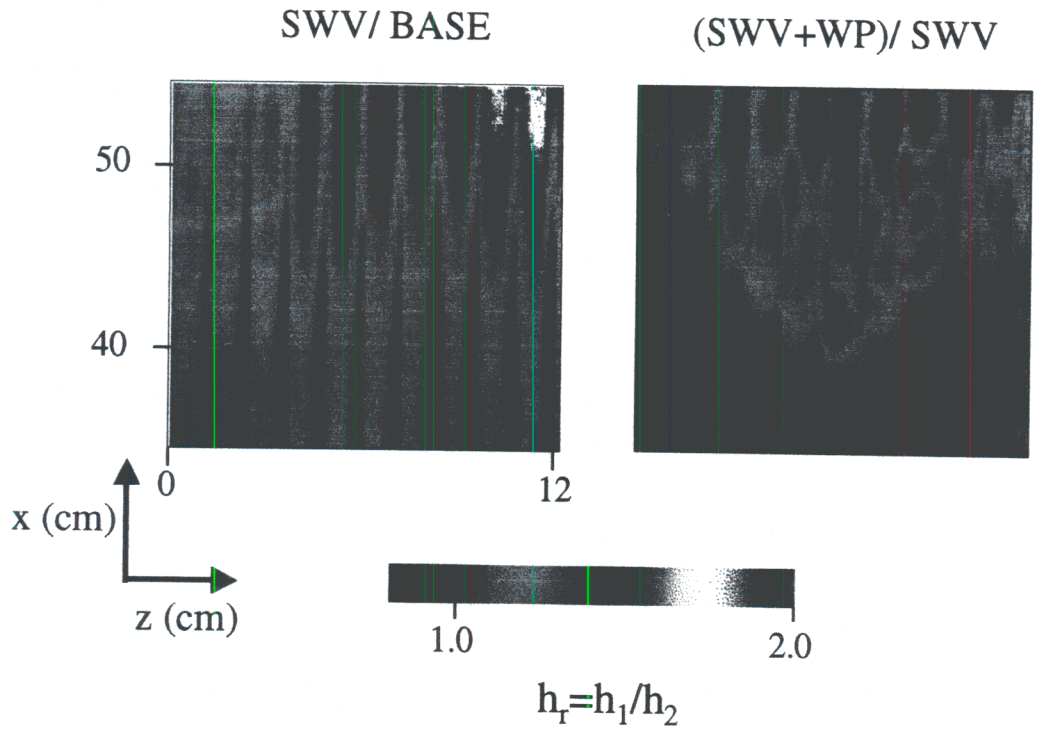

Figure 18a

Figure 18b

III.3.3 Streamwise Vortex Cancellation using Wave-Packets

In §III.2.5, it is demonstrated that it is possible to cancel spanwise variations in surface temperature that result from stationary streamwise vortices via phased seeding of streamwise vortices. It appears plausible that higher order cancellation can be achieved by combining phased control with propagating wave-packets to exploit the induced spanwise displacement of the streamwise vortices. If this spanwise displacement is on the order of the spanwise wavelength of the streamwise vortices, then "sliding" spanwise-periodic cooling and heating of the surface can be used across the span to achieve uniform surface temperature. Figure 19b shows the average disturbance temperature created by the passage of a single wave-packet through a system of streamwise vortices. The time averaged change in surface temperature (T_{ad}) created by the wave-packet is nearly 180° out of phase with respect to the surface temperature established by the streamwise vortices in figure 19a. This implies that if a wave-packet is used as a control of surface transport, the control input (i.e. change in surface temperature) is the correct sign for canceling the temperature variations imposed by the streamwise vortices. By changing the duty cycle, amplitude, and spanwise distribution of wave-packets, the spanwise variations created by the streamwise vortices could be smoothed in the mean.

IV CONCLUSIONS

Controlled excitation of spanwise instability modes have been employed to investigate the evolution of streamwise vortices in an inclined free convection boundary layer. It is found that the growth rate of spanwise instabilities depends strongly on plate inclination angles and only weakly on surface heat flux. Depending on the modified Reynolds number and the initial strength of the spanwise disturbances, the streamwise vortices can merge within the present range of observations. The appearance of the streamwise vortices leads to a substantial modification of the temperature distribution on the surface and with controlled, spanwise-periodic excitation an array of streamwise vortices can lead to a peak localized heat transfer increase of 200% and streamwise averaged increase of up to 35%. Controlled open loop excitation can also be used to cancel the formation of streamwise vortices resulting in substantial reductions in spanwise surface temperature variations.

Time-dependent pulsed excitation that leads to the appearance of isolated wave-packets has also been investigated in a nominally 2-D boundary layer and a boundary layer seeded with streamwise vortices. In the 2-D boundary layer, the wave-packet exhibits streamwise stretching that is nearly twice that of a packet in a momentum boundary layer. The packet is comprised of oblique waves of equal magnitude but opposite directions and their angles increase in the streamwise direction indicating the presence of vertical vorticity. Farther downstream, the wave-packet undergoes a bifurcation as a result of a subharmonic resonance that is characterized by the development of large side lobes symmetric about the disturbance centerline. At this stage the wave-packet has effectively split in two with each side lobe comprised of a pair of oblique waves. The spanwise temperature variations induced by the passage of the wave packet increase substantially when the wave packet propagates through seeded streamwise vortices thus leading to substantial enhancement in surface heat transfer.

Figure 19a

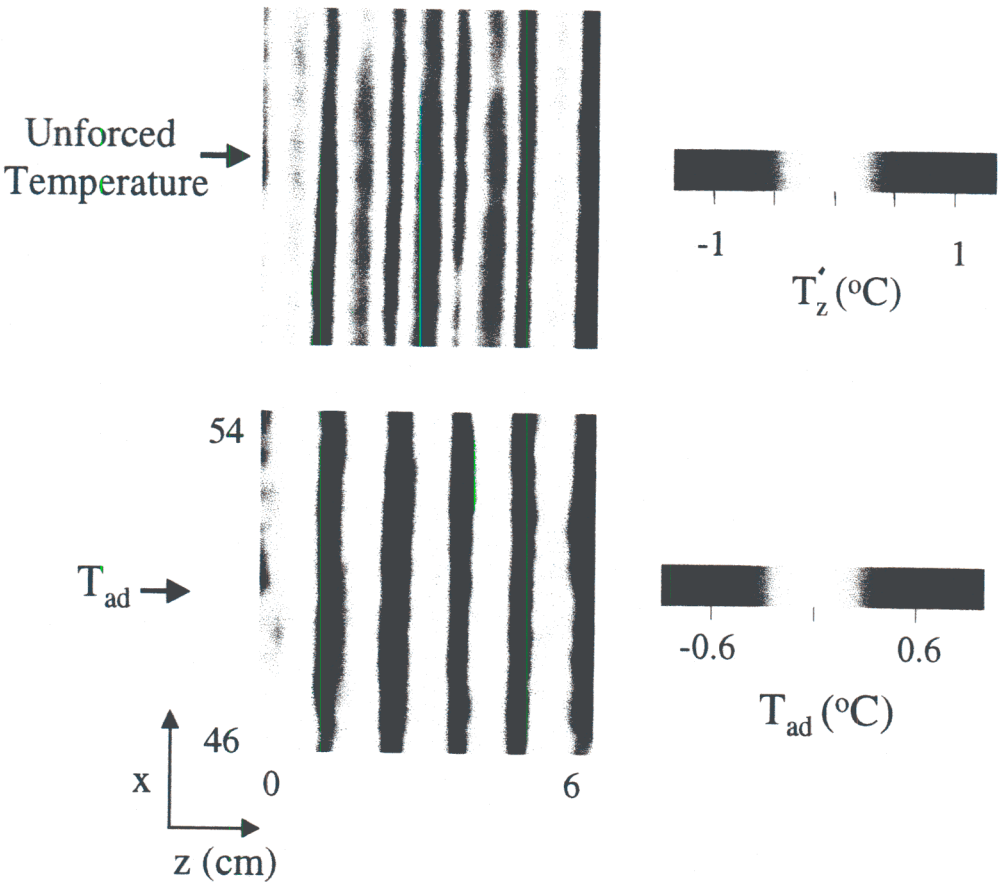

Figure 19b

IV. STATEMENT OF WORK TO BE COMPLETED

- Particle image velocimetry (PIV) will be used to measure velocities in planar cross sections of the boundary layer.
- The velocity data will be coupled to the previous heat transfer measurements.
- The streamwise vorticity field will be constructed to determine the evolution and dynamics of the streamwise vortices and, in particular, their merging.
- The effect of time varying forcing on heat transfer will be quantitatively determined using TLC thermometry.
- Further investigations of open-loop control configurations will be sought for maximum enhancement of heat transfer. Time-harmonic excitation waveforms including spanwise amplitude-modulated and spanwise phase-modulated excitation will be used.

References

1. Chen C.C., Labhabi A., Chang H.-C., Kelly R.E., "Spanwise pairing of finite-amplitude longitudianl vortex rolls in inclined free-convection boundary layers,", *J. Fluid Mech.*, **231**, 73-111, 1991.

2. Craik, A., "Non-linear resonant instability in boundary layers", J. Fluid Mech, **50**, 393-413, 1971

3. Farina, D.J. et. al.,"Illuminant invariant calibration of thermochromic liquid crystals," *Experimental Thermal and Fluid Science*, **9**, 1-12, 1994.

4. Gaster, M., "An experimental investigation of the formation and development of a wave packet in a laminar boundary layer", Proc. R. Soc. Lond. A., **347**, 253-269, 1975

5. Gebhart, B., "Natural convection flow, instability and transition," *J. Heat Transfer,* **18**, 293-309, 1969.

6. Godaux, F., Gebhart, B. "An experimental study of the transition of natural convection flow adjacent to a vertical surface," *Int. J. Heat Mass Transfer*, **17**, 93-107, 1974.

7. Gortler, H. "Uber eine Analogie zwischen den Instabilititen laminarer Grenzschichtstromungen an konkaven Wunden und an erwurmten Wunden, " *Ing. Arch.*, **28**, 251-255, 1969.

8. Haaland, S.E., Sparrow, E.M. "Vortex instability of natural convection flow on inclined surfaces," *J. Heat Mass Transfer*, **16**, 2355-2367, 1973.

9. Jaluria, Y., Gebhart, B."An experimental study of nonlinear disturbance behavior in natural convection", *J. Fluid Mech,* **61**, 337-365, 1973.

10. Kierkus, W.T. "An analysis of laminar free convection flow and heat transfer about an inclined isothermal plate,", *J. Heat Mass Transfer*, **11**, 241-253, 1968.

11. Knowles, C.P., Gebhart, B. , "The stability of the laminar natural convection boundary layer," *J. Fluid Mech.*, **34**, 657-686, 1968.

12. Liepmann, H. W., Brown, G. L. , and Nosenchuck, D. M. "Control of laminar-instability waves using a new technique," *J. Fluid Mech.*, **118**, 187-200, 1982.

13. Lloyd, J. R., Sparrow, E. M "On the instability of natural convection flow on inclined plates," *J. Fluid Mech.*, **42**, 465-470.

14. Lloyd, J. R., Sparrow, E. M., and Eckert, E. R. G., "Laminar, transition and turbulent natural convection adjacent to inclined vertical surfaces," *Int. J. Heat Mass Transfer*, **15**, 457-473, 1972.

15. Merkin, J.H., "The effect of buoyancy forces on the boundary-layer flow over a semi-infinite vertical flat plate in a uniform free stream," *J. Fluid Mech.*, **35**, 439-450, 1969.

16. Pauley, W.R., Eaton, J.K. "The effect of embedded longitudinal vortex arrays on turbulent boundary layer heat transfer," *J. Heat Transfer*, **116**, 871-879.

17. Sparrow, E.M., Gregg, J.L., "Laminar free convection from a vertical plate with uniform surface heat flux," *Trans. ASME*, 435-440, 1956.

18. Sparrow, E.M., Tsou, F.K., Kurtz, E.F., "Stability of laminar free-convection flow on a vertical plate," *Phys. Fluids*, **8**, 1559-1561, 1965.

19. Shankatullah, E. M. and Gebhart, B., "An experimental investigation of natural convection flow over and inclined surface," *Int. J. Heat Mass Trans.*, **21**, 1481-1490, 1978.

20. Vliet, G.C., Liu, C.K. "An experimental study of turbulent natural convection boundary layers," *J. Heat Transfer*, 517-531, Nov. 1969.